Easily Achievable Methods for Making Superamphiphobic Surfaces

Inger Lise Øhman Meisingset

Master's Thesis in Nano Science

Supervisor: Tore Skodvin

Department of Chemistry, University of Bergen

Allégaten 41, 5020 Bergen, Norway

June 1st, 2018

Acknowledgments

I want to express my gratitude towards my supervisor Tore Skodvin, for all his guidance, feedback and encouragement throughout this thesis work. I would also like to thank Irene Heggstad at the laboratory for electron microscopy, for spending hours helping me investigate my samples.

I would like to thank my family and friends for their support, and a special thanks to my father for constructive feedback and proofreading this thesis. I also want to thank my student choir for all the fun (and mandatory) rehearsals throughout this period, which made me take a break and take my mind of writing during stressful times.

Abstract

Superamphiphobic materials have surfaces that display a contact angle above 150° for both low and high-tension liquids[1]. Superamphiphobic surfaces present exciting and innovative properties for commercial and industrial applications. Fabrication of superamphiphobic surfaces often require advanced techniques and chemicals. Easier and cheaper methods for making these surfaces are desirable to produce them sustainably, durably and on a big-scale. In this thesis, we explore whether surfaces of different materials can be rendered superamphiphobic in an environmentally sound way and with easily accessible chemicals and instruments found in most labs.

Three different techniques described in the literature were taken as starting points for the pursuit of easily accommodable methods. For the first technique, glass and stainless steel substrates were dip-coated in a waterborne coating system consisting of a fluorinated compound and silica particles, to give the proper structured surfaces for superamphiphobicity[2]. In the second technique, thermal treatment was used on silicon oil to produce a layer of soot which deposited directly on to glass and steel substrates to give the proper surface structure and composition for superamphiphobicity[3]. Thirdly, aluminum was etched in hydrochloric acid in order to give a micro structured surface. The aluminum was then immersed in a solution of HNO_3 and $CuSO_4$ in order to provide a hierarchical structure by the addition of copper particles, and dip-coated in a fluorinated solution to minimize the surface energy[4].

The unmodified and modified substrates were characterized by electron microscopy imaging and elemental analysis to elucidate the structure and composition of the surfaces. The wetting properties and apparent surface energy of the substrates were determined from optical contact angle measurements.

Superhydrophobic surfaces were readily achieved for all the tested materials. Oleophobicity was not achieved without the addition of fluorinated compounds, and none of the methods chosen yielded superamphiphobic surfaces. The easily achievable methods have not provided surface structures of the necessary quality to uphold superamphiphobicity.

Table of Contents

List of Figures

List of Tables

1 Introduction

Imagine being able to make any surface self-healing, anti-corrosive, antibacterial, anti-fouling, and self-cleaning. Drops of rain will make cars spotless, and containers can yield 100% of their contents due to a non-adherent surface. Ships can be in contact with water for months without any need for algae removal or maintenance. This causes less energy to be lost due to drag, hence less fuel is needed. A surface can be given these properties by applying a superamphiphobic coating. Superamphiphobic surfaces can give a more environmental friendly society, reducing waste and the demand on resources.

1.1 Exploring Surface Chemistry

In 1997, Barthlott and Neinhuis published an article explaining the chemistry behind the "lotus effect" [5]. Lotus leaves have a superhydrophobic surface (see Figure 1.1b) with self-cleansing properties. Superhydrophobic surfaces will give a contact angle of minimum 150° with water droplets. When there is dirt on the lotus leaf, water droplets that roll off will also bring the dirt off the surface, making self-cleaning a common property for superhydrophobic surfaces. Barthlott and Neinhuis' research showed that the lotus leaf has a surface with roughness both on the microscale and the nanoscale, a so called hierarchical surface roughness[6] (see Figure 1.1a), which plays a dominant role in making a surface superhydrophobic. The new knowledge on the surface structure and chemistry of superhydrophobic surfaces sparked the interest in researching this field, trying to mimic the surfaces of other plants and animals.

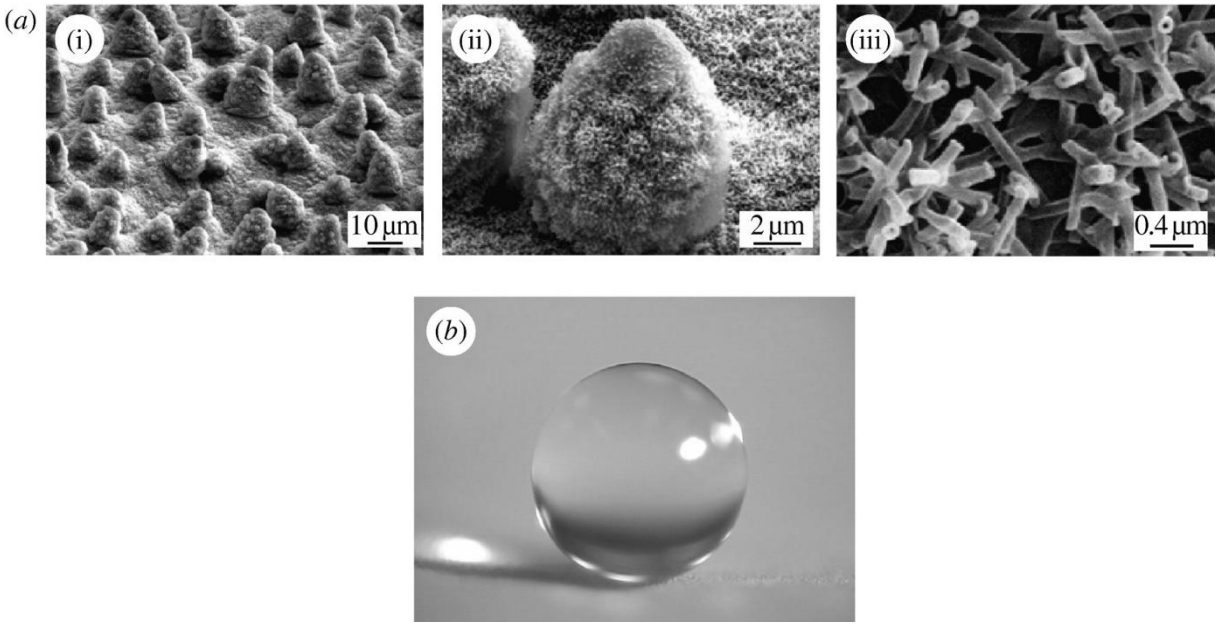

Figure 1.1. (a) SEM images of a lotus leaf at three different magnifications (i), (ii), (iii). The hierarchical surface structure can be seen by the roughness at each scale. (b) Water droplet sitting on top of a lotus leaf, illustrating the superhydrophobic property. Figure reprinted from Bhushan's Biomimetics[7].

Another naturally occurring liquid-repellent surface is an oleophobic surface. Oleophobic surfaces give rise to contact angles of 90°-150° with organic liquids with low surface tensions[1]. The surface of a liquid may be likened to a thin elastic sheet, and the force needed to expand this sheet, is the liquids surface tension. If a liquid has a high surface tension it will more easily have high contact angles when deposited on a surface. Liquids with low surface tensions will only form high contact angles with a surface that has an even lower surface energy. This makes it difficult to prevent organic liquids from wetting surfaces. Superoleophobic surfaces that gives contact angles above 150° with low tension liquids are yet to be found naturally occurring[8]. However, they have been made artificially

The superoleophobic surfaces are self-cleaning and anti-fouling from organic and biological contaminants both in air and in water, which makes them attractive for industrial applications like marine ship fouling, anti-smudge, transparency, anti-icing, and anti-fogging, on windows, solar panels, electronic touch screens, and computer displays, etc. Because of the low surface energy of superoleophobic surfaces, most of them will also repel water, but recently there have been cases where superoleophobic surfaces have proven to be superhydrophilic[9].

The need to distinguish between the superoleophobic surfaces that are superhydrophilic, and the ones that are superhydrophobic, gave rise to several new terms. The terminology for these

repellent surfaces are yet not well defined, and many researchers apply the same terms based on different definitions. In this thesis we define superamphiphobic surfaces as surfaces that are both superoleophobic and superhydrophobic in air, caused by a combination of the proper surface roughness and chemistry.

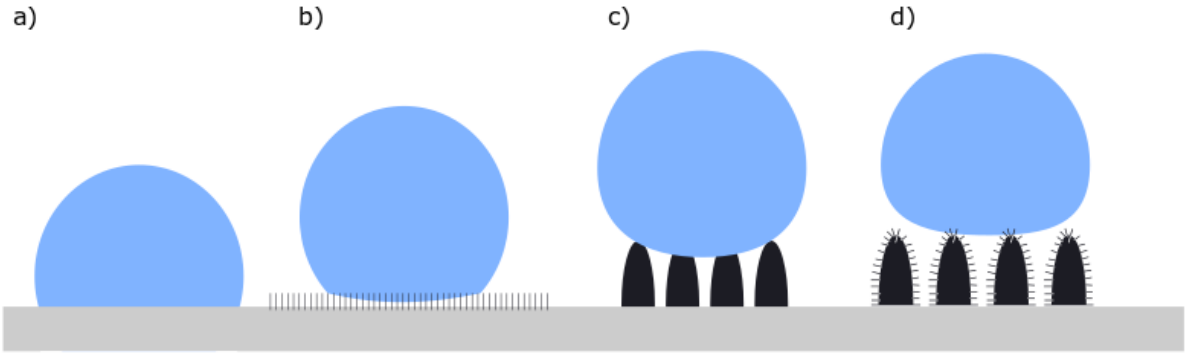

Figure 1.2. Illustration of the hierarchical surface structure. (a) A droplet on a smooth surface, the droplet has a relatively low contact angle hence wetting the surface. (b) A droplet on a rough nano-structured surface, the apparent contact angle is much higher than for a smooth surface. (c) A droplet on a rough micro-structured surface, the contact angle is higher than for a smooth surface. (d) A droplet on a hierarchical surface structure. This causes an even higher contact angle because of a small contact area and air bubbles trapped underneath.

The combination of a high contact angle and a low contact angle hysteresis is the basis for superamphiphobic surfaces. Superamphiphobic surfaces are surfaces that display contact angles higher than 150° for liquids with both low and high surface tension. The contact angle hysteresis should also be smaller than 5° so that liquids easily roll of the surface and give (among other) self-cleaning and anti-fouling properties[1]. The contact angle hysteresis of a surface is the difference between the advancing and receding angle of a droplet deposited on a surface[10]. This difference occurs because of the roughness and heterogeneity of a surface.

Neither water nor oil will be able to penetrate the structure or decrease the quality of a superamphiphobic surface. This makes a superamphiphobic surface more resistant to liquids, in comparison to superhydrophobic or superoleophobic surfaces. Superamphiphobic surfaces appear unreactive to most surroundings and thus are attractive for commercial and industrial applications. A challenge when making superamphiphobic surfaces is to make them sufficiently resistant to mechanical stress. It is also challenging to make a superamphiphobic coating with proper adhesion to the substrate, while keeping their superamphiphobic properties towards the surroundings.

Another challenge is the frequent use of fluorinated compounds. Fluorinated compounds are often used to achieve a surface with low surface energy since these compounds often display weak intermolecular forces. This, in addition to a hierarchical surface geometry, will further increase a contact angle. Unfortunately, some fluorinated compounds (like perfluorooctanesulfonic acid (PFOS) and perfluorooctanoic acid (PFOA)) are resistant to most typical environmental degradation processes and thus extremely persistent in the environment. The toxicity, mobility and bioaccumulation potential of these compounds may cause adverse effects for the environment and human health[11].

1.2 Properties of Superamphiphobic Surfaces

Current surface coatings with primary function of self-cleaning can broadly be classified into two types: photocatalysis-induced superhydrophilic coatings and superamphiphobic coatings[12]. Organic substances are converted to carbon dioxide and water by the photocatalytic effect, and the surfaces are cleansed by the sheeting effect of water. The superamphiphobic coating on the other hand, use air pockets in the rough hierarchical surface structure which are water repellent and form a composite interface for the solid and liquid, resulting in an increased contact angle for the droplet and enabling it to roll-off while taking away dirt and other pollutants. In contrast to photocatalysis, the superamphiphobic coating will also use water droplets to remove dirt and pollutants, making it more versatile and efficient.

To prevent icing on devices like airplanes and radars, anti-freezing is another important property for surface materials. Large amounts of ice can destroy or severely damage outdoor infrastructures. Efficient methods to prevent icing may reduce pollution by eliminating the need to frequently add coatings like antifreeze on airplanes. To prevent water from freezing on a surface it should be superhydrophobic with a low contact angle hysteresis so the water droplets rapidly can roll off before they freeze. Quèrè *et al.*[13] found that an air sublayer on the surface will sufficiently increase the thermal insulation, slowing down the freezing process for the water droplets. Hierarchical structures on superamphiphobic surfaces will provide air pockets in the nano – and microstructures of the surface, giving higher contact angles, lower contact angle hysteresis and better thermal insulation. Hence, superamphiphobic surfaces could be more efficient than superhydrophobic surfaces for anti-freezing properties.

Metals and alloys often suffer from corrosion and oxidation in humid surroundings, which causes problems like accelerated aging of devices, waste, and environmental contamination.

This is a major problem in shipping and on offshore installations. Superhydrophobicity is not sufficient to prevent corrosion, since oil pollutants and organic materials in seawater may penetrate the coating. A way to successfully prevent corrosion is surface modification. Superamphiphobic coatings have proven to be an efficient method by acting as a durable barrier film. Zhao *et al.*[14] formed a nano - and microstructured hierarchical surface on CaLi-based bulk metallic glass, by etching with water and coating with a low tension fluorinated compound. The surface was exposed to ambient atmospheric condition for three months without any damage to the surface, in comparison to an untreated CaLi-based metallic glass surface that was severely oxidized within 1-2 weeks of similar exposure. This shows that the superamphiphobic coating is an efficient way to prevent corrosion and oxidation.

Superamphiphobic surfaces have also proven to have antibacterial properties. This could be useful for medical equipment by reducing the risk of bacterial contaminations, and it can prevent biofouling on ships and platforms in seawater, increasing the durability of the materials. Liu *et al.*[15] used silver nanoparticles on a superamphiphobic aluminum surface, which insulates the aluminum from exposure to humid surroundings, preventing corrosion. The silver nanoparticles have antiseptic properties, and by deposition on the superamphiphobic surface they will promote biofouling properties. However, silver nanoparticles may be toxic.

1.3 Current Methods for the Formation of Superamphiphobic Surfaces

There are several different techniques available for making superamphiphobic surfaces, all of which include some kind of roughening and coating of the surface. The surface can be roughened by methods like etching, lithography or sputter deposition, and afterwards coated with a low surface energy compound. Another method is to coat flat surfaces directly with compounds that will attain a rough surface structure after deposition and give a low surface energy. This can occur through dip-coating, spin-coating, spray-coating, or other physical coating techniques.

Some of the methods for making superamphiphobic surfaces require more equipment and expertise than others. Fujii *et al.*[16] used sputter deposition for making the rough surface structure on their substrate, by sputtering Al-Nb alloys onto aluminum substrate followed by anodization. In comparison, Zhou *et al.*[2] used a simpler method by dip-coating the substrate in a mixture of

teflon particles and a fluorinated compound in a waterborne coating system (see Figure 1.3). The fluorinated compound adhered to the teflon particles. After the dip-coating, the fluorinated teflon particles self-aggregated into a hierarchical structure when dried. Dip-coating in a waterborne system prevents use of organic solvents that can pollute the environment and cause safety issues.

The method used by Zhou *et al*.[2] formed a superamphiphobic coating on a diverse selection of materials which showed durability against mechanical friction. However, while the superamphiphobic surface could withstand abrasion and showed good self-healing properties, the contact angle for low tension liquids decreased after washing and abrasions. This was explained by an increase in the adhesive forces between the superamphiphobic surface and oil. Self-healing after physical abrasion gave several contact angles close to, but not higher, than 150°. A contact angle lower than 150° no longer makes the surface superamphiphobic. The surfaces were not tested for anti-corrosion nor antibacterial properties.

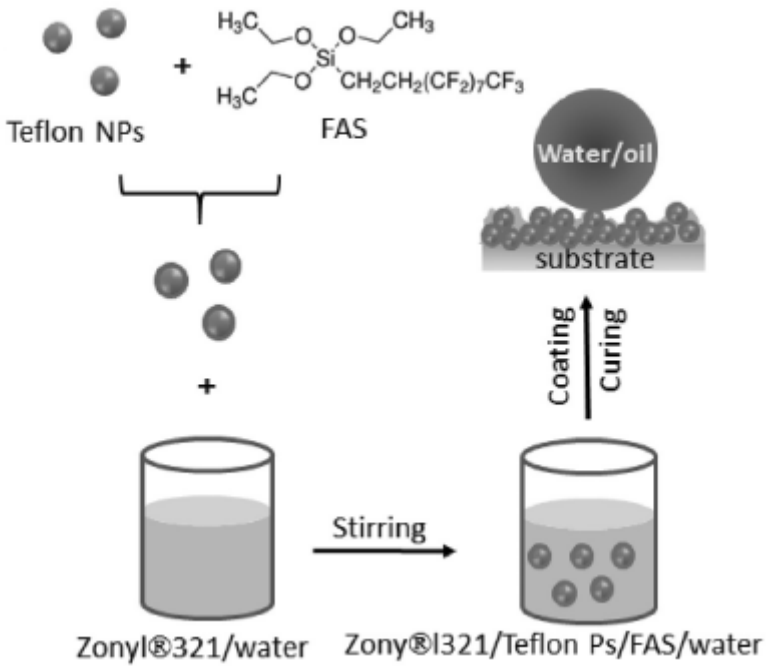

Figure 1.3. Illustration of the dip-coating procedure for solution preparation and surface treatment, giving a superamphiphobic surface. Figure reprinted from Zhou et al[2].

Published literature on aluminum surfaces that presents superoleophobicity, anti-smudge properties, mechanical durability and self-cleaning are scarce. *Peng et al*.[4] produced microstep and nanoreticula structures on aluminum surfaces to form a hierarchical structure. A two-step

chemical etching process was employed, and the hierarchical structure was modified with fluorosilane to get superamphiphobic properties. The surfaces were found to be wear resistant, self-cleaning, corrosion resistant and had anti-smudge properties.

Another simple and more environmentally friendly method was developed by Long *et al.*[3], who used one-step thermal treatment of polydimethylsiloxane (PDMS, Sylgard 184) to create a transparent super-repellent surface on glass slides, and super-repellent powder. The PDMS was heated for 2 hours and the soot was deposited directly onto various substrates. No fluorosilane modification was made on the coatings, and the wettability of the coated substrates was regulated by controlling temperature and heating time. The ability to provide superamphiphobic coatings without fluorosilane is highly desirable, and these coatings showed both chemical and mechanical durability towards stress. This makes these coatings applicable for solar cell panels, smart windows, safety glasses and more.

1.4 Thesis Objectives

The aim of this thesis is to investigate easy and efficient techniques for making superamphiphobic coatings applicable to a variety of materials, without the use of advanced instrumentation or specialized chemicals. We also want to elucidate to what degree one can avoid fluorinated compounds when preparing superamphiphobic surfaces.

The works by Zhou *et al.*[2], Long *et al.*[3] and Peng *et al.*[4] are used as the basis for our research. Their methods are applied to a range of different materials to see if the methods are generally applicable. The effect on the wetting properties and surface structure by adjusting the methods is also elucidated. Where fluorinated compounds have been used, we investigate whether these are required in order to render the coatings superamphiphobic.

Two main techniques are used for characterizing the coated and uncoated substrates. Scanning electron microscopy imaging is used for determining the surface structure, and the surface composition is determined at the same instance (from the integrated elemental analysis equipment (an energy-dispersive X-ray spectroscopy detector (EDS) and wavelength-dispersive X-ray spectroscopy detector (WDS) is at our disposal). The wetting properties and apparent surface energy are determined using an optical contact angle instrument.

We intended to replicate the work done by Long *et al.*[3] with a broader range of substrates in order to investigate whether superamphiphobicity can be achieved regardless of the substrates

composition. Also, it was planned to study the effects of variations in temperature and heating time on the deposit structure and wetting properties. However, the oil used by Long *et al.*[3], Sylgard 184, arrived 6 months late, close to the end of the project. This led us to replace Sylgard 184 with another quality of silicone oil (the much more viscous Silicon Oil DC 200) in the meantime. The experiments were limited to comprise a comparison of the surface structure and wetting properties of soot from Sylgard 184 and Silicon Oil DC 200.

1.5 Thesis Outline

In the following, a brief theoretical introduction to superamphiphobicity will be given. This is followed by a description of the instrumentation used for this work. Subsequently, the experimental methods applied to the substrates are presented. Finally, the most important results are discussed before the conclusion is drawn. The appendix holds further details on the treated substrates, contact angle hysteresis and surface energy calculations.

2 Theory

There are several properties at the interface between a liquid and a solid surface that affects the way the two substances will interact. These basic interactions must be considered and understood when making surface coatings to achieve the wanted results. In this chapter the following concepts are presented; surface tension of liquids and solids, contact angle, contact angle hysteresis, wetting regimes, the importance of surface structure, and superamphiphobic surfaces.

2.1 Surface Tension of Liquids and Solids

All liquids are held together by intermolecular forces, i.e. hydrogen bonds, dipole interactions and van der Waals forces. These forces follow Coulombs law, hence higher charged poles on the molecules will give stronger intermolecular forces. The molecules in the interior of the liquid will experience intermolecular forces in all directions, while the molecules at the surface will only experience forces from the interior of the liquid (see Figure 2.1). This tends to give the liquid a spherical shape when it is dispersed in another liquid. The droplets are easily distorted from the spherical shape, for instance by gravitational pull[17].

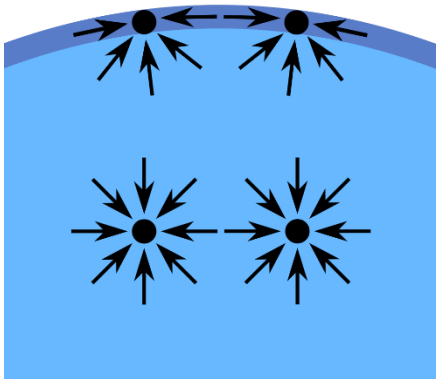

Figure 2.1. The intermolecular forces acting upon molecules in the bulk of a liquid, and at the surface. The molecules in the bulk experience forces from all directions, while the molecules at the surface only experience forces from the interior[18].

Droplets contract to the minimum surface area to achieve the lowest and most stable state of energy. The surface tension of a droplet depends on the magnitude of the intermolecular forces. Liquids with stronger bonds, i.e. water with a lot of hydrogen bonds will have a greater surface tension than organic liquids where van der Waals forces are the major contributors[17]. The surface tension is defined as the energy required to expand the surface per unit area, J/m^2, or the force required to expand per unit length, N/m.

$$\gamma = \frac{\Delta W}{\Delta A} \tag{1.1}$$

γ is the surface energy, W is the work done on the surface and A is the area. When using the units of N/m one usually refers to surface energy as surface tension. Liquids with low surface tension will easily spread out on a surface, giving a lower *contact angle* than liquids with high surface tension[17]. Table 2.1 gives the surface tension for both polar and non-polar liquids.

Table 2.1 Surface tension for selected liquids. Increasing charge in the molecule gives stronger intermolecular forces, hence higher surface tension[19].

Liquid	**Surface Tension (mN/m)**
Sodium Chloride	114.0
Water	72.7
Diiodomethane	50.8
Olive oil	33.1
n-Hexadecane	22.4
Ethanol	22.0

To expand the surface of a solid material, energy is required. This surface energy is not readily measured but it may be calculated using various theories[20]. Fluorination is often used for preparing repellent surfaces due to the high electronegativity and low polarizability of the fluorine atom, a property that promotes low surface energies. There are no exact theories for calculating the surface energy of a solid material, because none of the theories can model reality perfectly. For indirect estimations of the surface energy of solid surfaces, the interactions between the solid surface and liquids with different surface tensions may be determined. One common theory used for finding surface energy experimentally is a method developed by Owens, Wendt, Rabel and Kaelble (OWRK)[21]. This method is based on the idea that the interfacial tension can be separated according to the underlying interactions between the molecules. The test liquids contact angles, and the dispersive and polar parts of their surface

tension, is used to create a regression line. At least two test liquids are required in order to construct the regression line, but a minimum of three test liquids are recommended for more accurate results[21].

2.2 Contact Angle

A liquid in contact with a solid surface can spread out like a film, of form spherically shaped droplets laying on top of the solid surface. The amount of spreading for a specific liquid depends on the surface tension of the liquid and the surface energy, structure and chemical composition of the materials in contact. The contact angle for the liquid may be used as a measure of the degree of spreading and is measured at the "triple line", the line of contact of the liquid, solid and gas[22] (see Figure 2.2).

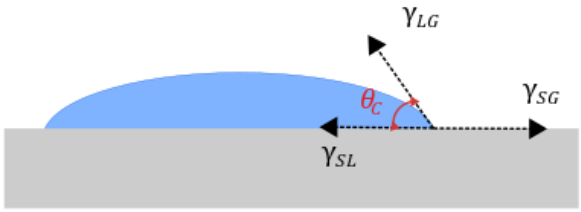

Figure 2.2 The contact angle is measured at the interface for all three phases, the triple line.

If the contact angle is below 90°, the solid surface is described as liquidphilic and we say that the liquid wets the surface. If the contact angle is between 90° and 150°, the surface is described as liquidphobic, while contact angles of more than 150° describes a superliquidphobic surface[1].

The energy of a system where a liquid is in contact with a surface will decrease below that of the two separate surfaces. This occurs because of the molecular attractions and is expressed by the Duprè equation[23],

$$W_{SL} = \gamma_{SG} + \gamma_{LG} - \gamma_{SL} \tag{1.2}$$

W_{SL} is the work of adhesion per unit area for creating two separate surfaces, and γ_{SG}, γ_{SL} and γ_{LG} is the surface tension for solid-gas, solid-liquid and liquid-gas, respectively.

When a liquid is placed on a smooth and homogeneous solid surface, the liquid and solid will come together under equilibrium at the characteristic static contact angle. The static contact angle is determined when the net free energy of the system is zero[23].

$$E_{tot} = \gamma_{LG}(A_{LG} + A_{SL}) - W_{SL}A_{SL} = 0 \tag{1.3}$$

A_{SL} and A_{LG} are the contact areas of the liquid with the solid and gas, respectively.

From Figure 2.2, geometrical considerations show that

$$\frac{dA_{LG}}{dA_{SL}} = \cos\theta_c \tag{1.4}$$

By combining equations (1.2), (1.3) and (1.4), Young's equation for the static contact angle is obtained[23],

$$\cos\theta_c = \frac{\gamma_{SG} - \gamma_{SL}}{\gamma_{LG}} \tag{1.5}$$

The contact angle from equation (1.4) is a macroscale parameter and can often be referred to as the "apparent contact angle"[24]. The actual contact angle at the interface between solid, gas and liquid often have a lower value at micro – and nanoscale for several reasons. Firstly, liquids tend to form a thin film layer on top of many materials because of long-distance van der Waals forces, and this forms the disjoining pressure. The disjoining pressure depends on the liquid layer thickness and may cause the formation of stable thin films. Droplets near the triple line gradually transform from spherical to flat which gives a much lower nanoscale contact angle than the apparent contact angle. Next, even surfaces that are carefully prepared to be atomically smooth will have a certain level of roughness and heterogeneity. When liquid is in contact with the surface it will first spread on the liquidphilic spots that have high surface energy and in turn give low contact angles. Then, the static contact angle is determined when a droplet placed on a surface stop propagating. This definition is not well defined since there are other factors giving dynamic effects to the droplet. For instance, the droplet gains liquid when it is deposited on the surface and evaporate after deposition, hence no real static contact angle can be measured[24].

2.3 Contact Angle Hysteresis

When measuring the contact angle for a droplet on a surface it is also important to consider the contact angle hysteresis. Contact angle hysteresis occurs because of surface roughness and

heterogeneity. The contact angle hysteresis is a measure of the difference between the advancing and receding contact angles, and it reflects a droplets ability to move on a surface (see Figure 2.3)[10]. It is defined as,

$$H = \theta_{adv} - \theta_{rec} \tag{1.6}$$

where θ_{adv} and θ_{rec} are the advancing and receding contact angles, respectively.

If the receding contact angle is relatively low it means that the droplet pins to the surface and is hard to remove. If the contact angle hysteresis is low, it means that the advancing and receding contact angles are close in value, and the droplet can roll off a tilted surface[10].

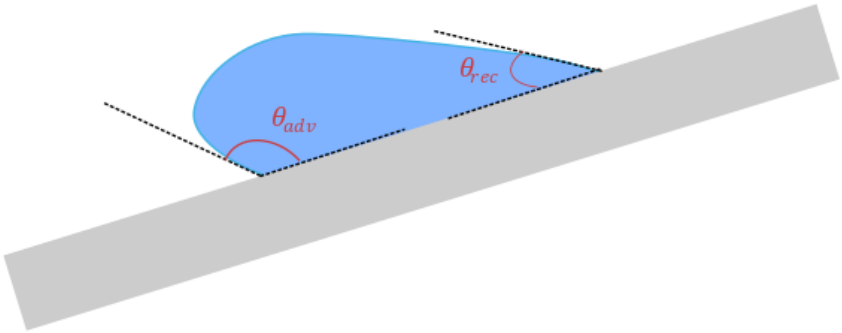

Figure 2.3. Illustration of a droplet on a tilted surface, showing the advancing and receding angles.

2.4 Wetting Regimes

How does a liquid spread on a rough surface compared to a smooth? When a liquid is in contact with a rough surface, one of two models is often used for describing the interaction, the so called Wenzel regime and the Cassie-Baxter regime[25-26].

The Wenzel regime describes wetting on a homogeneous rough surface, where the droplet fills all the curvatures (see Figure 2.4a). The contact angle for the Wenzel regime is given by,

$$\cos\theta = \frac{A_{SL}}{A_F} = R_f \cos\theta_c \tag{1.7}$$

where R_f is the roughness factor which gives the ration between the area of the flat surface, A_F, and the total area of the rough surface, A_{SL}. Equation (1.7) is called the Wenzel equation[25].

The Wenzel regime predicts that a liquidphobic surface becomes more liquidphobic with an increase in the roughness factor, while a liquidphilic surface becomes more liquidphilic with an increase in the roughness factor. This can be seen from Figure 2.4b[25].

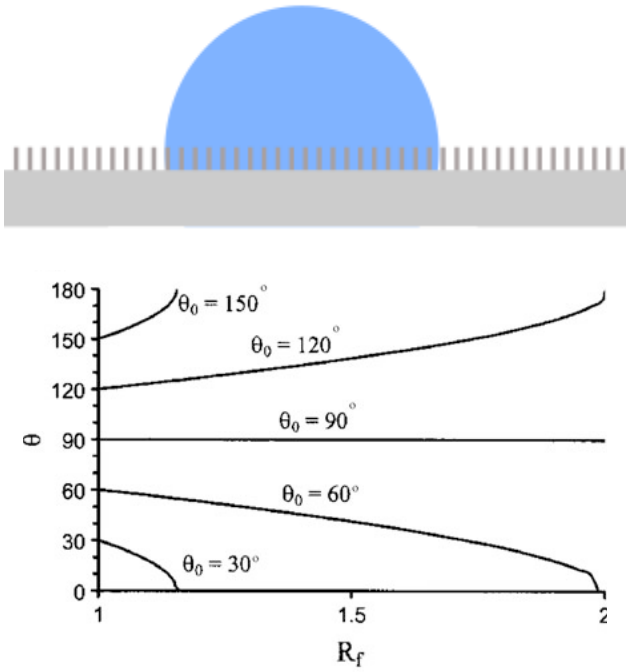

Figure 2.4. (a) A droplet wetting the surface in the Wenzel regime. The curvatures are fully filled with liquid. (b) The relationship between R_f and the contact angle. Liquidphilic will become more liquidphilic, while liquidphobic will become more liquidphobic. Figure 2.4b reprinted from Bushan's Biomimetics[25].

The Cassie-Baxter regime describes wetting of a heterogenous surface which gives a composite interface[25]. The droplet will sit on top of the curvatures in the rough structure without penetrating it, leaving pockets of air between the liquid and surface as illustrated in Figure 2.5. The composite interface consists of a fractional geometrical area of the solid-liquid interface under the droplet and the liquid-gas interface.

The contact angle for the Cassie-Baxter regime is defined by,

$$cos\,\theta = R_f\,cos\,\theta_C - 1 + f_{SL} \tag{1.8}$$

where R_f is the roughness factor and f_{SL} is the fraction of the geometrical area of the solid-liquid interface. From equation (1.8) it is clear that a smaller solid-liquid contact area will give a higher contact angle.

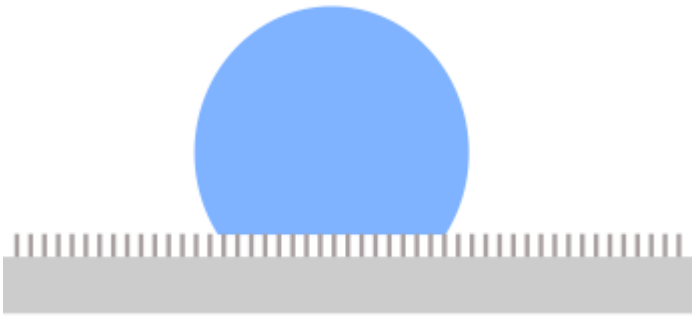

Figure 2.5 Cassie-Baxter wetting regime. The liquid does not penetrate the cavities, making a composite interface.

Pure Wenzel or Cassie-Baxter wetting rarely occur. The more common situation is a state between the Wenzel and Cassie-Baxter regimes where the liquid partially fills the cavities underneath, the so called impregnated state[25] (see Figure 2.6). This state will still lead to higher contact angles than the Wenzel regime, due to the air trapped beneath the liquid.

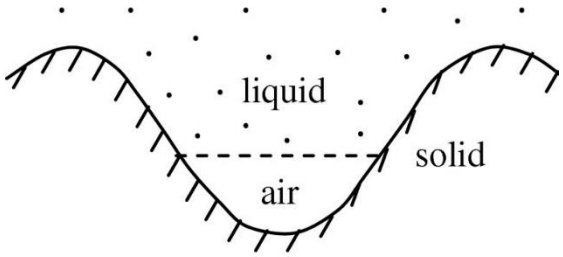

Figure 2.6. Illustration of the impregnated state, a mix between Wenzel and Cassie-Baxter. Figure reprinted from Bushan's Biomimetics[25].

The different wetting regimes will influence the liquid behavior on the surface, i.e. how strong the adhesion to the surface is or the hydrophobicity. A Cassie-Baxter regime give rise to higher hydrophobicity than a Wenzel regime because of hydrophobic properties of the air trapped in the cavities[25].

2.5 The Importance of Surface Structure

A hierarchical surface structure has levels of roughness from macrostructures to nanostructure, which provides hydrophobic air pocket formation[6] (see Figure 1.2d). This causes water droplets to have lower contact area with the surface, which in turn reduces the contact angle hysteresis,

promotes self-cleaning, low adhesion, and antifouling properties. Hierarchical structures favor Cassie-Baxter wetting which causes higher contact angles for water droplets on the surface.

If a hierarchical surface has a long distance between the peaks on the surface (i.e. a higher pitch value) it will promote Cassie impregnated wetting. This increase the adhesion forces since the water droplets can penetrate the micro – and partially the nanostructure. This phenomenon is seen on rose petals, which can have superhydrophobic surfaces with both low – and high adhesion[6].

In some cases, an irreversible transition from Cassie-Baxter to Wenzel wetting can occur. This destabilization of the Cassie-Baxter wetting regime may be caused e.g. by droplet vibration or pressure, and a complete Wenzel wetting will be more energetically favorable. For a liquid with low surface tension, such as organic liquids, and a contact angle less than 90° on a flat surface, a Wenzel regime will never be able to increase the contact angle further[25]. Hence, it is important to have Cassie-Baxter wetting to give oleophobicity.

The geometry of the surface structure will influence the surface properties. A surface structure with re-entrant geometry is useful for stabilizing a Cassie-Baxter wetting regime and prevent transition[27] (see Figure 2.7). For a re-entrant geometry, each roughness feature will create an overhang, hence become narrower closer to the surface. If the sum of the inclination angle (α) of the overhang, and the contact angle of a liquid on the flat surface (θ_{flat}) is ≥ 90°, the geometry will support a liquid-vapor interface where the surface tension points upward. This leaves a composite interface; hence the liquid does not fully wet the surface[28-29].

For liquids where $\theta_{flat} \approx 0°$, a double re-entrant geometry might be necessary to keep the liquid from wetting the surface. The presence of a positive pressure in a droplet means that the liquid-vapor interface shape with an upward surface tension is required. This is achieved by the double re-entrant geometry where vertical overhangs normal to the surface is incorporated, in addition to horizontal overhangs parallel to the surface (see Figure 2.7e).

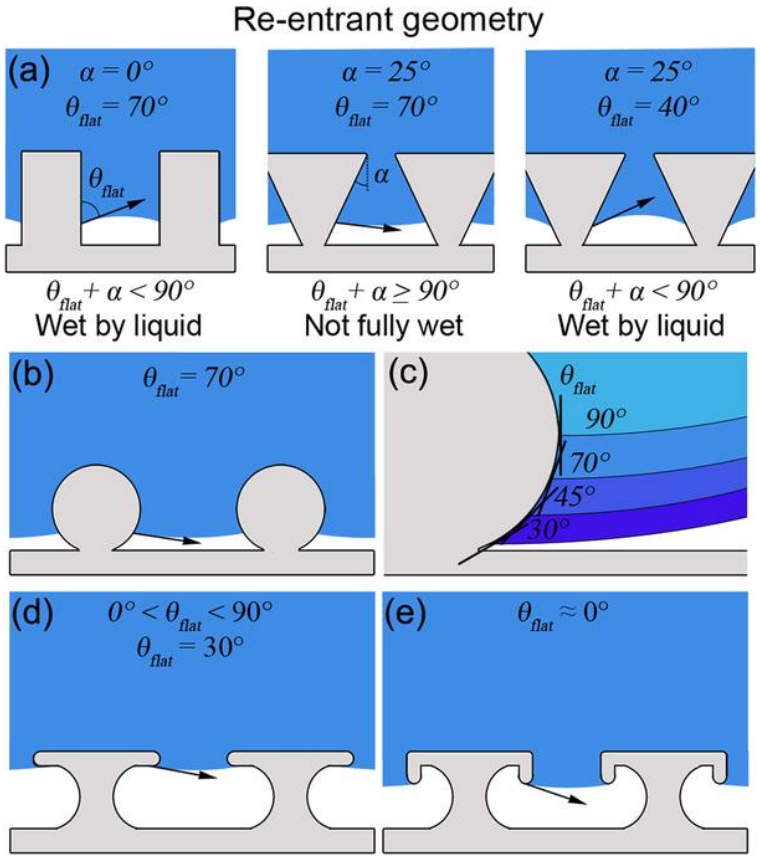

Figure 2.7. Liquid in contact with three types of a re-entrant geometries. a) liquid behavior on non-re-entrant and re-entrant geometries of cylindrical and trapezoidal features b) re-entrant geometry of cylindrical features supporting θ_{flat} = 70° c) re-entrant geometry supporting various θ_{flat} angles ≤90° d) re-entrant geometry supporting θ_{flat} = 30°, and e) double re-entrant geometry supporting $\theta_{flat} \approx 0°$ The arrows indicate the direction of the surface tension for liquid-gas. Figure reprinted from Brown *et al.*[29].

2.6 Superamphiphobic Surfaces

Superamphiphobic surfaces are surfaces that have a contact angle higher than 150° with both oil and water, hence it is both superoleophobic and superhydrophobic. True superamphiphobic surfaces should also display a contact angle hysteresis of less than 5° (this is important for the self-cleaning and anti-fouling properties). Superhydrophobicity can be achieved by preparing a hierarchical surface structure. Due to the relative high surface tension of water, there may in principle be no need for further coating to enhance this feature.

Superoleophobicity on the other hand is harder to achieve. All superhydrophilic surfaces will be superoleophobic in water, but no naturally occurring superoleophobic surfaces have been

observed in air. For a surface to become superoleophobic, the surface energy of the material in contact with the oil must be lower than the surface tension of the liquid itself. By combining a hierarchical structure with a re-entrant geometry and low surface energy coating, superamphiphobicity may be obtained in air, as shown by Zhou *et al.*[2], Long *et al.*[3] and Peng *et al.*[4].

3 Experimental Equipment

This chapter describes the equipment used for characterization of the treated and untreated glass, steel and aluminum substrates, and analysis of surface structure and composition. Firstly, it describes the instrument used for determining contact angle and surface energies. Next, it describes the dip-coating instrument used for depositing coatings onto substrates. Finally, the electron microscope used for imaging and elemental analysis is presented. A list of additional equipment used in the experiments is given at the end of the chapter.

3.1 Optical Contact Angle Measuring Instrument

For measuring the contact angle, contact angle hysteresis and calculating the apparent surface energy of the (coated and un-coated) materials, a video-based optical contact angle measuring instrument was used (model OCA20, Datatechnics, Germany). The OCA20 consists of a light source, sample stage, a high-resolution CCD camera, and an automatic dispensing unit. The light source is LED-lightning with software controlled adjustable intensity. The sample stage can be adjusted both horizontally and vertically to get an optimal sample position. The camera has a 6-fold zoom lens with 0.7-4.5 magnification and integrated fine focus, giving a measuring precision of ± 0.1° [30]. The automatic dispensing unit is mounted above the sample stage and can hold a syringe with volume up to 50 mL. The instrument is connected to a computer where the SCA software (Datatechnics, Germany) is used to analyze and store the images from the camera. In the SCA software, the volume and velocity is set for an automatic drop deposition on to the sample stage. On the sample stage, the droplet will be visible to the camera and the image appears in the SCA software where it can be further analyzed. A sketch showing the principal components of the OCA20 is given in Figure 3.1.

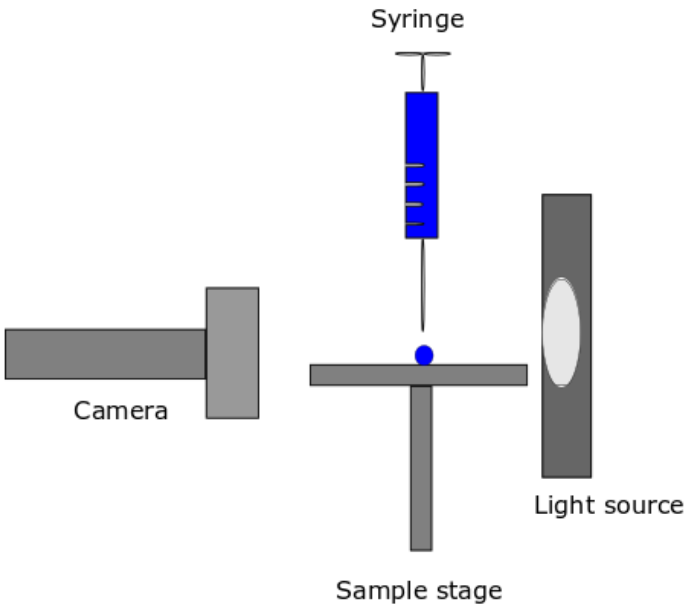

Figure 3.1. Illustration of the optical contact angle measuring instrument, model OCA20.

The static contact angle was measured by the SCA software at the triple line. A horizontal base line was manually placed at the triple line of the droplet and the SCA software fitted the extracted profile of the droplet. This gives the left and right contact angle for the droplet. This technique for contact angle measurements is called the sessile drop technique[31].

When measuring the contact angle hysteresis, the instrument was tilted (maximally to 90°) and the droplet movement was recorded and then analyzed. If the droplet rolled of the sample stage, the advancing and receding angle was found by the same method as for the static contact angle.

The SCA software used the OWRK method for calculating the surface energy of the materials. Water, diiodomethane and hexadecane were used as reference liquids with known surface tensions.

3.2 Dip-coating

Dip-coating of the glass and steel slides was done by a mini dip-coater from KSV Instruments Ltd., Finland. The LayerBuilder software is used for controlling the dip-coating process. The substrates are held by a plastic clip, and a solution or particle suspension is placed in appropriate distance beneath the handle. Parameters for dipping velocity, depth of immersion, amount of immersions, and how long the substrate is immersed before withdrawal, are entered in to the software and the dipping runs automatically. An illustration of the set-up is given in Figure 3.2.

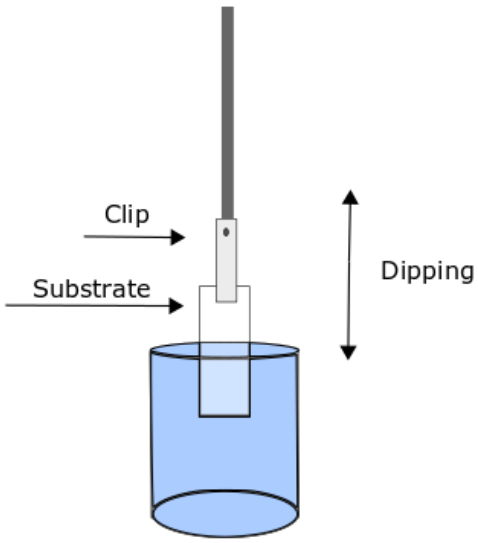

Figure 3.2. Illustration of the dip-coating instrument.

3.3 Electron Microscope

A Zeiss Supra 55VP Scanning Electron Microscope (SEM) was used for characterizing surface structure with and perform elemental analysis of the substrates and coatings. The Supra 55VP uses a field emission gun as an electron source, the accelerating voltage is in the range from 100 V-30 kV with a magnification up to 1.5 million times. The Supra 55VP is equipped with a Scanning Transmission Electron Microscope detector, backscatter detector, and a cathodoluminescence detector for imaging. For elemental analysis[32], an energy-dispersive X-ray spectroscopy detector (EDS) and wavelength-dispersive X-ray spectroscopy detector (WDS) can be used. It is estimated that the elemental analysis is made on the upper 2 μm of the samples.

3.4 Other Equipment

Heating and drying oven (Heraeus, Thermo Fisher Scientific, USA), used for drying and curing samples.

Ultrasonic bath (Sonorex Super RK 102 H, Bandelin, Germany).

Tube furnace (1200C, Carbolite, UK).

Analytical balance (XA204 DeltaRange, Mettler Toledo, USA) with a maximum capacity of 220 g and a readability of 0.1 mg.

4 Experimental Procedure

This chapter firstly presents the chemicals used in the experiments and the methods used for cleaning the glass, steel and aluminum substrates. Next, the experimental procedure for preparing coatings of Capstone and silica particles is presented, with the parameters used in the dip-coating of glass and steel substrates. Then, the deposition of heated silicon oil on glass and steel substrates, followed by the procedures for etching and coating of aluminum is presented. The methods used for the characterization of the coatings are given at the end of the chapter.

4.1 Chemicals

Table 4.1. Chemicals used in the experiments.

Compound	**Molecular formula**	**Molecular weight [g/mol]**	**Density [g/mL]**	**Manufacturer**
Capstone ST-100	Aqueous fluorochemical polymer dispersion	-	1.06	DuPont
Capstone ST-110	Aqueous fluorochemical polymer dispersion	-	-	DuPont
1H, 1H, 2H, 2H-perfluorodecyl-triethoxysilane (PDES)	$C_{16}H_{19}F_{17}O_3Si$	610.38	1.39	Sigma-Aldrich
1H, 1H, 2H, 2H-perfluorooctyl-trichlorosilane(POCS)	$CF_3(CF_2)_5CH_2CH_2SiCl_3$	481.54		Sigma-Aldrich
Potassium Hydroxide	KOH	56.11	2.12	Fluka
Acetone	C_3H_6O	58.08	0.78	-
Ethanol	C_2H_6O	46.07	0.79	-
Aerosil R972, hydrophobic	Fumed silica particles	-	-	Evonik
Aerosil OX50, hydrophilic	Fumed silica particles	-	-	Degussa
Silicon oil DC 200	$[-Si(CH_3)_2O-]_n$	-	0.96	Fluka
Sylgard 184	$(C_2H_6OSi)_n$	-	1.03	Sigma-Aldrich
Hexadecane	$C_{16}H_{34}$	226.44	0.77	Sigma-Aldrich
Diiodomethane	CH_2I_2	267.83	3.32	Sigma-Aldrich

Compound	Molecular formula	Molecular weight [g/mol]	Density [g/mL]	Manufacturer
Hydrochloric acid	HCl	36.46	0.00149	Sigma-Aldrich
Nitric acid	HNO_3	1.51	1.39	Sigma-Aldrich
Cupper(II) sulfate	$CuSO_4$	159.61	3.60	-

Distilled, ion-exchanged water has been used throughout.

Table 4.2. List of substrates.

Substrate	Composition	Surface area [mm^2]	Thickness [mm]
Glass slide	SiO_2 (72%) Na_2O (13,3%) CaO (8,8%) MgO (4,3%) Al_2O_3 (0,5%) K_2O (0,4%)	75 x 26	1.00
Steel slide	Fe (69,0%) Cr (18,0%) Ni (10,0%) Mo (3,0%)	45 x 15	0.92
Aluminum slide	Al	30 x 10	40.00

4.2 Procedure for Cleaning Glass, Steel and Aluminum Substrates

The glass substrates were treated according to the procedure describe by Cras *et al.* [33]. In short, the substrates were washed in a solution of potassium hydroxide and isopropanol for 30 minutes, rinsed with distilled water and dried with nitrogen gas, before being placed in an oven at 130° C to remove all water residue.

The steel substrates were placed in a container with acetone in the ultrasonic bath to remove glue residue from the steel surface.

The aluminum substrates were cleaned by ultrasonication sequently in acetone, ethanol, and distilled water.

4.3 Preparation of Colloidal Suspensions

Capstone ST-100 and Capstone ST-110 were diluted to the working strength recommended by DuPont in the data sheets[34-35].

4.3.1 Colloidal suspensions with PDES (1H, 1H, 2H, 2H-perfluorodecyl-triethoxysilane)

110-OX50(PDES)

10 mL of acetone is added to a mixture of 0.5 mL PDES and 0.25 g Aerosil OX50. 4.7 mL Capstone ST-110 is diluted in 100 mL H_2O and added to the mixture while stirring.

110-R972(PDES)

0.5 mL PDES is added to 0.25 g of Aerosil R972. 4.7 mL Capstone ST-110 is diluted in 100 mL H_2O, and mixed with Aerosil R972 and PDES while stirring.

100-OX50(PDES)

10 mL acetone is added to a mixture of 0.5 mL PDES and 0.25 g Aerosil OX50. 6.7 mL Capstone ST-100 is diluted with 100 mL H_2O and added to the solution while stirring.

100-R972(PDES)

0.5 mL PDES is added to 0.25 g of Aerosil R972. 6.7 mL Capstone ST-100 is diluted in 100 mL H_2O, and mixed with Aerosil R972 and PDES while stirring.

4.3.2 Colloidal suspensions with POCS (1H, 1H, 2H, 2H-perfluorooctyl-trichlorosilane)

Four additional suspensions were made with Capstone and POCS. Due to the chlorine functionality in POCS, it may be expected to more readily react with the hydrophilic silica particles as compared to PDES. This may be advantageous when it comes to the formation of stable suspensions.

110-OX50(POCS)

0.79 mL POCS is added to 0.9 g Aerosil OX50. 3.30 mL Capstone ST-110 is diluted in 50 mL H_2O and added to the solution. After stirring for 10 minutes, the solution is further diluted by 100 mL H_2O.

110-R972(POCS)

0.79 mL POCS is added to 0.9 g Aerosil R972. 3.30 mL Capstone ST-110 is diluted with 50 mL H_2O and added to the solution. After stirring for 10 minutes, the solution is further diluted by 100 mL H_2O.

100-OX50(POCS)

0.79 mL POCS is added to 0.9 g Aerosil OX50. 3.30 mL Capstone ST-100 is diluted with 50 mL H_2O and added to the solution. After stirring for 10 minutes, the solution is further diluted by 100 mL H_2O.

100-R972(POCS)

0.79 mL POCS is added to 0.9 g Aerosil OX50. 3.30 mL Capstone ST-110 is diluted with 50 mL H_2O and added to the solution. After stirring for 10 minutes, the solution is further diluted by 100 mL H_2O.

The PDES and POCS suspensions were coated on glass and steel slides, respectively, by using the mini dip-coater described in chapter 3.2. The downward rate was 90 mm/min, the upward rate was 45 mm/min, and the immersion time was 120 seconds. The coated substrates were dried at room temperature for 10 min and cured at 135°C for 1 h.

4.4 Deposition of Silicon Oil Soot

Following the method in the work done by Long *et al*.[3], 10 mL of silicon oil was placed in a container made of glass and a substrate (glass or steel) was placed on top, with a distance to the oil of approximately 1 cm. The oil was placed in a tube furnace with a temperature increase of 10°C/min from 0°C-350°C, and left at 350°C for 2 hours. The heating caused a layer of soot to deposit on to the substrate.

4.5 Etching of Aluminum, and Subsequent Coating

Following the method in the work done by Peng *et al.* [4], the aluminum slides were etched in 100 mL, 2.5 M HCl for 10 minutes to make a micro structured surface. Dislocation sites on the aluminum surface have relatively higher energy which causes the acid to selectively etch these

sites first. This leads to the formation of micro-pits on the surface. Following the etching, the aluminum slides were rinsed with distilled water and dried with nitrogen gas.

The aluminum slides were next immersed in 10 mg/ml solution of $CuSO_4$ in concentrated HNO_3 for 6 minutes at 80°C and dried in air at room temperature. The copper ions, (Cu^{2+}), are reduced to elementary copper (Cu). Copper nanoparticles deposits on the micro structured surface, resulting in a hierarchical surface structure.

Next, the aluminum slide was dip-coated for 2 hours in a 1.0 wt% PDES in ethanol solution, before being cured at 100°C for 30 minutes. The dip-coater is described in chapter 3.2. The downward and upward rate was set to 90 mm/min, between each dip the slide dried in air for 120 seconds, and the slide was dipped 55 times.

This procedure was repeated on three more samples, but with the immersion time in HCl set to 22 minutes in order to increase the degree of etching on the slide. For one sample, the solutions were continuously stirred.

4.6 Contact Angle Measurements

Static contact angles were measured for each sample using the sessile drop technique described in chapter 3.1, with both distilled water, diiodomethane and hexadecane. Typically, the droplet volume was 15 μL, occasionally smaller or larger volumes were employed, depending on the liquids ability to dispatch from the dispensing nozzle. The droplets were deposited on the surfaces using a plastic syringe with a stainless-steel nozzle. A camera displayed the droplets shape on a screen, the brightness and magnification were adjusted manually to give an optimal image. For measuring contact angles, magnification lines where used to calibrate the measurements, and a baseline was placed along the base of the droplet. The software automatically extracted the drop profile and calculated the contact angles. The contact angles are recorded as the mean value of the left and right contact angle measured of each droplet.

Tilting was used to determine contact angle hysteresis. A droplet was again deposited on a surface and the droplet shape is recorded, while the whole instrument is tilted to a maximum of 90°. Recordings of the tilted droplets were used to measure the advancing and receding contact angles. Plots of the contact angle hysteresis are given in Appendix B and equation 1.6 was used for calculating the contact angle hysteresis.

4.7 Surface Energy Calculations

SCA software was used to calculate the apparent surface energy of each surface. The software used the OWRK method and the contact angle for water, diiodomethane and hexadecane on each surface. For some surfaces data from only two liquids were used in the calculations of the apparent surface energy, leaving a more This happened when either complete wetting by the third liquid was observed, or if the droplet rolled of the surface, leaving no measurable contact angle. The surface energy plots made in this thesis are found in Appendix C.

4.8 Scanning Electron Microscopy Imaging and Elemental Analysis

The surface structure of the samples was characterized by SEM imaging with both high and low magnification. Both InLens and secondary electron detector was used for imaging. Samples must be conducting in order to achieve images without scanning faults or other artifacts. Since glass is nonconducting, the samples with glass substrates were coated with an ultrathin layer of carbon from sputter coating, prior to SEM imaging. The substrates are mounted to a sample holder using a conductive adhesive. If the SEM images presents white areas, it may suggest that the contact between the coating and the substrate is not optimal[36]. Elemental analysis was performed on all slides.

5 Results

All samples presented in Chapter 4 are characterized by electron microscope images, elemental analysis and contact angle measurements. The results are presented in the following order; characterization of uncoated glass, steel and aluminum surfaces, characterization of the capstone/silica coatings on glass and steel slides, characterization of silicon oil soot on glass and steel slides and characterization of etched and coated aluminum.

5.1 Uncoated Glass, Steel and Aluminum Substrates

All the glass, steel and aluminum substrates were characterized by SEM imaging to investigate surface structure and roughness before being treated as described in Chapter 4. Elemental analysis was performed to identify and compare the composition of the surfaces before and after coating. The slides were cleaned before characterization. It should be noted that according to the elemental analysis, beryllium seems to be present in considerable amounts in all samples. This is probably an artefact due to contamination in the vacuum chamber of the scanning electron microscope.

Contact angle measurements were performed on the glass, steel and aluminum surfaces prior to, and after coating. Using water, diiodomethane and hexadecane as liquids with known surface tensions, the apparent surface energy of the surfaces was calculated.

Uncoated Glass Slide

Electron microscopy images of the cleaned and uncoated glass slide show a homogenous surface. No surface features were visible, therefore no image is shown.

Figure 5.1 shows an elemental analysis of the glass slide which indicates presence of silicon, oxygen and calcium. The peak at 1 keV could suggest the presence of sodium. These components may imply that the glass slide is composed of silicon dioxide, calcium oxide and sodium dioxide. From table 4.2 we see that these are the major compounds of the glass slide.

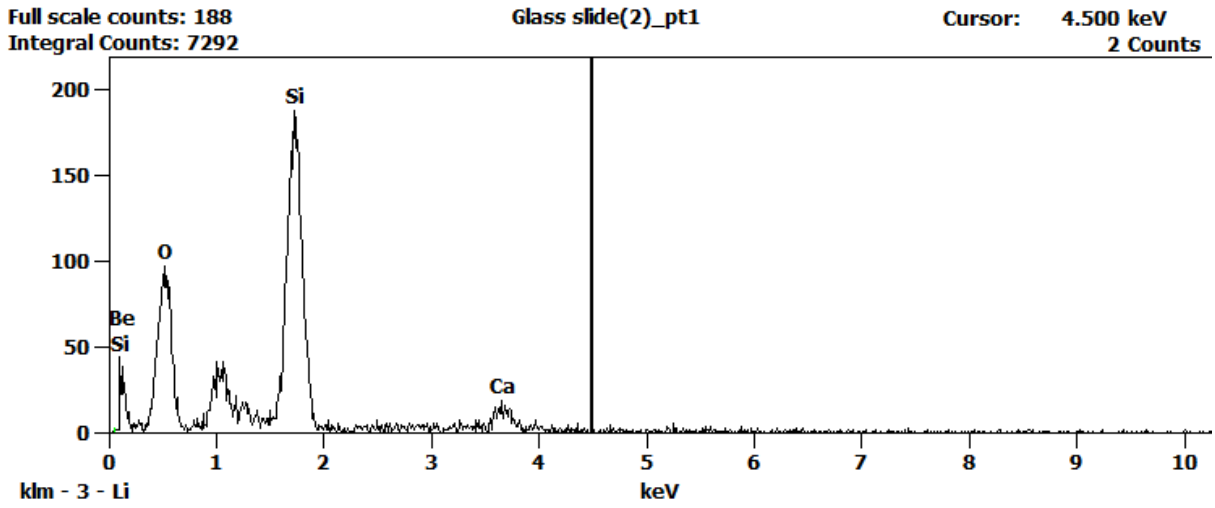

Figure 5.1. Element analysis of an uncoated glass slide. The presence of beryllium is probably an instrument error.

Contact angle measurements show that the cleaned glass slides are wetted by water and hexadecane, and partially wetted by diiodomethane. Figure 5.2 show the optical contact angle measurement with water, diiodomethane and hexadecane with contact angles of 9.1°, 39.0° and 1.9°, respectively.

The contact angle hysteresis for diiodomethane on the glass slide is 11.44°. Contact angle hysteresis was not measured for the water and hexadecane droplets because the liquids wets the surface.

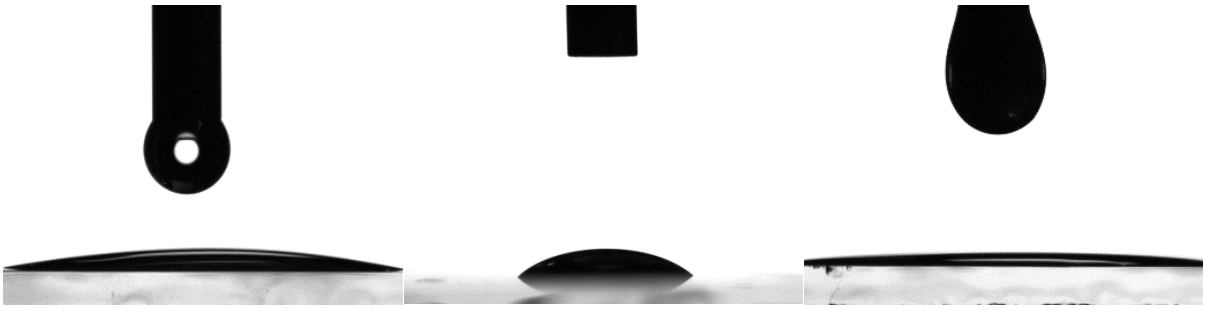

Figure 5.2 Optical contact angle measurements show water, diiodomethane and hexadecane droplets, respectively, on an uncoated glass slide.

Apparent surface energy calculations could not be performed on the glass slide because two of the liquids wet the surface, and the apparent surface energy is calculated with the use of at least to non-wetting liquids.

Uncoated Steel Slide

Figure 5.3 shows an electron microscope image of an uncoated steel slide. The surface has a microscopic roughness with ridges about 1-2 µm wide, in addition to more narrow ridges evenly distributed over the surface. The horizontal marks on the surface are probably from filing down the edges of the steel with a metal file.

The image in Figure 5.3 was taken with a secondary electron detector, 7000 times magnification and an accelerating voltage of 5.0 kV.

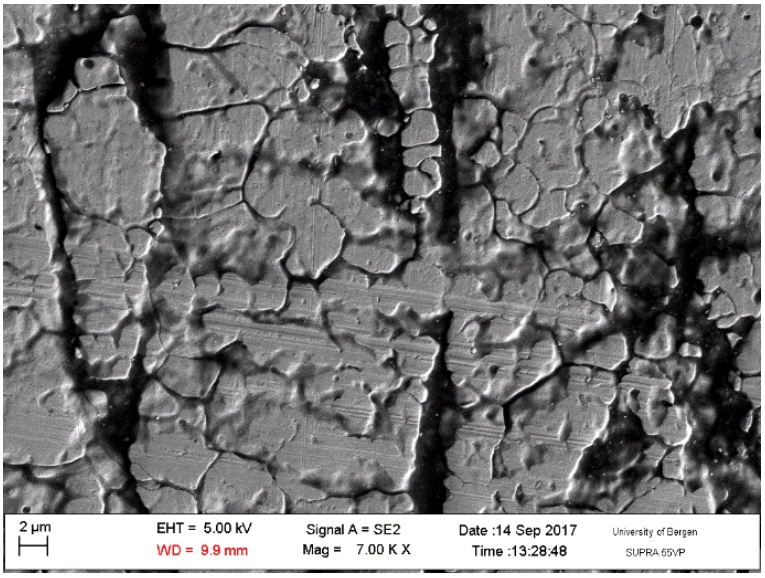

Figure 5.3. Scanning electron microscopy image of a steel slide.

Figure 5.4 shows an elemental analysis of the uncoated steel slide which indicates presence of iron and chromium. The analysis could also indicate the presence of nickel and molybdenum on the surface. These compounds are all present in the steel slide, as seen from table 4.2.

The contact angle measurements show that the steel slide is partially wetted by water and diiodomethane, and completely wetted by hexadecane. Figure 5.5 shows the optical contact angle measurement of water, diiodomethane and hexadecane with contact angles of 88.4°, 60.3° and 1.6°, respectively.

The contact angle hysteresis for water and diiodomethane on the steel slide is 20.62° and 20.58°, respectively. These values are relatively large and proves that the surface does not have self-cleaning properties. Contact angle hysteresis for hexadecane is not measured because the liquid wets the surface.

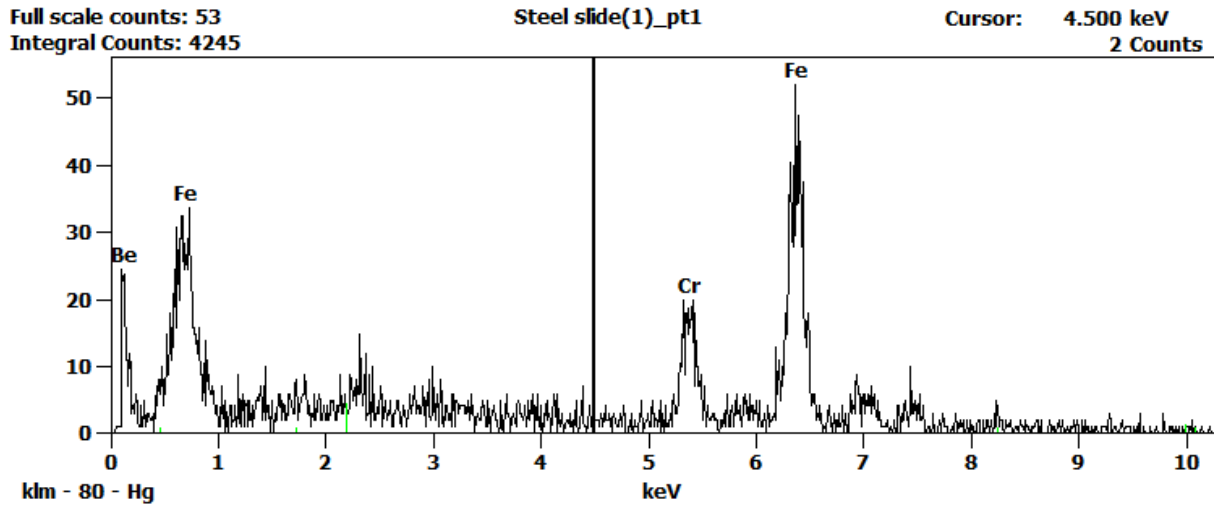

Figure 5.4 Elemental analysis of an uncoated steel slide. The presence of beryllium is probably an instrument error.

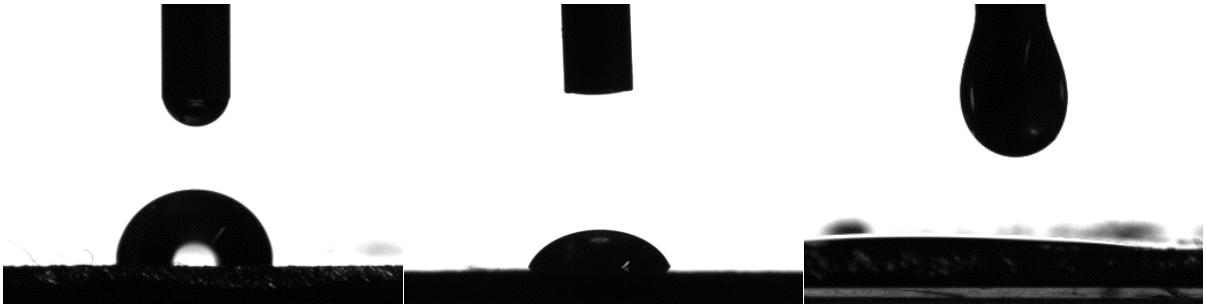

Figure 5.5. Optical contact angle measurements show water, diiodomethane and hexadecane droplets, respectively, on an uncoated steel slide.

The apparent surface energy of the steel slide was found to be 28.41 mN/m.

Uncoated Aluminum Slide

Figure 5.6 shows an electron microscope image of the uncoated aluminum slide. The image shows vertical marks on the surface of the slide that are 5-10 micrometers wide, probably from the cutting of the aluminum.

The image in Figure 5.6 is taken with a secondary electron detector, 2000 times magnification and an accelerating voltage of 5.00 kV.

Figure 5.7 shows an elemental analysis of the uncoated aluminum slide which indicates the presence of aluminum and no other elements. This implies that the slide is composed of aluminum. Oxygen was expected to be found at the surface of the aluminum slide, caused by a layer of aluminum oxide. This may be thinner then what the elemental analysis can detect.

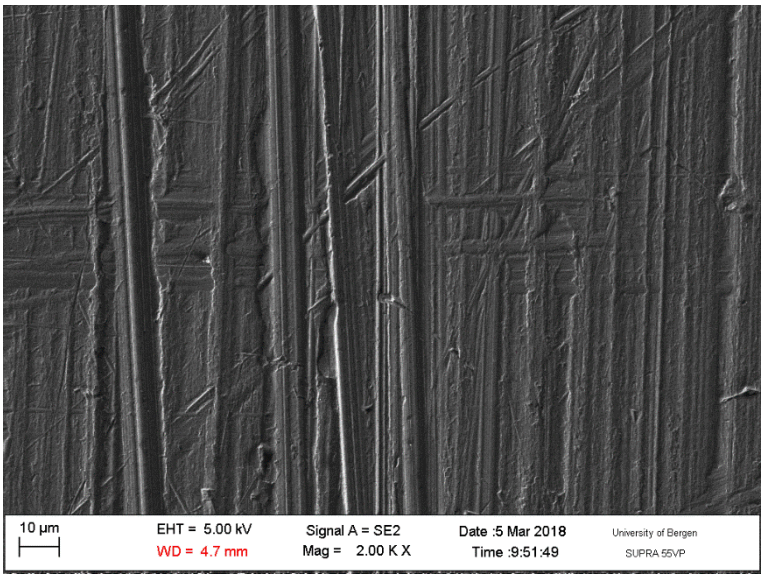

Figure 5.6. Scanning electron microscopy image of an uncoated aluminum slide.

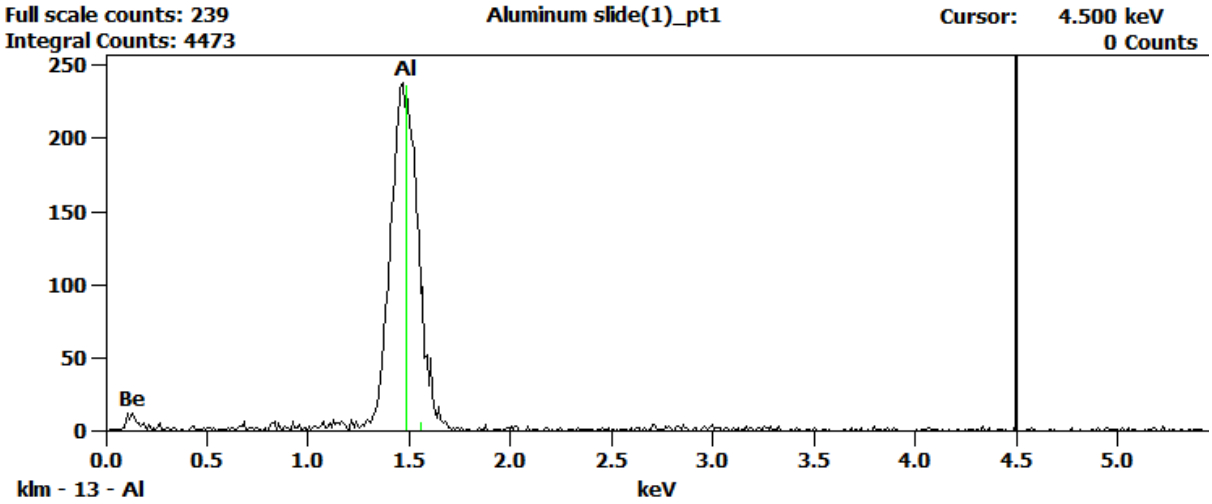

Figure 5.7. Elemental analysis of an uncoated aluminum slide. The presence of beryllium is probably an instrument error.

The contact angle measurements show that the uncoated aluminum slide is partially wetted by water and diiodomethane, and completely wetted by hexadecane. Figure 5.8 shows the optical contact angle measurement of water, diiodomethane and hexadecane with contact angles of 86.9°, 45° and 7.4°, respectively.

The contact angle hysteresis for water and diiodomethane on the uncoated aluminum slide is 32.04° and 39.16°, respectively. These values are relatively large and proves that the surface does not have self-cleaning properties. Contact angle hysteresis for hexadecane is not measured because the liquid wets the surface.

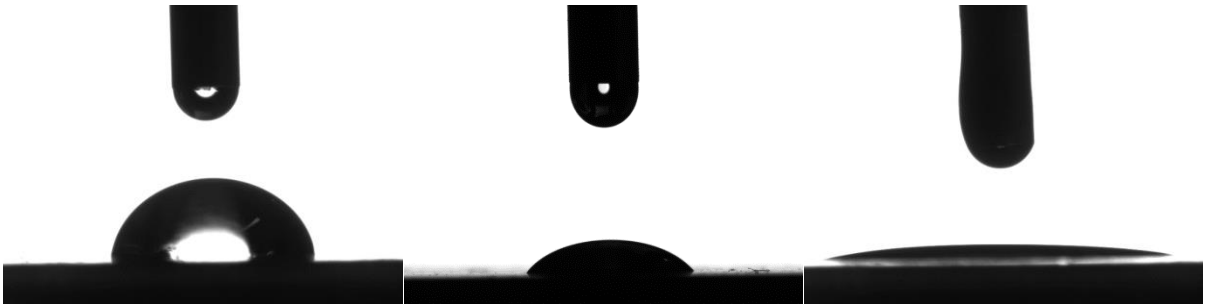

Figure 5.8. Optical contact angle measurements show water, diiodomethane and hexadecane droplets, respectively, on an uncoated aluminum slide.

The apparent surface energy of the aluminum slide was found to be 38.76 mN/m.

5.2 Colloidal Suspensions of Capstone and Silica Particles

The following coated glass and steel slides are characterized by SEM images to investigate surface structure and roughness after coating. Elemental analysis was performed to identify the composition of the coated slides, and the analysis are performed on the areas as seen in the respective SEM images (unless stated otherwise).

Contact angle measurements with water, diiodomethane and hexadecane were performed on the coated glass and steel surfaces. Contact angle hysteresis was measured for the liquids that did not completely wet the surfaces. Apparent surface energy is calculated for each coated slide. Droplets that display a contact angle of more than 90° indicates that the coating presents a low surface energy, a rough structure, or a combination of both.

5.2.1 Coating 110-OX50(PDES)

This suspension was quite unstable and has a lot of precipitate when not stirred, and a light-yellow color. It was not homogenous during dip-coating which caused accumulations of particles on some parts and no visible coating on other parts of the slides. The characterizations were done on the areas on the slides with the highest accumulation of particles.

Coated Glass Slide

Figure 5.9 shows an electron microscopy image of the coated glass slide. Several white areas in the image suggests that there are weak interaction between the slide and the coating. This made it difficult to get images with high magnification and resolution. The image shows that

the accumulated particles have a rough structure, but they are not evenly distributed across the slide.

The image in Figure 5.9 was taken with a secondary electron detector, 2000 times magnification and an accelerating voltage of 15.0 kV.

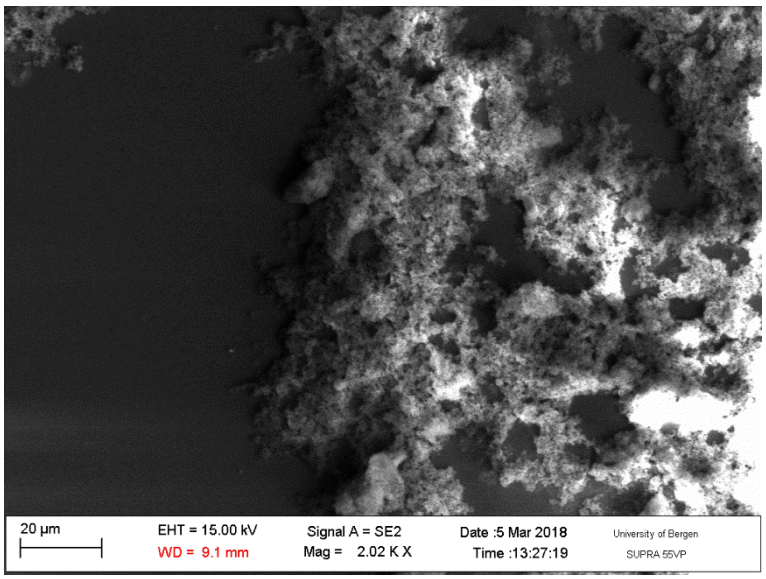

Figure 5.9. Scanning electron microscopy image of a glass slide coated with 110-OX50(PDES).

Figure 5.10 shows an elemental analysis of a glass slide coated with 110-OX50(PDES) which indicates the presence of silicon, fluorine and oxygen. These components may indicate the presence of silica. Sodium may also be present which can originate from the sodium oxide in the glass slide.

Contact angle measurements show that the coated glass slide is not wetted by water but partially wetted by diiodomethane and hexadecane. Figure 5.11 show the optical contact angle measurements for water, diiodomethane and hexadecane droplets with contact angles of 105.3°, 87.9° and 60.6°, respectively.

The contact angle hysteresis for water, diiodomethane and hexadecane on the coated glass slide is 26.59°, 21.18° and 37.66°, respectively. These values are relatively large and proves that the surface does not have self-cleaning properties.

The apparent surface energy of the coated glass slide is estimated to be 10.65 mN/m.

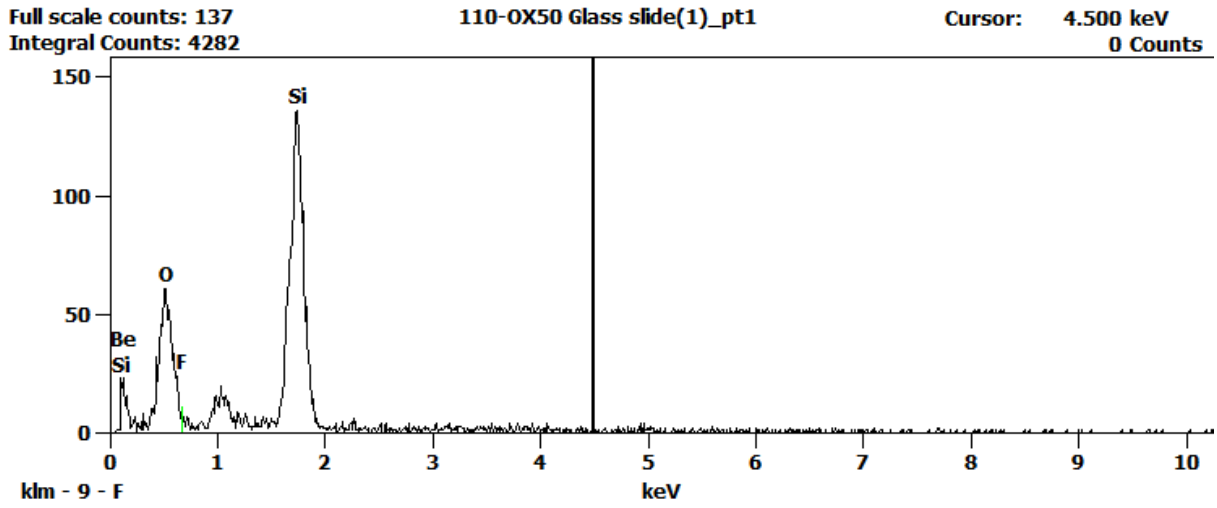

Figure 5.10. Elemental analysis of a glass slide coated with 110-OX50(PDES). The presence of beryllium is probably an instrument error.

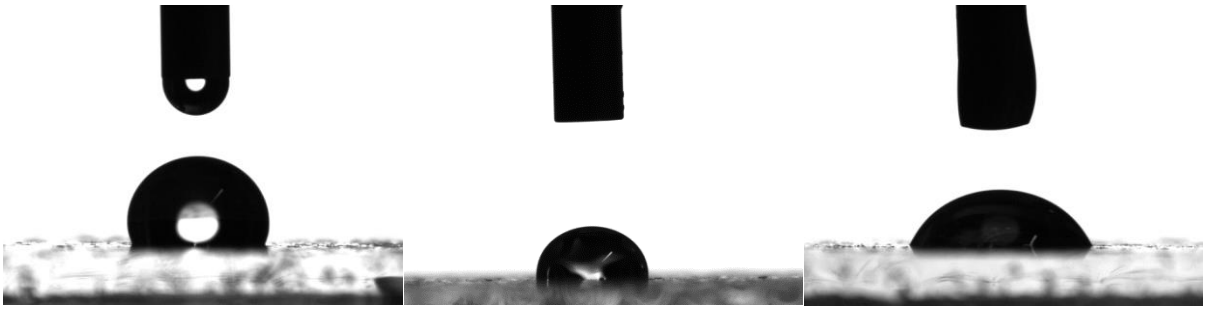

Figure 5.11. Optical contact angle measurements show water, diiodomethane and hexadecane droplets, respectively, deposited on a glass slide coated with 110-OX50(PDES).

Coated Steel Slide

Figure 5.12 show an electron microscopy image of the coated steel slide. The image shows that the coating has a rough structure in the places with the accumulated particles, but the particles are not evenly distributed across the slide.

The image in Figure 5.12 was taken with a secondary electron detector, 2000 times magnification and an accelerating voltage of 5.0 kV.

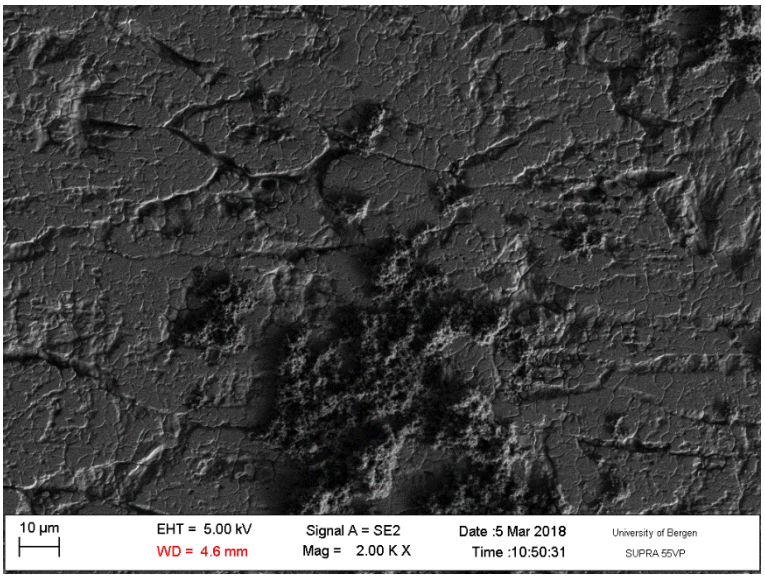

Figure 5.12. Scanning electron microscopy image of a steel slide coated with 110-OX50(PDES).

Figure 5.13 shows an elemental analysis of a steel slide coated with 110-OX50(PDES) which indicates the presence of fluorine, iron, silicon, oxygen and chromium. These components may indicate the presence of silica, polydimethylsiloxane and the fluorochemical polymer. Figure 5.13 may indicate unidentified elements present in the sample, or noise.

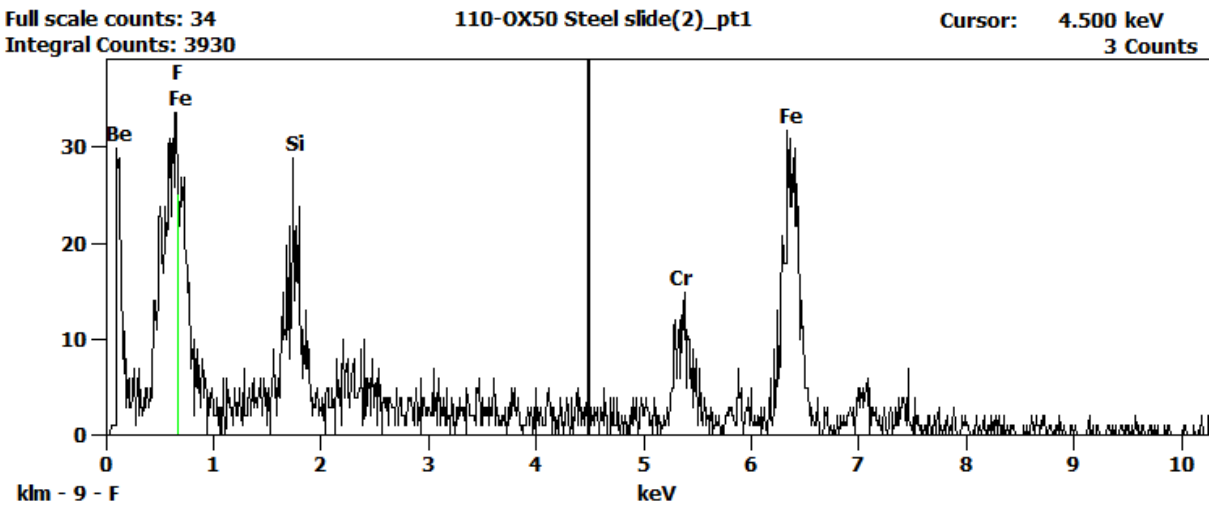

Figure 5.13. Elemental analysis of a steel slide coated with 110-OX50(PDES). The presence of beryllium is probably an instrument error.

Contact angle measurements show that the coated steel slide is not wetted by water or diiodomethane and partially wetted by hexadecane. Figure 5.14 shows the optical contact angle measurements for water, diiodomethane and hexadecane droplets with contact angles of 114.1°, 105.7° and 65.0°, respectively.

The contact angle hysteresis for water, diiodomethane and hexadecane on the coated steel slide is 37.54°, 37.29° and 24.99°, respectively. These values are relatively large and proves that the surface does not have self-cleaning properties.

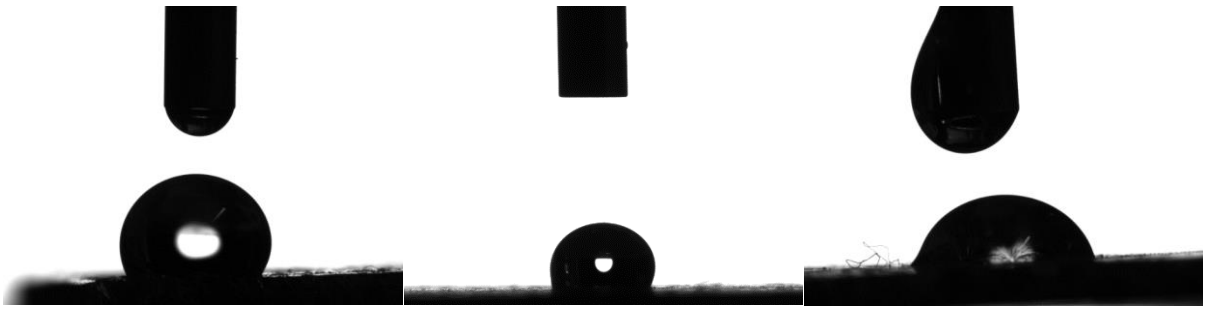

Figure 5.14. Optical contact angle measurements show water, diiodomethane and hexadecane droplets, respectively, deposited on a steel slide coated with 110-OX50(PDES).

The apparent surface energy of the coated steel slide is estimated to be 9.64 mN/m.

5.2.2 Coating 110-R972(PDES)

This suspension was not completely homogenous, but seemed to be more homogenous than 110-OX50(PDES). The solution has a light-yellow color as well. The dip-coated surfaces have visible particles spread out on the slide but not a homogenous coating.

Coated Glass Slide

Electron microscopy images of a glass slide coated with 110-R972(PDES) gave poor results because of weak interactions between the coating and the glass, and therefore no image is shown.

Figure 5.15 shows an elemental analysis of a glass slide coated with 110-R972(PDES) which indicates the presence of silicon, oxygen, carbon and fluorine. These components may indicate the presence of silica, polydimethylsiloxane and the fluorochemical polymer. Figure 5.15 may indicate the presence of more unidentified elements between 0 – 1 keV.

Contact angle measurements show that the coated glass slide is not wetted by water, and partially wetted by diiodomethane and hexadecane. Figure 5.16 show the optical contact angle measurements for water, diiodomethane and hexadecane droplets with contact angles of 96.6°, 78.5° and 59.7°, respectively.

The contact angle hysteresis for water, diiodomethane and hexadecane on the coated glass slide is 8.52°, 16.01° and 17.01°, respectively.

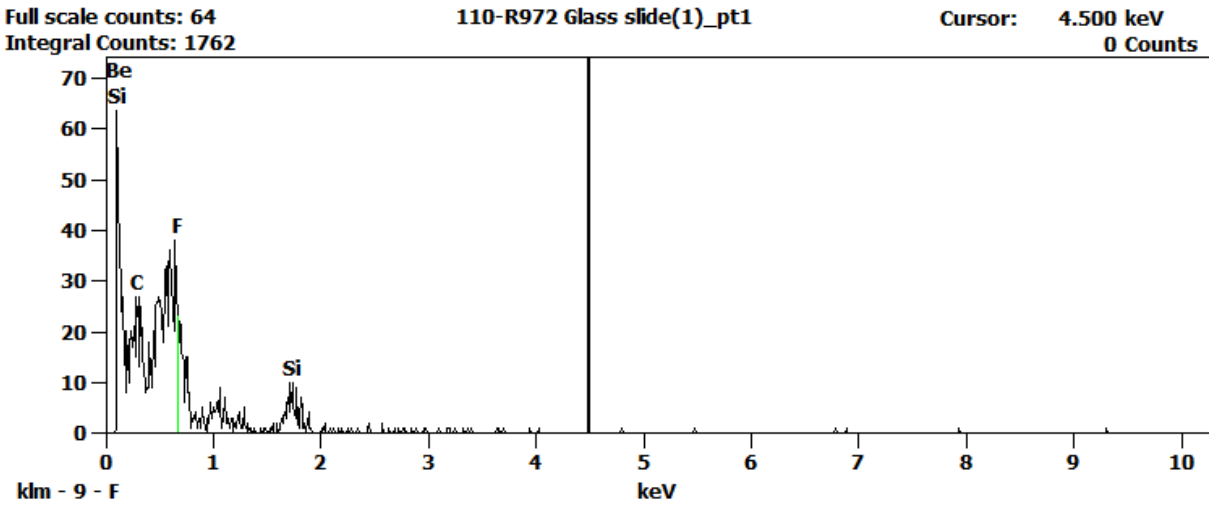

Figure 5.15. Elemental analysis of a glass slide coated with 110-R972(PDES). The presence of beryllium is probably an instrument error.

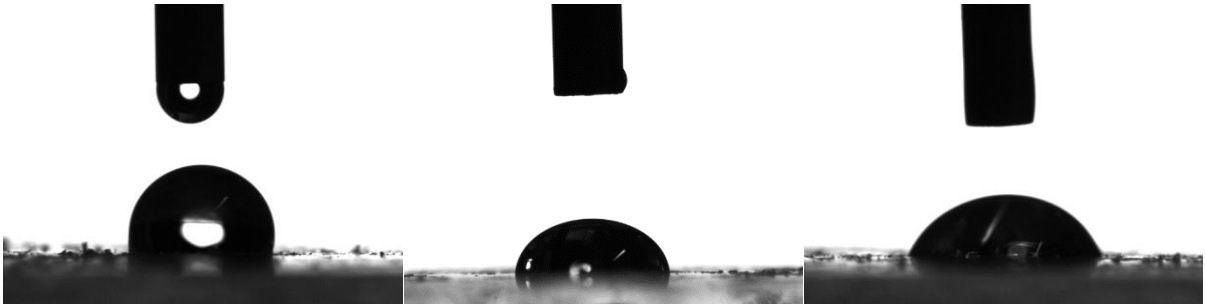

Figure 5.16. Optical contact angle measurements show water, diiodomethane and hexadecane droplets, respectively, deposited on a glass slide coated with 110-R972(PDES).

The apparent surface energy of the coated glass slide is estimated to be 21.65 mN/m.

Coated Steel Slide

Figure 5.17 show an electron microscopy image of a coated steel slide. The particles in the coating have accumulated on the surface, and the coating has not spread out evenly on the slide. The areas of accumulated particles appear to have a rougher surface structure.

The image in Figure 5.17 was taken with a secondary electron detector, 2000 times magnification and an accelerating voltage of 5.0 kV.

Figure 5.18 shows an elemental analysis of a steel slide coated with 110-R972(PDES) which indicates the presence of silica, oxygen, carbon, fluorine, iron and chromium. These components may indicate the presence of silica, polydimethylsiloxane and the fluorochemical polymer. Figure 5.18 may imply the presence of unidentified elements from 0 – 2 keV.

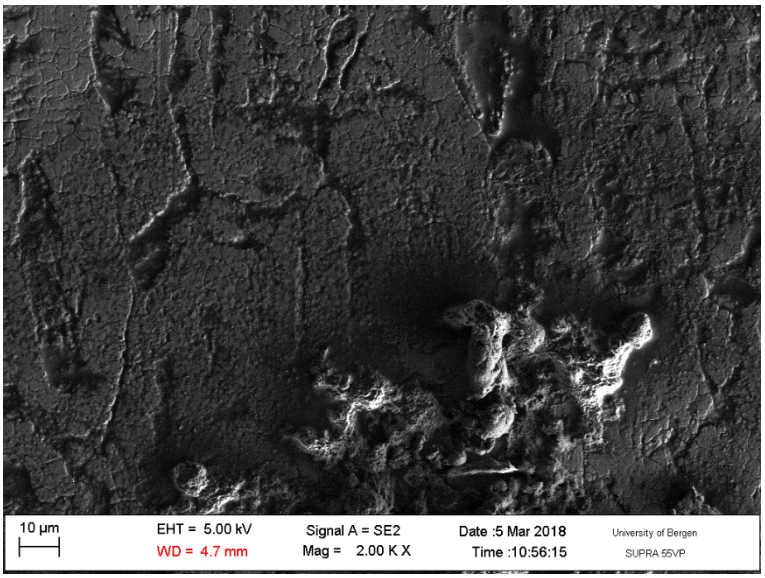

Figure 5.17. Scanning electron microscopy image of a steel slide coated with 110-R972(PDES).

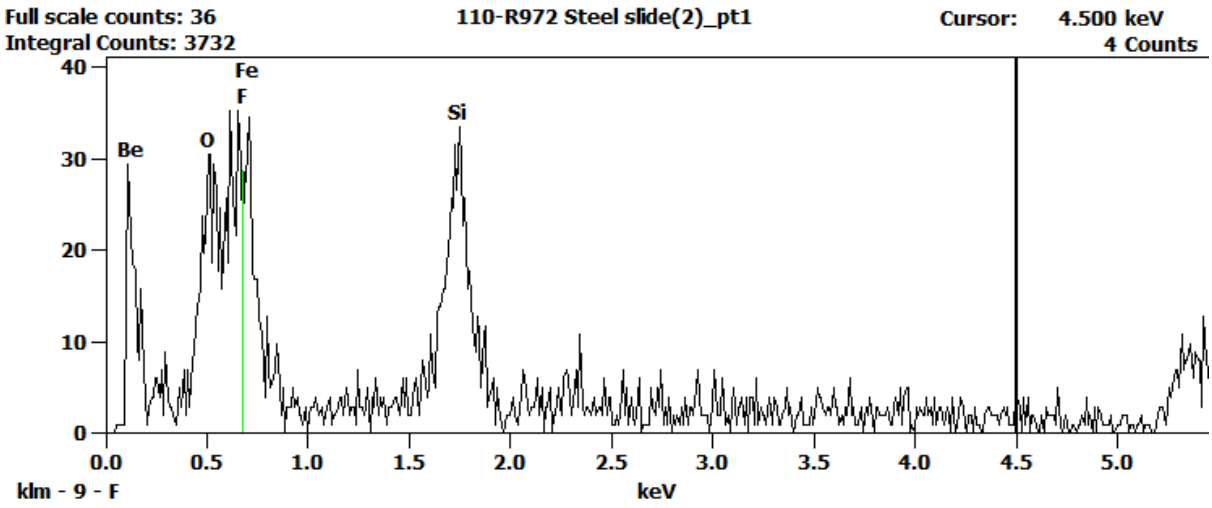

Figure 5.18. Elemental analysis of a steel slide coated with 110-R972(PDES). The presence of beryllium is probably an instrument error.

Contact angle measurements show that the coated steel slide is not wetted by water, and partially wetted by diiodomethane and hexadecane. Figure 5.19 show the optical contact angle measurements for water, diiodomethane and hexadecane droplets with contact angles of 109.2°, 84.7° and 41.6°, respectively.

The contact angle hysteresis for water, diiodomethane and hexadecane on the coated steel slide is 13.67°, 18.22° and 14.85°, respectively.

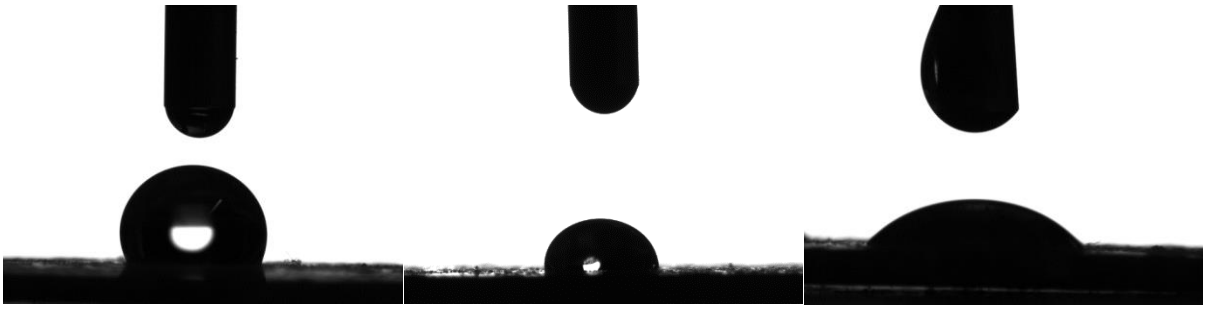

Figure 5.19. Optical contact angle measurements show water, diiodomethane and hexadecane droplets, respectively, deposited on a steel slide coated with 110-R972(PDES).

The apparent surface energy of the coated steel slide is estimated to be 14.05 mN/m.

5.2.3 Coating 100-OX50(PDES)

This suspension seems to be homogeneous and has a light grey color, also when not stirred. The dip-coated slides seem to have a thin and even distribution of particles on the surface from visual observations.

Coated Glass Slide

Figure 5.20 shows an electron microscopy image of a coated glass slide. It is not possible to evaluate the surface. The coating on the slide was difficult to detect, but by using the InLens detector, 18 000 times magnification and an accelerating voltage of 15.0 kV, the particles on the glass slide were detectable.

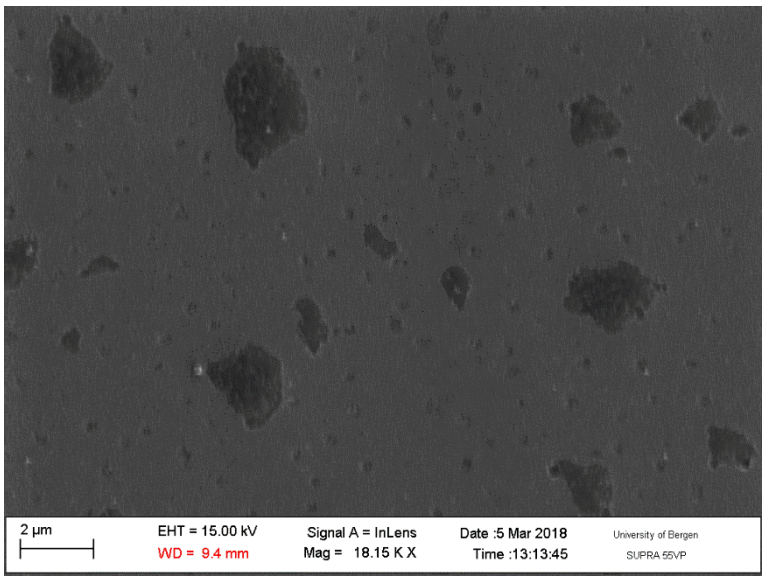

Figure 5.20. Scanning electron microscopy image of a glass slide coated with 100-OX50(PDES).

Figure 5.21 shows an elemental analysis of a glass slide coated with 100-OX50(PDES). The elemental analysis was taken at lower magnification and on a bigger area than seen in Figure 5.20. The elemental analysis indicates the presence of silicon, oxygen, sodium and calcium. These components may indicate the presence of silica, calcium dioxide, sodium dioxide and polydimethylsiloxane, several of which are components in the glass slide. Figure 5.21 is very similar to the elemental analysis of an uncoated glass slide (see Figure 5.1) which may suggest a layer of coating that is thinner then what the elemental analysis can detect.

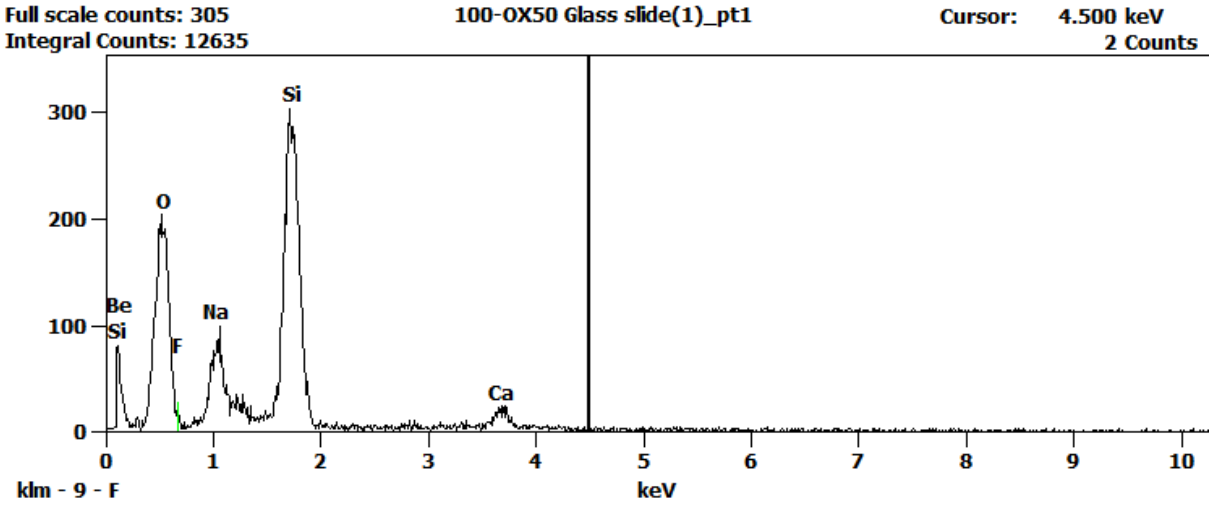

Figure 5.21. Elemental analysis of a glass slide coated with 100-OX50(PDES). The presence of beryllium is caused by an error in the instrument.

Contact angle measurements show that the coated glass slide is not wetted by water, diiodomethane or hexadecane. Figure 5.22 show the optical contact angle measurements for water, diiodomethane and hexadecane droplets with contact angles of 111.3°, 105.2° and 89.3°, respectively. These contact angles are much larger than what was measured on the uncoated glass slide, hence this glass slide has a significant amount of coating.

The contact angle hysteresis for water, diiodomethane and hexadecane on the coated glass slide is 35.13°, 37.78° and 22.71°, respectively.

The apparent surface energy of the coated glass slide is estimated to be 8.43 mN/m.

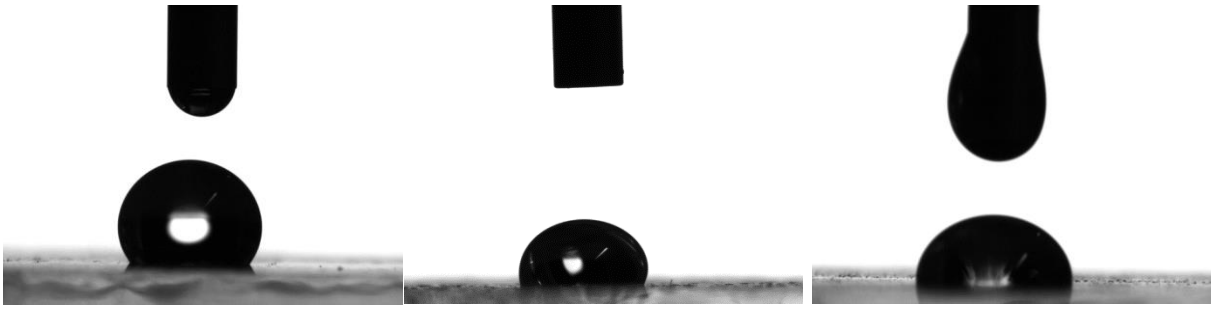

Figure 5.22. Optical contact angle measurements show water, diiodomethane and hexadecane droplets, respectively, deposited on a glass slide coated with 100-OX50(PDES).

Coated Steel Slide

Figure 5.23 shows an electron microscopy image of a steel slide coated with 100-OX50(PDES). The particles in the coating have accumulated on the slide. The coating is not evenly distributed, but the areas with particles appears to have a rougher surface structure.

The image in Figure 5.23 is taken with a secondary electron detector, 2000 times magnification and an accelerating voltage of 5.0 kV.

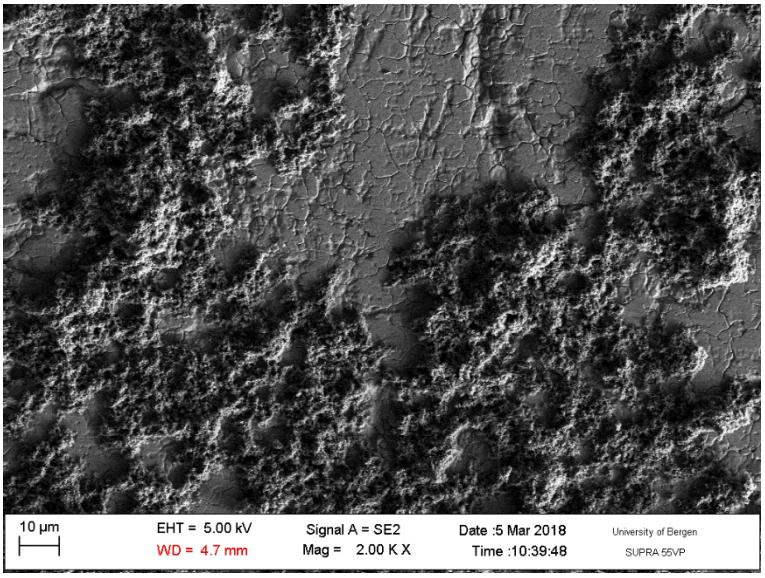

Figure 5.23. Scanning electron microscopy image of a steel slide coated with 100-OX50(PDES).

Figure 5.24 shows an elemental analysis of a steel slide coated with 100-OX50(PDES) which indicates the presence of silicon, oxygen, carbon, fluorine, iron and chromium. These components may indicate the presence of silica, polydimethylsiloxane and the fluorochemical polymer. Figure 5.24 suggests that there may also be several unidentified elements present.

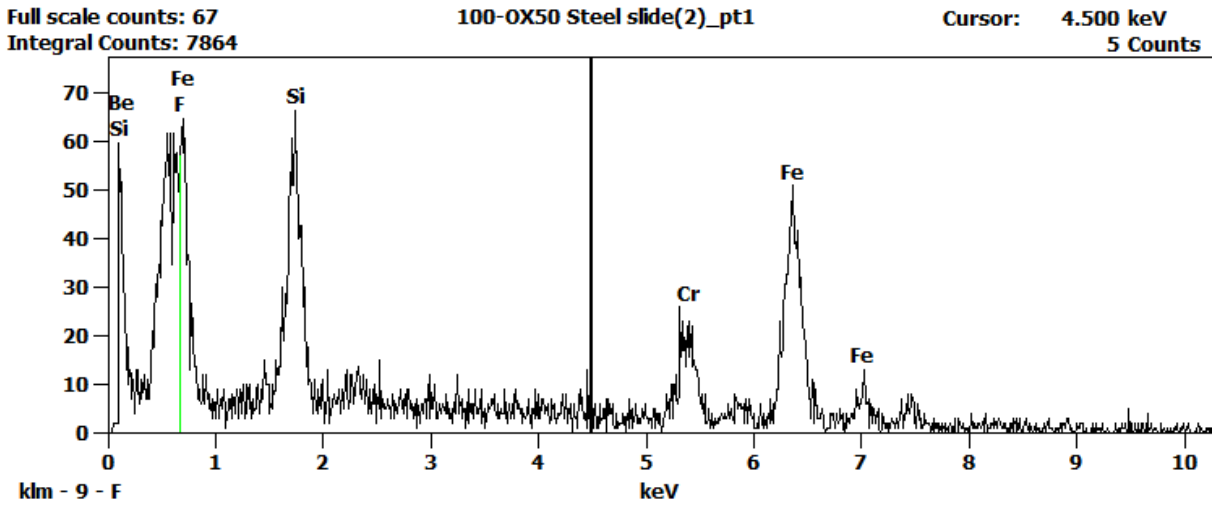

Figure 5.24. Elemental analysis of a steel slide coated with 100-OX50(PDES). The presence of beryllium is probably an instrument error.

Contact angle measurements show that the coated steel slide is not wetted by water or diiodomethane, and partially wetted by hexadecane. Figure 5.25 show the optical contact angle measurements for water, diiodomethane and hexadecane droplets with contact angles of 106.7°, 95.9° and 79.3°, respectively.

The contact angle hysteresis for water and hexadecane on the coated steel slide is 22.01° and 25.12°, respectively. Contact angle hysteresis for diiodomethane was not possible to measure because of uneven movements of the droplets when the surface was tilted.

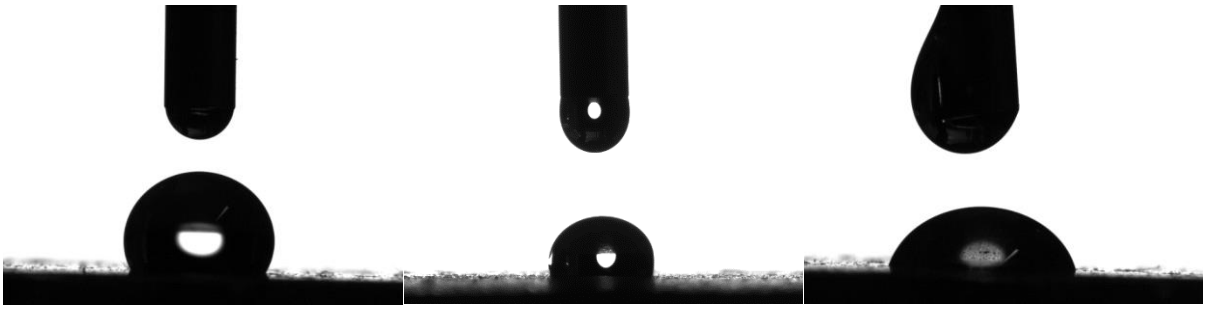

Figure 5.25. Optical contact angle measurements show water, diiodomethane and hexadecane droplets, respectively, deposited on a steel slide coated with 100-OX50(PDES).

The apparent surface energy of the coated steel slide is estimated to be 5.21 mN/m.

5.2.4 Coating 100-R972(PDES)

This suspension is relatively stable but will precipitate shortly after stirring. The color is light grey, similar to 110-OX50(PDES). The dip-coating was done on what seems to be a homogenous suspension, but the coated slides have areas of accumulation.

Coated Glass Slide

Electron microscopy examination of a glass slide coated with 100-R972(PDES) did not return any information about the coating. Except for contaminations on the surface, there was nothing to see on the images other than a smooth surface, therefore the image is not shown.

Figure 5.26 shows an elemental analysis of a glass slide coated with 100-R972(PDES) which indicates the presence of silicon, oxygen, sodium and calcium. These components may indicate the presence of silica, sodium oxide, calcium oxide and polydimethylsiloxane. This elemental analysis is similar to the elemental analysis for the uncoated glass slide (see Figure 5.1), which suggests that the coated layer is too thin to be detected.

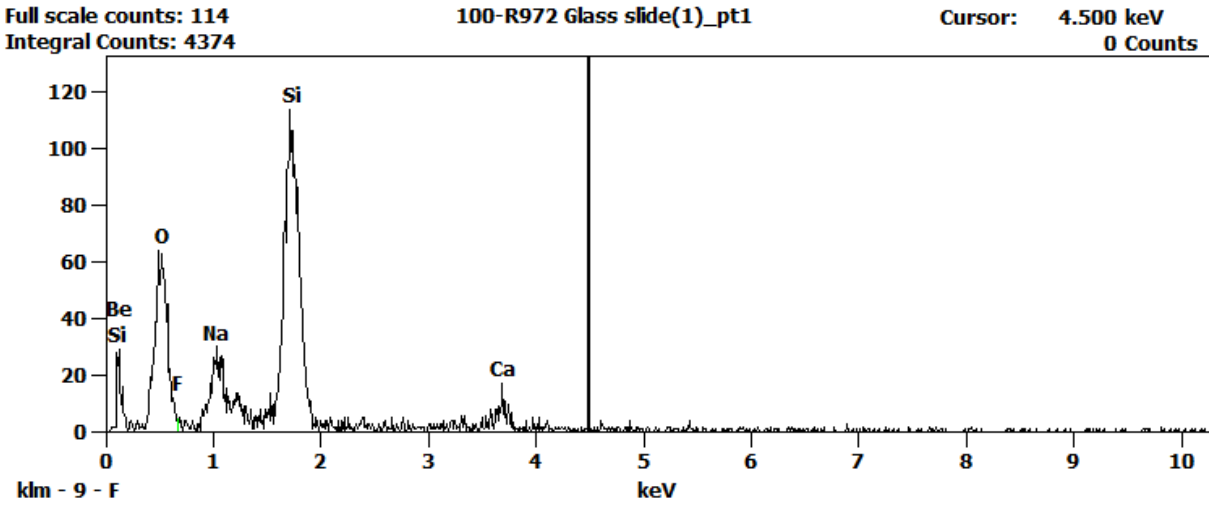

Figure 5.26. Elemental analysis of a glass slide coated with 100-R972(PDES). The presence of beryllium is probably an instrument error.

Contact angle measurements show that the coated glass slide is not wetted by water and partially wetted by diiodomethane and hexadecane. Figure 5.27 shows the optical contact angle measurements for water, diiodomethane and hexadecane droplets with contact angles of 108.8°, 84.9° and 70.0°, respectively. These values are much higher than for the uncoated glass slide, hence this glass slide has a significant amount of coating.

The contact angle hysteresis for water, diiodomethane and hexadecane on the coated glass slide is 23.89°, 46.88° and 31.46°, respectively.

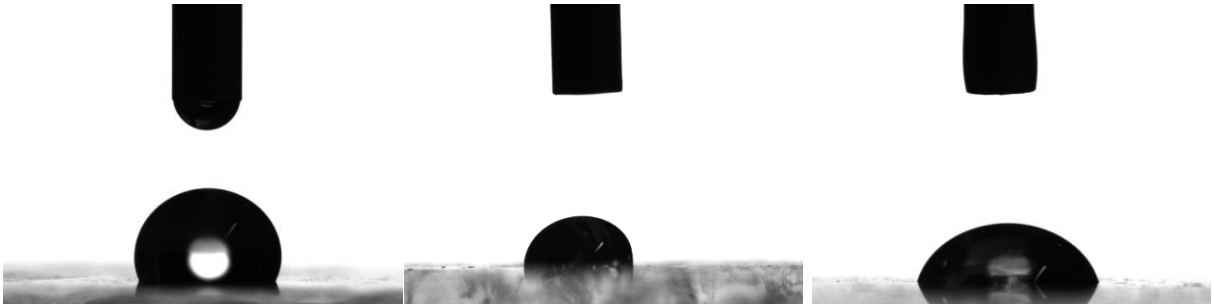

Figure 5.27. Optical contact angle measurements show water, diiodomethane and hexadecane droplets, respectively, deposited on a glass slide coated with 100-R972(PDES).

The apparent surface energy of the coated glass slide is estimated to be 17.03 mN/m.

Coated Steel Slide

Figure 5.28 shows an electron microscopy image of the coated steel slide, with several white areas that suggest that the coating has a weak interaction with the slide underneath. The particles in the coating have accumulated on the surface, not forming an even distribution of the coating. The surface structure is rougher when there is a higher density of particles.

The image in Figure 5.28 was taken with a secondary electron detector, 2000 times magnification and an accelerating voltage of 5.0 kV.

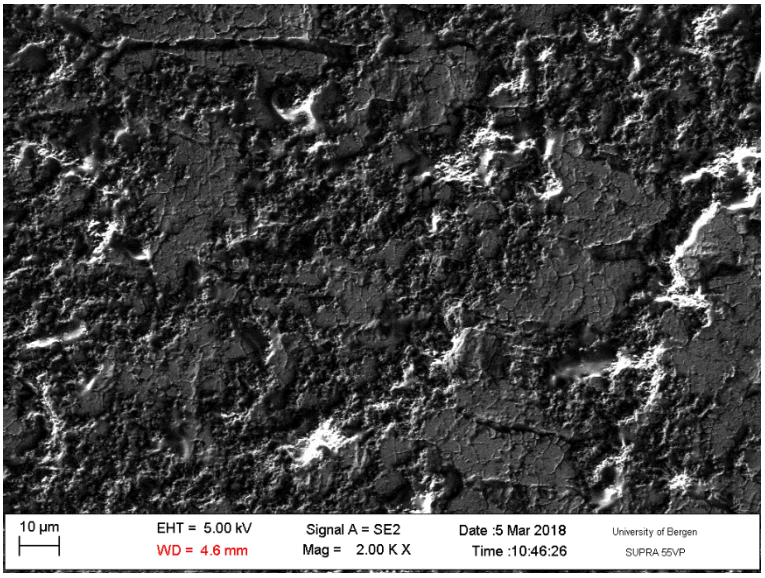

Figure 5.28. Scanning electron microscopy image of a steel slide coated with 100-R972(PDES).

Figure 5.29 shows an elemental analysis of a steel slide coated with 100-R972(PDES) which indicates the presence of silicon, oxygen, carbon, fluorine, iron and chromium. These components may indicate the presence of silica, polydimethylsiloxane and the fluorochemical polymer.

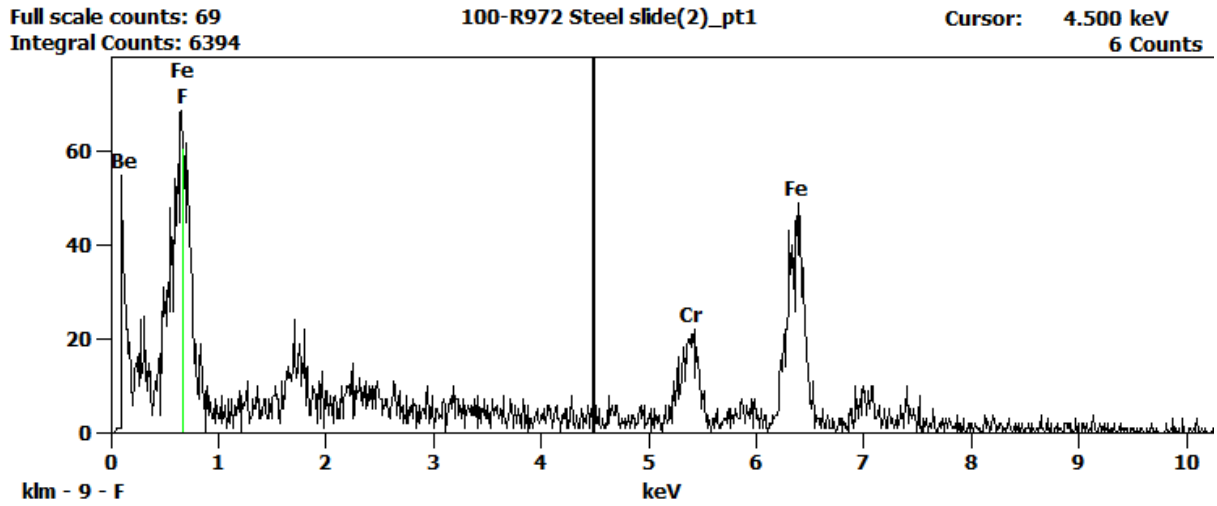

Figure 5.29. Elemental analysis of a steel slide coated with 100-R972(PDES). The presence of beryllium is probably an instrument error.

Contact angle measurements show that the coated steel slide is not wetted by water and partially wetted by diiodomethane and hexadecane. Figure 5.30 shows the optical contact angle measurements for water, diiodomethane and hexadecane droplets with contact angles of 108.1°, 85.6° and 67.6°, respectively.

The contact angle hysteresis for water, diiodomethane and hexadecane on the coated steel slide is 18.10°, 33.59° and 26.50°, respectively.

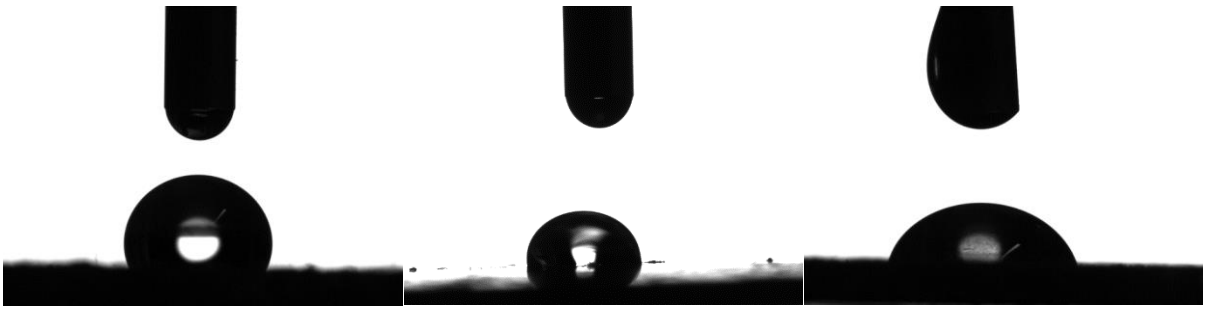

Figure 5.30. Optical contact angle measurements show water, diiodomethane and hexadecane droplets, respectively, deposited on a steel slide coated with 100-R972(PDES).

The apparent surface energy of the coated steel slide is estimated to be 14.62 mN/m.

5.2.5 Coating 110-OX50(POCS)

This suspension has a white color and is homogenous during stirring and dip-coating, but over time it will start to accumulate and make a foam layer on top of the solution. There was a thin foam layer on top of the solution when the slides where withdrawn, making the coating uneven and thick.

Coated Glass Slide

Figure 5.31 shows an electron microscopy image of the coated glass slide and the white areas suggest that the coating has weak interaction with the slide underneath. This made it difficult to get images with high magnification and resolution. The coating is distributed evenly across the slide in a thin layer, and some areas have higher accumulation of particles.

The image in Figure 5.31 was taken with a secondary electron detector, 141 times magnification and an accelerating voltage of 15.0 kV.

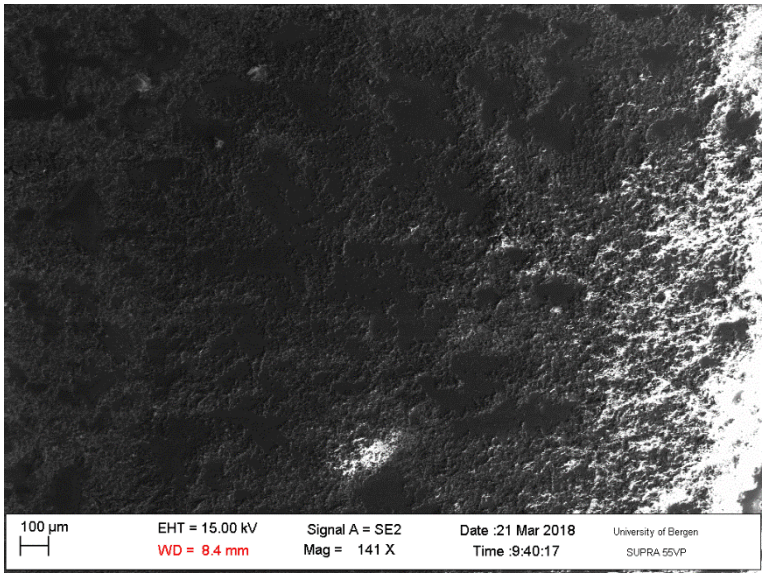

Figure 5.31. Scanning electron microscopy image of a glass slide coated with 110-OX50(POCS).

Figure 5.32 shows an elemental analysis of a glass slide coated with 110-OX50(POCS) which indicates the presence of silicon, chlorine, carbon, oxygen, fluorine and sodium. These components may indicate the presence of silica, perfluorooctyl-trichlorosilane and fluorochemical polymer, in addition to sodium oxide and calcium oxide, which are components of the glass slide.

Contact angle measurements show that the coated glass slide is not wetted by water, diiodomethane or hexadecane. Figure 5.33 show the optical contact angle measurements for

water, diiodomethane and hexadecane droplets with contact angles of 158.7°, 121.3° and 116.9°.

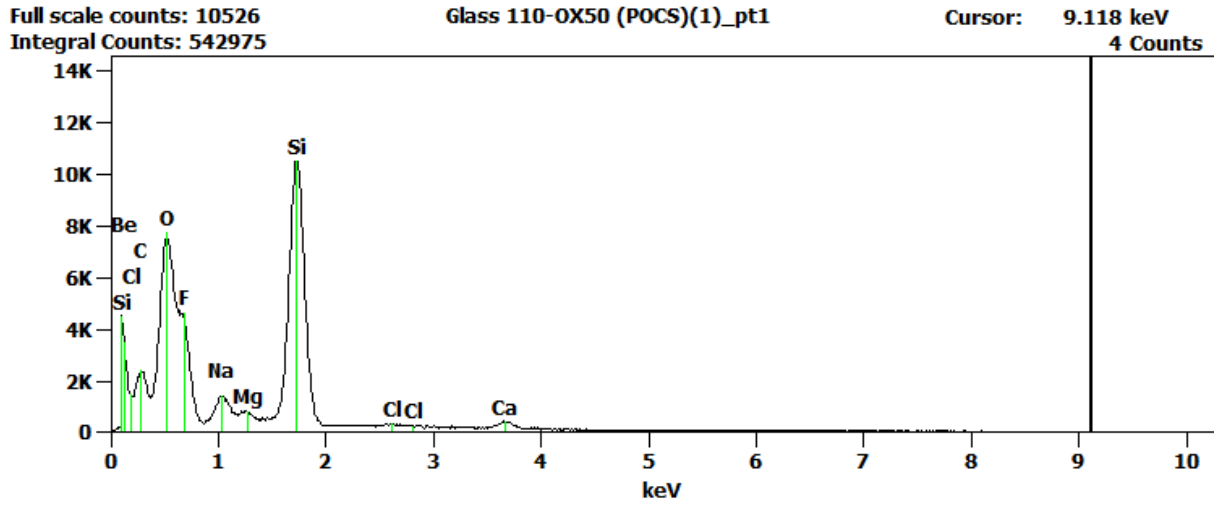

Figure 5.32. Elemental analysis of a glass slide coated with 110-OX50(POCS). The presence of beryllium is probably an instrument error.

The contact angle hysteresis for water, diiodomethane and hexadecane on the coated glass slide is 9.83°, 36.85° and 42.18°, respectively.

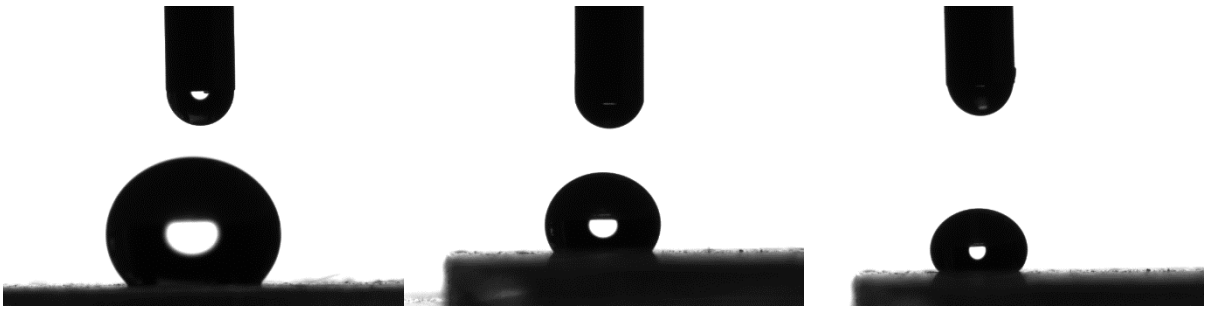

Figure 5.33. Optical contact angle measurements show water, diiodomethane and hexadecane droplets, respectively, deposited on a glass slide coated with 110-OX50(POCS).

The apparent surface energy of the coated glass slide is estimated to be 3.50 mN/m.

Coated Steel Slide

Figure 5.34 shows an electron microscopy image of the coated steel slide. The image shows the coating accumulating in relatively thick layers on the steel slide. The white areas suggest that the coating has weak interactions with the slide underneath.

The image in Figure 5.34 was taken with a secondary electron detector, 2000 times magnification and an accelerating voltage of 15.0 kV.

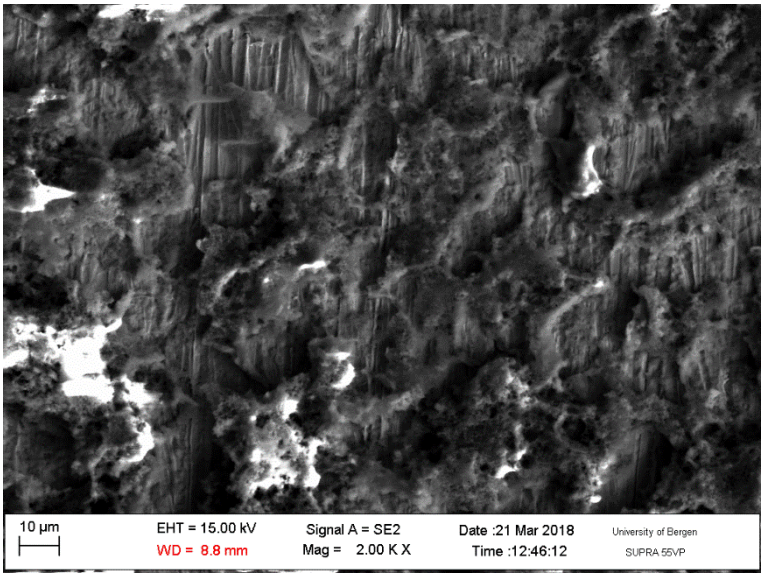

Figure 5.34. Scanning lectron microscopy image of a steel slide coated with 110-OX50(POCS).

Figure 5.35 shows an elemental analysis of a steel slide coated with 110-OX50(POCS) which indicates the presence of silicon, chlorine, oxygen, chromium, iron and fluorine. These components may indicate the presence of silica, perfluorooctyl-trichlorosilane and fluorochemical polymer.

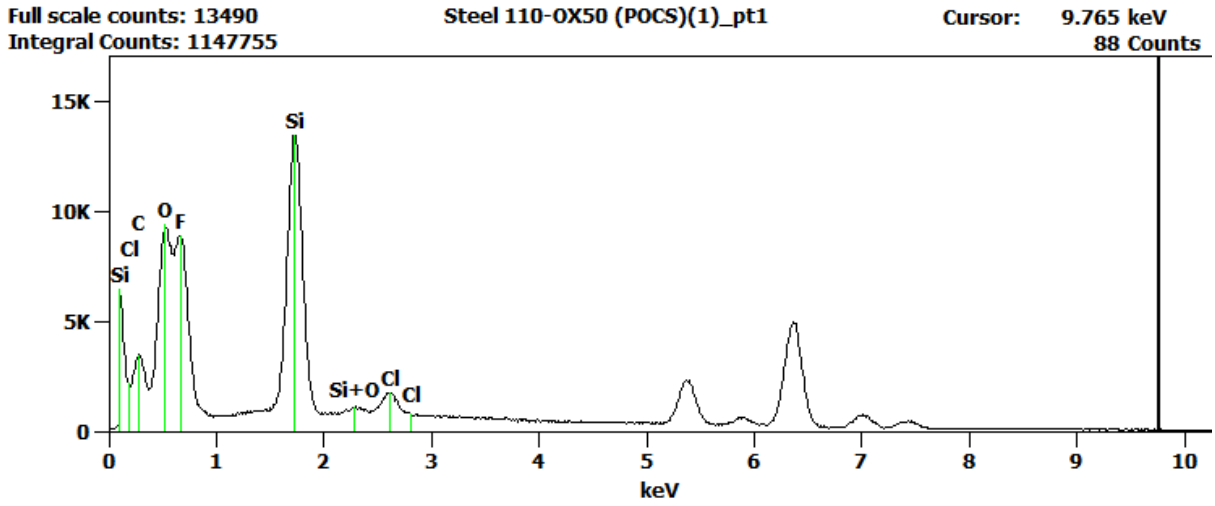

Figure 5.35. Elemental analysis of a steel slide coated with 110-OX50(POCS). The presence of beryllium is probably an instrument error.

Contact angle measurements show that the coated steel surface is not wetted by water, diiodomethane or hexadecane. Figure 5.36 show the optical contact angle measurements for

water, diiodomethane and hexadecane droplets with contact angles of 125.2°, 119.3° and 115.4°, respectively.

The contact angle hysteresis for water, diiodomethane and hexadecane on the coated steel slide is 34.96°, 28.63° and 53.33°, respectively.

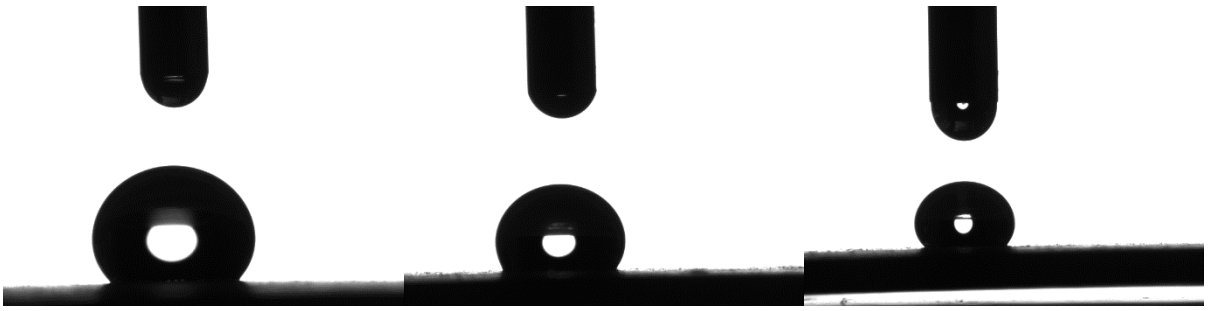

Figure 5.36. Optical contact angle measurements show a water, diiodomethane and hexadecane droplet, respectively, spread on a steel slide coated with 110-OX50(POCS).

The apparent surface energy of the coated steel slide is estimated to be 3.11 mN/m.

5.2.6 Coating 110-R972(POCS)

This solution is similar to 110-OX50(POCS), with a white homogenous suspension during stirring. The suspension accumulates, leaving a foam layer on top of the solution after a short period of time. The slides where withdrawn through a foam layer, making the coating uneven and thick.

Coated Glass Slide

Electron microscopy imaging of a coated glass slide does not give any useful information about the coating or the structure. The coating has weak interaction with the slide underneath which presents a majority of white areas on the image, and therefore no figure is shown.

Figure 5.37 shows an elemental analysis of a glass slide coated with 110-R972(POCS) which indicates the presence of silicon, sodium, calcium, magnesium and oxygen. These components indicate the presence of silica,sodium oxide, calcium oxide and magnesium oxide. The oxides are components of the glass slide.

Contact angle measurements show that the coated glass is not wetted by water or diiodomethane, and partially wetted by hexadecane. Figure 5.38 shows the optical contact angle measurements for water, diiodomethane and hexadecane droplets with contact angles of 152.8°,

127.6° and 72.8°, respectively. The contact angle measurement for water had to be performed by the needle-in method, to keep the droplet from rolling of the surface.

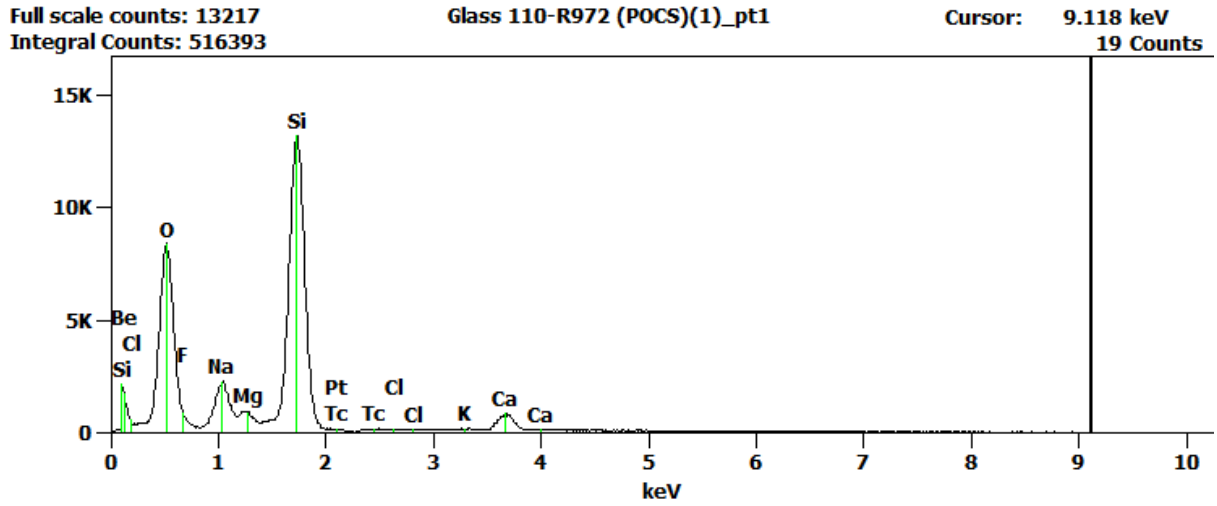

Figure 5.37. Elemental analysis of a glass slide coated with 110-R972(POCS). The presence of beryllium is probably an instrument error.

The contact angle hysteresis for diiodomethane and hexadecane on the coated glass slide is 94.92° and 20.32°, respectively.

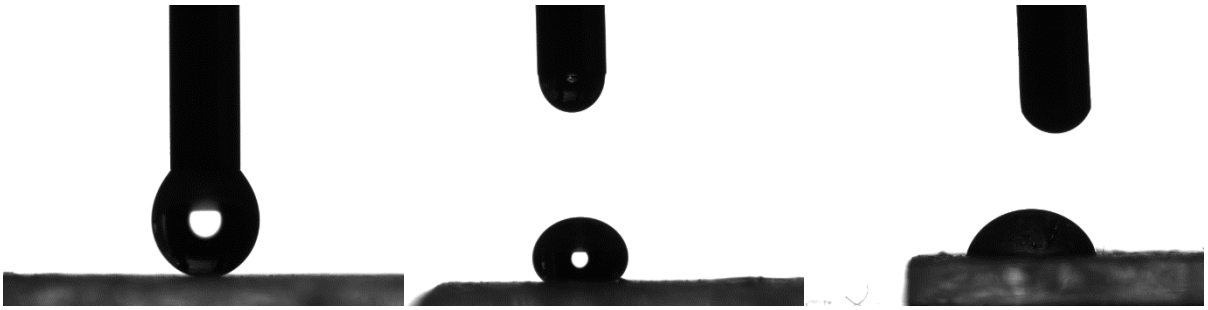

Figure 5.38. Optical contact angle measurements show diiodomethane and hexadecane droplets, respectively, deposited on a glass slide coated with 110-R972(POCS).

The apparent surface energy of the coated glass slide is estimated to be 12.23 mN/m.

Coated Steel Slide

Figure 5.39 shows an electron microscopy image of a coated steel slide. The coating is evenly distributed on the slide in a relatively thick layer with microscopic cracks in the structure.

The image in Figure 5.39 was taken with a secondary electron detector, 200 times magnification and an accelerating voltage of 15.0 kV.

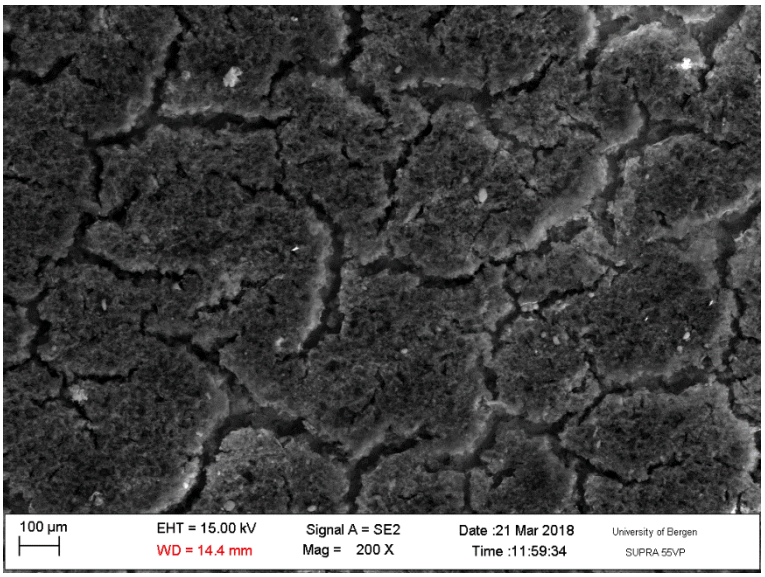

Figure 5.39. Scanning electron microscopy image of a steel slide coated with 110-R972(POCS).

Figure 5.40 shows an elemental analysis of a steel slide coated with 110-R972(POCS) which indicates the presence of silicon, chlorine, carbon, oxygen and fluorine. These components may indicate the presence of silica, perfluorooctyl-trichlorosilane and the fluorochemical polymer.

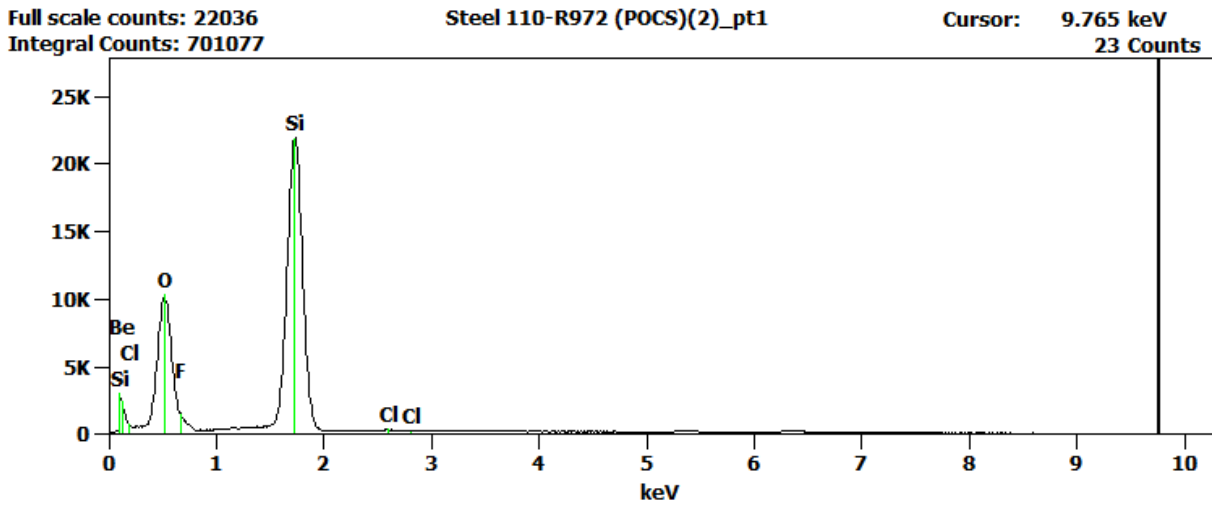

Figure 5.40. Elemental analysis of a steel slide coated with 110-R972(POCS). The presence of beryllium is probably an instrument error.

Contact angle measurements show that the coated steel slide is not wetted by water or diiodomethane, but partially wetted by hexadecane. Figure 5.41 shows the optical contact angle measurements for water, diiodomethane and hexadecane droplets with contact angles of 155.2°, 122.2° and 50.2°. The contact angle for hexadecane is not accurate because the droplet was continuously spreading out on the surface, increasing the contact angle. The contact angle

measurement for water had to be performed by the needle-in method, to keep the droplet from rolling of the surface.

The contact angle hysteresis for diiodomethane and hexadecane on the coated steel slide is 23.01° and 8.79°, respectively. The hysteresis for the hexadecane droplet is not accurate since the droplet was pinned to the surface and barely moved when tilted.

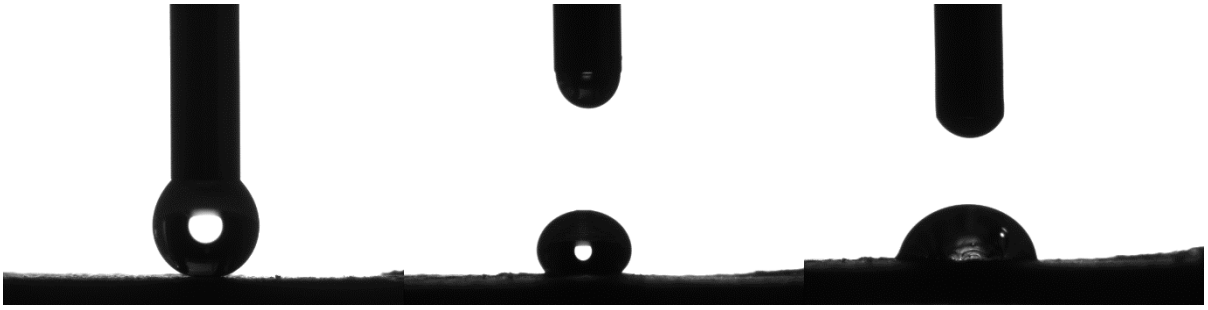

Figure 5.41. Optical contact angle measurements show water, diiodomethane and hexadecane droplets, respectively, deposited on a steel slide coated with 110-R972(POCS).

The apparent surface energy of the coated steel slide is estimated to be 17.56 mN/m.

5.2.7 Coating 100-OX50(POCS)

This solution has a white color, is homogenous and will not precipitate over time. The dip-coated slides have an uneven coating with areas of accumulated particles. The measurements were performed on the areas of the slide with higher concentration of particles.

Coated Glass Slide

Figure 5.42 shows an electron microscopy image of the coated glass slide which has several white areas that suggests the coating has weak interaction with the slide underneath. The coating is not evenly distributed on the slide and the particles have accumulated in separate areas. From Figure 5.42 it appears the accumulated particles have a rough surface structure.

The image in Figure 5.42 is taken with a secondary electron detector, 200 times magnification and an accelerating voltage of 15.0 kV.

Figure 5.43 shows an elemental analysis of a glass slide coated with 100-OX50(POCS) which indicates the presence of silicon, oxygen, carbon, chlorine, fluorine and sodium. These components may indicate the presence of silica, sodium oxide, calcium oxide, magnesium oxide, perfluorooctyl-trichlorosilane and the fluorochemical polymer.

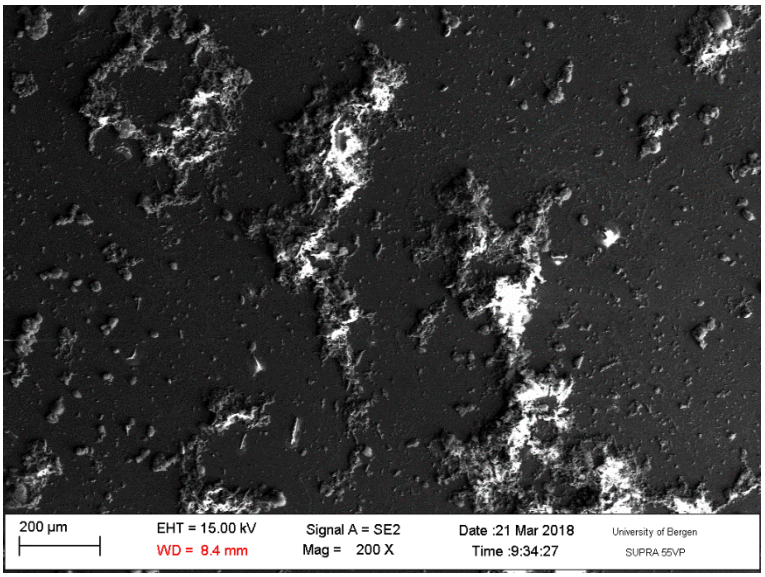

Figure 5.42. Scanning electron microscopy image of a glass slide coated with 100-OX50(POCS).

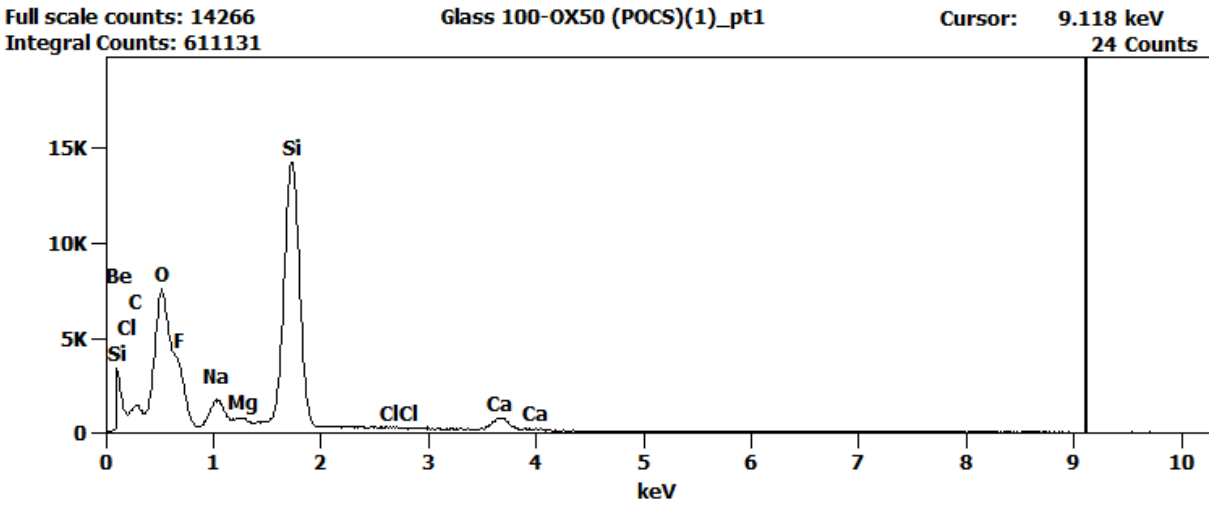

Figure 5.43. Elemental analysis of a glass slide coated with 100-OX50(POCS). The presence of beryllium is probably an instrument error.

Contact angle measurements show that the coated glass slide not wetted by water or diiodomethane, and partially wetted by hexadecane. Figure 5.44 shows the optical contact angle measurements for water, diiodomethane and hexadecane droplets with contact angles of 123.2°, 94.5° and 68.6°, respectively.

The contact angle hysteresis for water, diiodomethane and hexadecane on the coated glass slide is 20.52°, 40.79° and 36.70°, respectively.

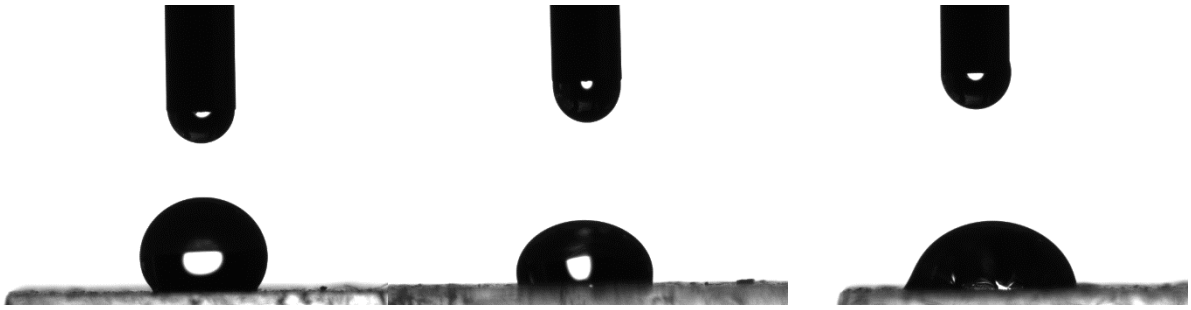

Figure 5.44. Optical contact angle measurements show water, diiodomethane and hexadecane droplets, respectively, deposited on a glass slide coated with 100-OX5O(POCS).

The apparent surface energy of the coated glass slide is estimated to be 12.06 mN/m.

Coated Steel Slide

Figure 5.45 shows an electron microscopy image of the coated steel slide. The coating is not evenly distributed on the slide and the particles have accumulated in small areas scattered on the surface.

The image was taken with a secondary electron detector, 200 times magnification and an accelerating voltage of 15.0 kV.

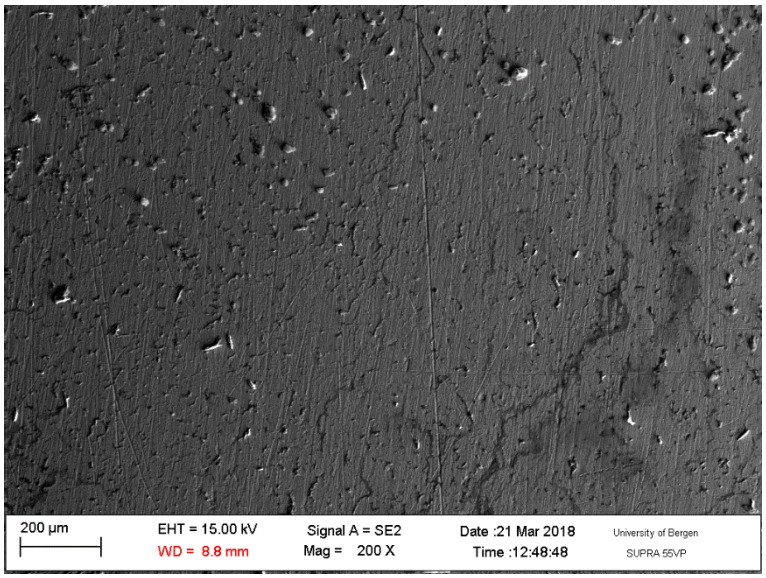

Figure 5.45. Scanning electron microscopy image of a steel slide coated with 100-OX50(POCS).

Figure 5.46 shows an elemental analysis of a steel slide coated with 100-OX50(POCS) which indicates the presence of silicon, chlorine, carbon, oxygen, iron, molybdenum, nickel, manganese and copper. These components may indicate the presence of silica, perfluorooctyl-trichlorosilane and fluorochemical polymer. Several of the metals originate from the steel slide.

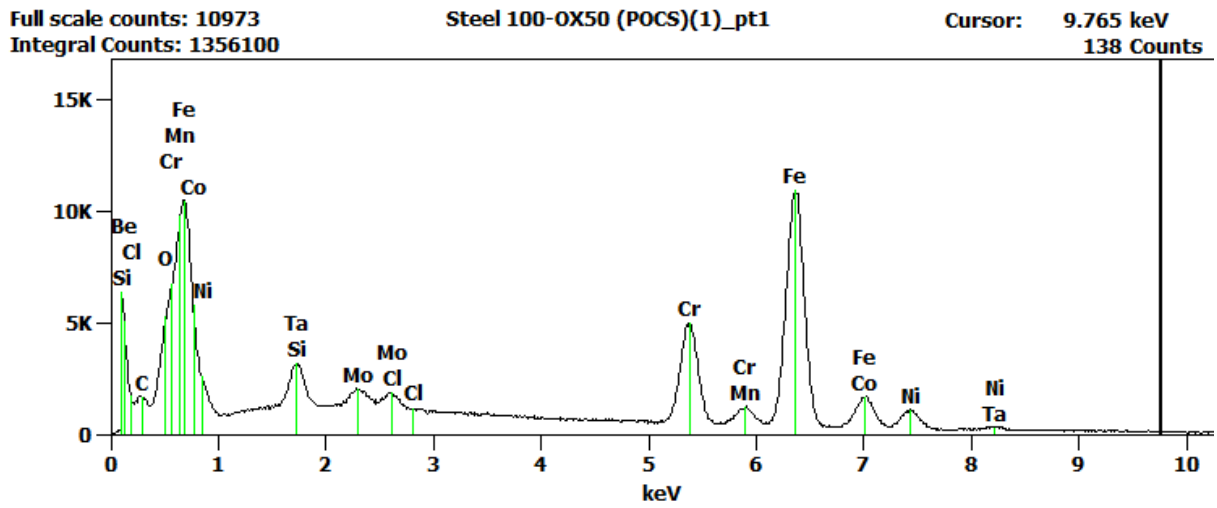

Figure 5.46. Elemental analysis of a steel slide coated with 100-OX50(POCS). The presence of beryllium is probably an instrument error.

Contact angle measurements show that the surface is not wetted by water or diiodomethane, and partially wetted by water. Figure 5.47 shows the optical contact angle measurements for water, diiodomethane and hexadecane droplets with contact angles of 93.0°, 87.2° and 80.9°. The contact angle for water is not accurate because the droplet was continuously spreading out on the surface, increasing the contact angle.

The contact angle hysteresis for water, diiodomethane and hexadecane on the coated glass slide is 26.48°, 45.81° and 32.65°, respectively.

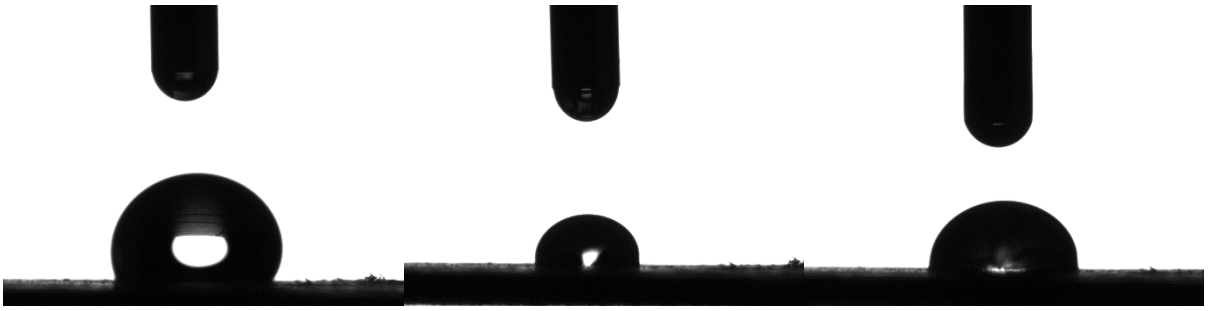

Figure 5.47. Optical contact angle measurements show water, diiodomethane and hexadecane droplets, respectively, on a steel slide coated with 100-OX50(POCS).

The apparent surface energy of the coated steel slide is estimated to be 17.63 mN/m.

5.2.8 Coating 100-R972(POCS)

This mixture was not homogenous and close to completely phase separated with a clear bottom phase and with a white foam layer on top. During stirring the mixture is a white seemingly homogenous solution, but it retracts to its original state when the stirring stops.

Coated Glass Slide

Figure 5.48 shows an electron microscope image of the coated glass slide. The top of the slide is uncoated. The coated area has an even layered coating with microscopic cracks in the structure. The white areas suggest weak interaction between the coating and the glass slide underneath.

The image was taken with a secondary electron detector, 200 times magnification and an accelerating voltage of 15.0 kV.

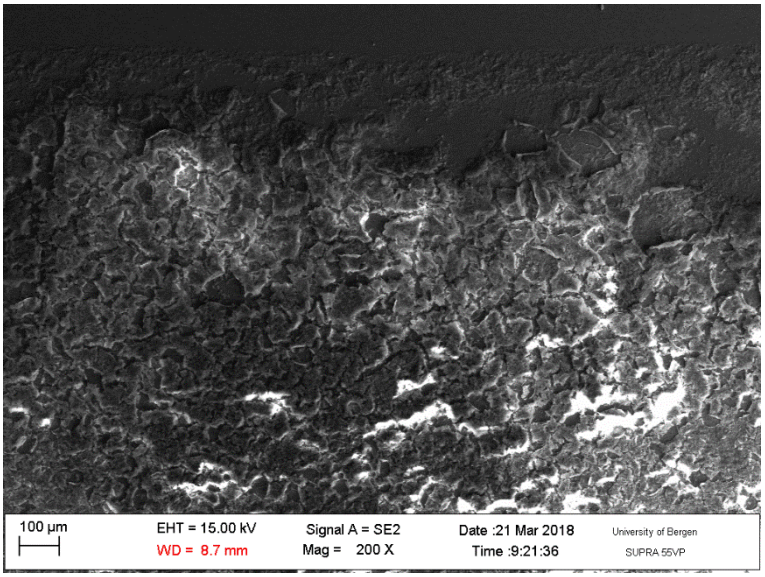

Figure 5.48. Scanning electron microscopy image of a glass slide coated with 100-R972(POCS).

Figure 5.49 shows an elemental analysis of a glass slide coated with 100-R972(POCS) which indicates the presence of carbon, sodium, calcium, magnesium, oxygen, fluorine and silicon. These components may indicate the presence of silica, sodium oxide, calcium oxide, magnesium oxide and the fluorochemical polymer. The oxides are components of the glass slide.

Contact angle measurements show that the coated glass slide is not wetted by water, diiodomethane or hexadecane. Figure 5.50 shows the optical contact angle measurements for

water, diiodomethane and hexadecane droplets with contact angles of 157.7°, 136.5° and 95.6°, respectively.

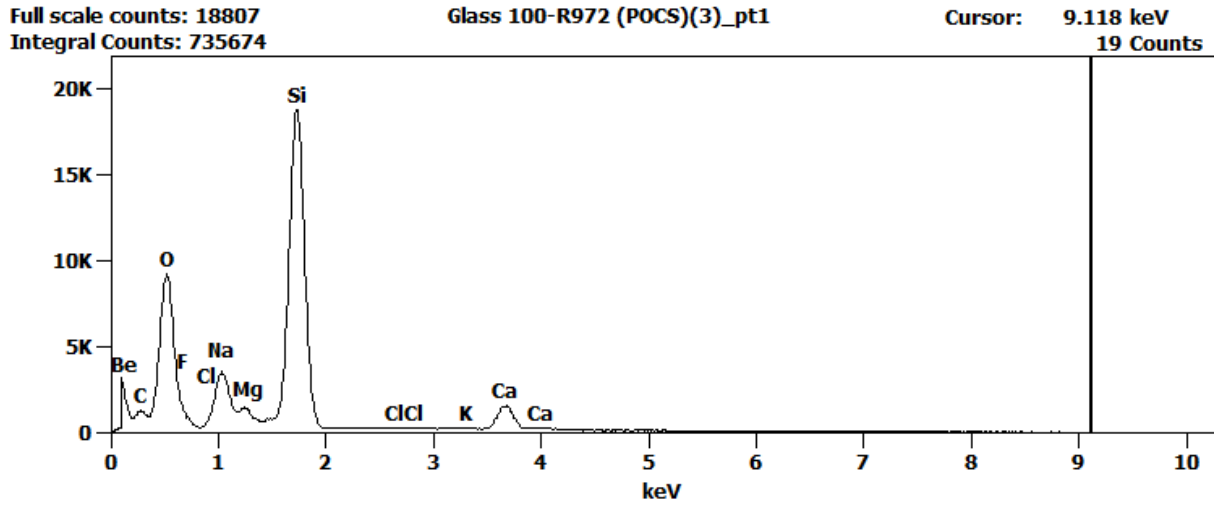

Figure 5.49. Elemental analysis of a glass slide coated with 100-R972(POCS). The presence of beryllium is probably an instrument error.

The contact angle hysteresis for water, diiodomethane and hexadecane on the coated glass slide is 4.32°, 20.73° and 14.60°, respectively.

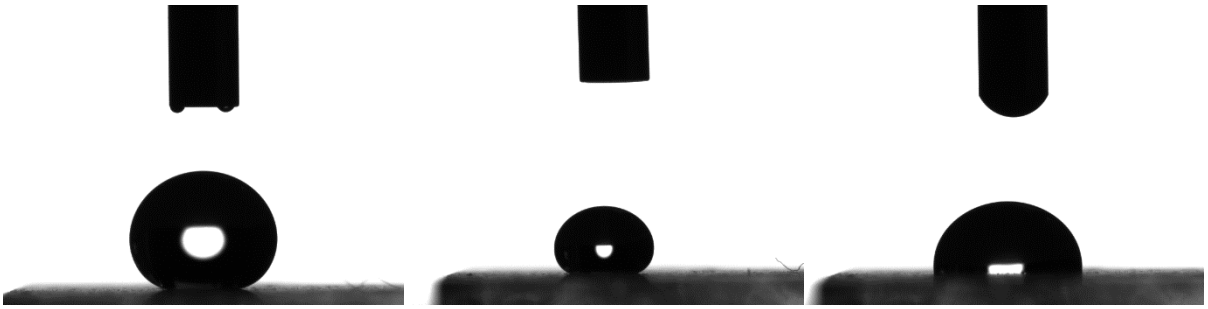

Figure 5.50. Optical contact angle measurements show water, diiodomethane and hexadecane droplets, respectively, deposited on a glass slide coated with 100-R972(POCS).

The apparent surface energy of the coated glass slide is estimated to be 6.28 mN/m.

Coated Steel Slide

Figure 5.51 shows an electron microscopy image of the coated steel slide. The image shows that the coating is evenly distributed across the slide with a rough surface structure. Some areas on the slide have a thinner layer of coating where the vertical lines from the steel surface are visible.

The image as was taken with a secondary electron detector, 200 times magnification and an accelerating voltage of 15.0 kV.

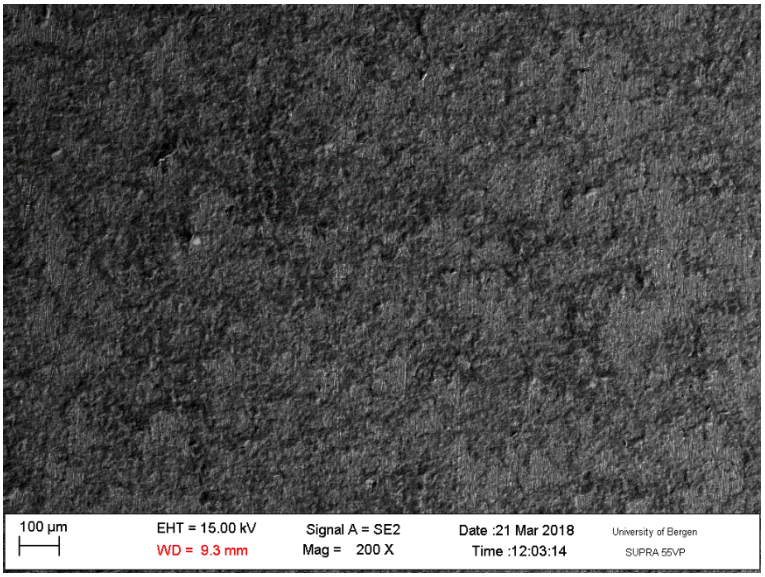

Figure 5.51. Scanning electron microscopy image of a steel slide coated with 100-R972(POCS).

Figure 5.52 shows an elemental analysis of a steel slide with 100-R972(POCS) which indicates the presence of silicon, chlorine, carbon, fluorine, oxygen, chromium, iron, molybdenum, manganese, copper and nickel. These components may indicate the presence of silica, perfluorooctyl-trichlorosilane and fluorochemical polymer. Several of the metals originate from the steel slide.

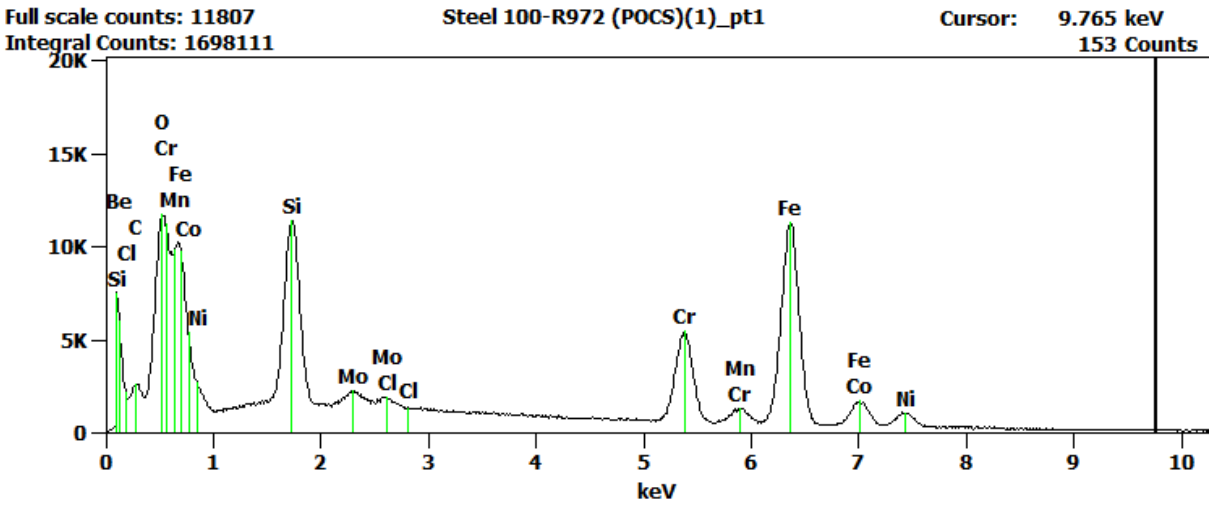

Figure 5.52. Elemental analysis of a steel slide with 100-R972(POCS). The presence of beryllium is probably an instrument error.

Contact angle measurements show that the coated steel slide is not wetter by water or diiodomethane, and partially wetted by hexadecane. Figure 5.53 shows the optical contact angle measurements for water, diiodomethane and hexadecane droplets with contact angles of 154.1°, 118.1° and 68.3°, respectively.

The contact angle hysteresis for water, diiodomethane and hexadecane on the coated glass slide is 79.65°, 35.74° and 31.68°, respectively.

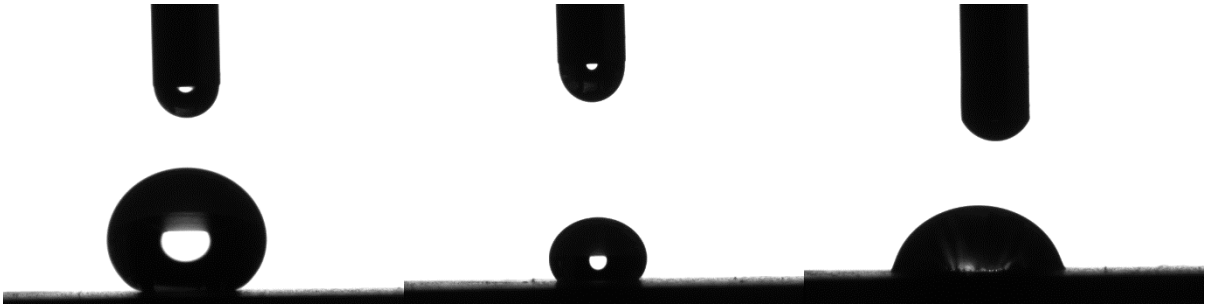

Figure 5.53. Optical contact angle measurements show water, diiodomethane and hexadecane droplets, respectively, deposited on a steel slide coated with 100-R972(POCS).

The apparent surface energy of the coated steel slide is estimated to be 12.16 mN/m.

5.3 Silicon Oil Soot

The following coated glass and steel slides are characterized by SEM images to investigate surface structure and roughness after deposition of a soot layer created by heating the silicon oil. Elemental analysis was performed to identify the composition of the deposited layer.

Contact angle measurements with water, diiodomethane and hexadecane were performed on the coated glass and steel surfaces. Contact angle hysteresis was measured for the liquids that did not completely wet the surfaces. Apparent surface energy is calculated for each coated slide.

5.3.1 Silicon oil DC 200

Soot from the silicon oil formed a transparent layer on the glass and steel slides which is visible because of the band of colors of the oil.

Coated Glass Slide

Figure 5.54 shows electron microscopy images of a glass slide coated with soot from Silicon Oil DC 200. The images show particles on the glass slide with a size of about 1 µm.

The image in Figure 5.54a was taken with a secondary electron detector, 2000 times magnification and an accelerating voltage of 15.0 kV. The image in Figure 5.54b was taken with a secondary electron detector, 20 000 times magnification and an accelerating voltage of 5.0 kV.

a) **b)**

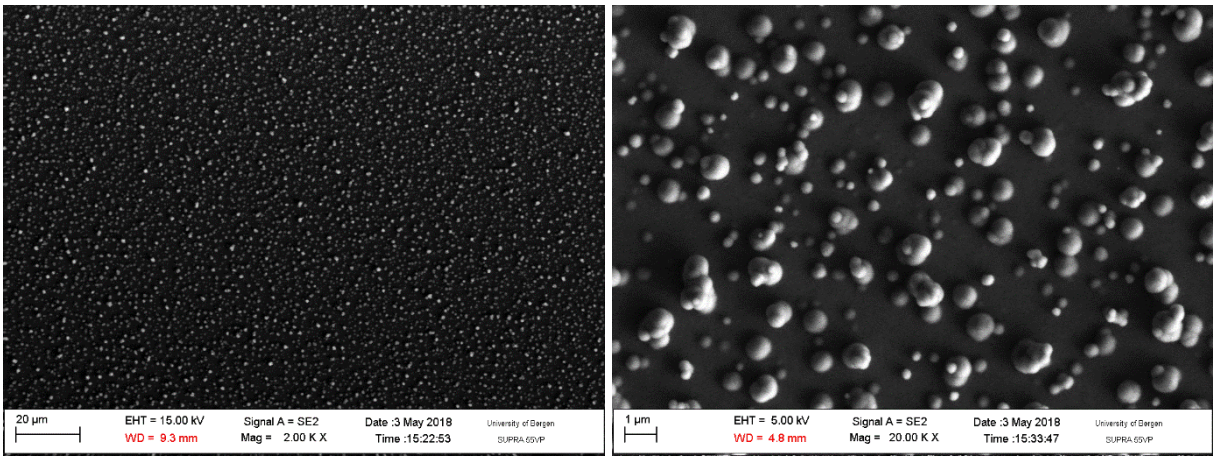

Figure 5.54. Scanning electron microscopy images of glass slide coated with soot from Silicon Oil DC 200 at a) 2000 times magnification and b) 20 000 times magnification.

Figure 5.55 shows an elemental analysis of a glass slide coated with soot from Silicon Oil DC 200, which indicates the presence of oxygen, sodium, magnesium, silicon and calcium. These components may indicate the presence of silica, sodium oxide, calcium oxide and magnesium oxide. The oxides are components of the glass slide.

Contact angle measurements show that the coated glass slide is not wetted by water or diiodomethane, but completely wetted by hexadecane. Figure 5.56 shows the optical contact angle measurements for water, diiodomethane and hexadecane droplets with contact angles of 157.1°, 93.9° and 4.3°, respectively. The contact angle measurement for the water droplet had to be performed by the needle-in method, to keep the droplet from rolling of the surface.

The contact angle hysteresis for diiodomethane on the coated glass slide is 39.99°. The contact angle hysteresis for water was not possible to measure because the droplet instantly rolls of the

surface. This indicates a low contact angle hysteresis. The contact angle hysteresis for hexadecane is not calculated because hexadecane fully wets the surface.

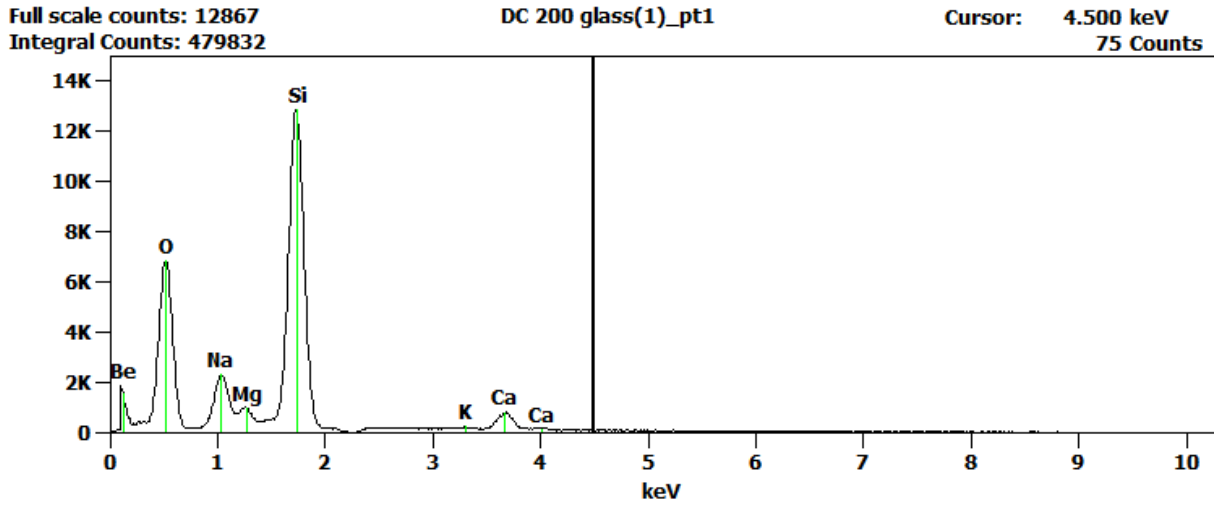

Figure 5.55. Elemental analysis of a glass slide coated with soot from Silicon Oil DC 200. The presence of beryllium is probably an instrument error.

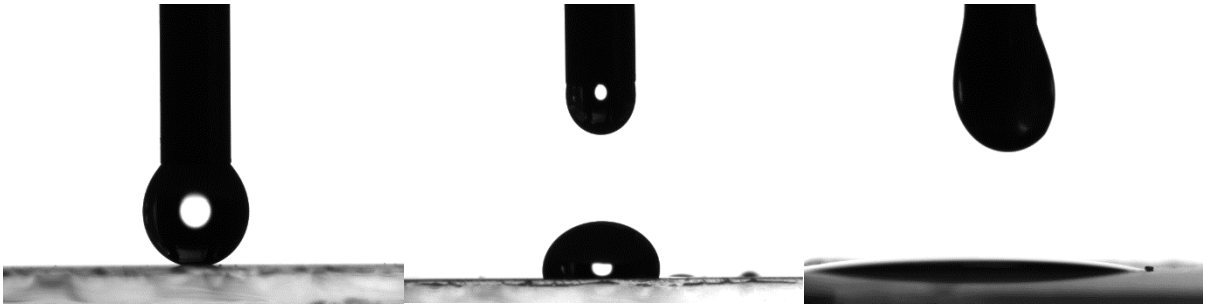

Figure 5.56. Optical contact angle measurements show water, diiodomethane and hexadecane droplets, respectively, deposited on a glass slide coated with soot from heating Oil DC 200.

The apparent surface energy of the coated glass slide is estimated to be 31.94 mN/m.

Coated Steel Slide

Figure 5.57 show an electron microscopy image of a steel slide coated with soot from heating Silicon Oil DC 200. Visible observations indicate a relatively thin film on the steel surface. White spots are observed, indicating larger particles less adhered to the surface.

The image in Figure 5.57 was taken with a secondary electron detector, 2000 times magnification and an accelerating voltage of 15.0 kV.

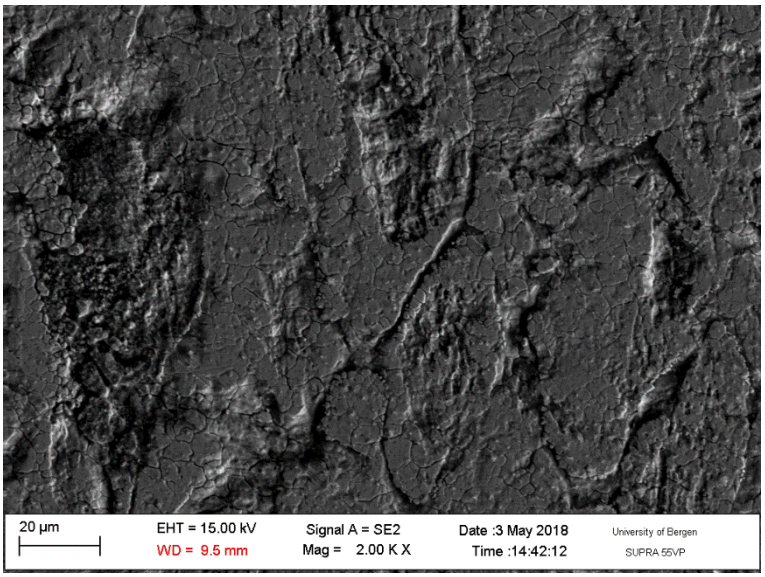

Figure 5.57. Scanning electron microscopy imaging of a steel slide coated with soot from Silicon Oil DC 200.

Figure 5.58 shows an elemental analysis of a steel slide coated with soot from heating Silicon Oil DC 200. The analysis indicates the presence of oxygen, manganese, chromium, iron, nickel, tantalum, silicon and molybdenum. These elements may imply the presence of silica on the steel slide. Elemental analysis performed directly on the white spots, showed higher presence of silicon and oxygen which indicates larger soot particles.

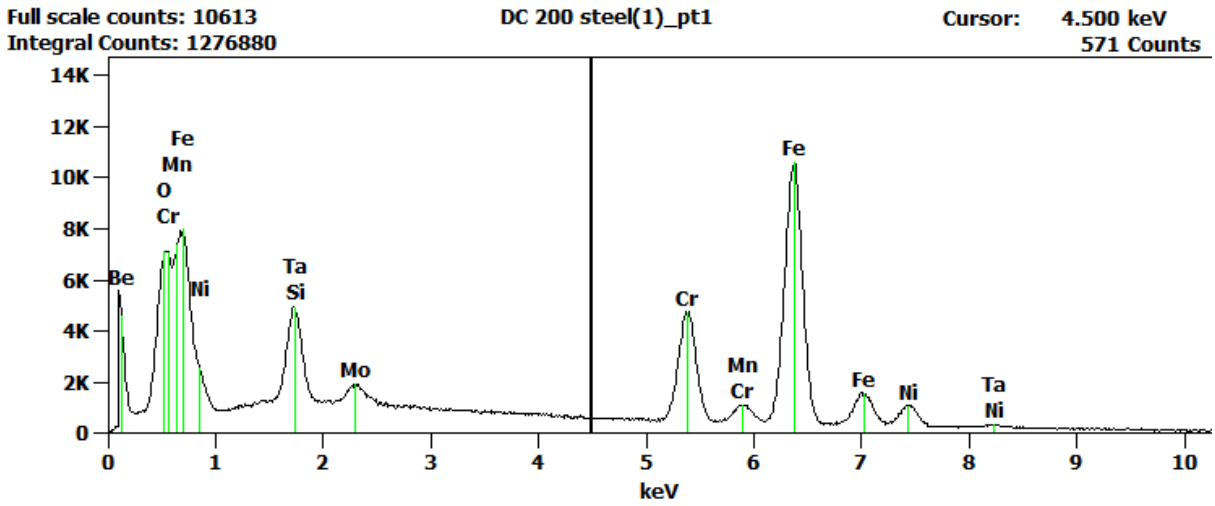

Figure 5.58. Elemental analysis of a steel slide coated with soot from heating Silicon Oil DC 200. The presence of beryllium is probably an instrument error.

Contact angle measurements show that the coated steel slide is not wetted by water, partially wetted by diiodomethane and completely wetted by hexadecane. Figure 5.59 show the optical

contact angle measurements for water, diiodomethane and hexadecane droplets with contact angles of 163.1°, 62.6° and 1.5°, respectively.

The contact angle hysteresis for water and diiodomethane on the coated glass slide is 6.81° and 27.97°, respectively. The contact angle hysteresis for hexadecane is not calculated because hexadecane fully wets the surface.

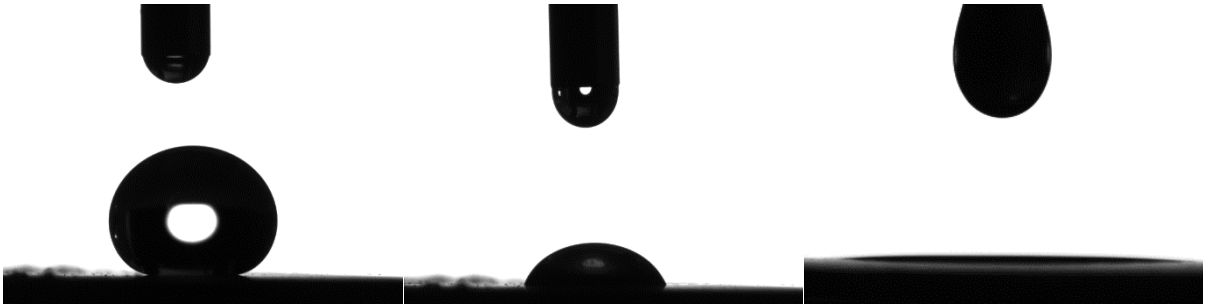

Figure 5.59. Optical contact angle measurements show water, diiodomethane and hexadecane droplets, respectively, deposited on a steel slide coated with soot from Silicon Oil DC 200.

The apparent surface energy of the coated steel slide is estimated to be 63.02 mN/m.

5.3.2 Sylgard 184

Soot from Sylgard 184 gave a transparent layer on the glass and steel slide that was visible because of the band of colors of the oil, and some white areas.

Coated Glass Slide

The electron microscopy images of the coated glass slide did not present any information about the coating, and therefore no figure is shown.

Figure 5.60 shows an elemental analysis of a glass slide coated with soot from Sylgard 184 which indicates the presence of silicon, oxygen, sodium and magnesium. These components may indicate the presence of silicon soot.

Contact angle measurements show that the coated glass slide is not wetted by water or diiodomethane, but completely wetted by hexadecane. Figure 5.61 shows the optical contact angle measurements for water and diiodomethane droplets with contact angles of 161.7°, 90.2° and 0.4°, respectively.

The contact angle hysteresis for water and diiodomethane on the coated glass slide is 0.3° and 29.11°, respectively. The contact angle hysteresis for hexadecane is not calculated because hexadecane fully wets the surface.

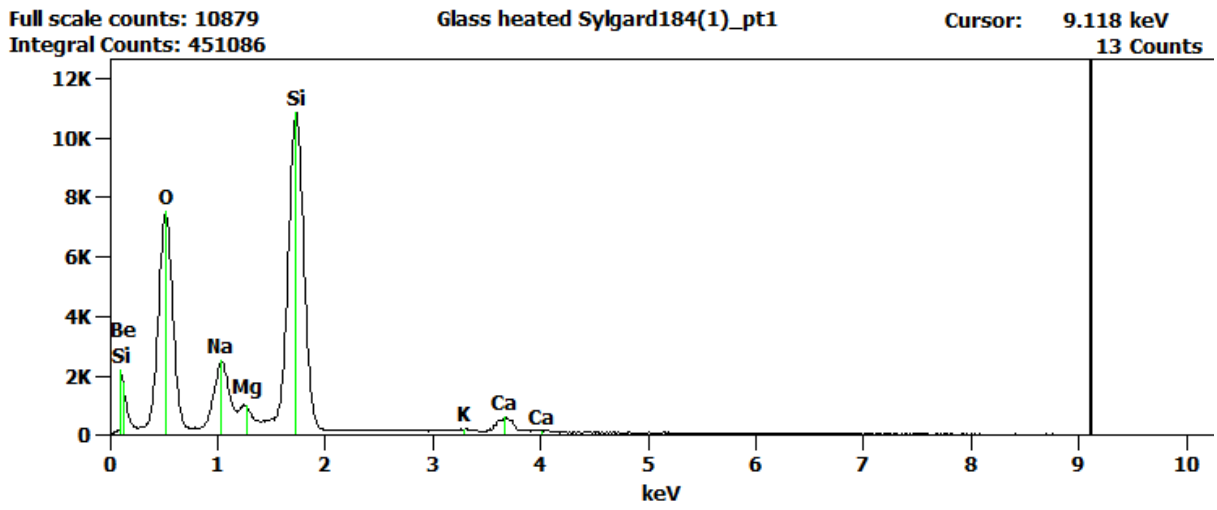

Figure 5.60. Elemental analysis of a glass slide coated with soot from heated Sylgard 184. The presence of beryllium is probably an instrument error.

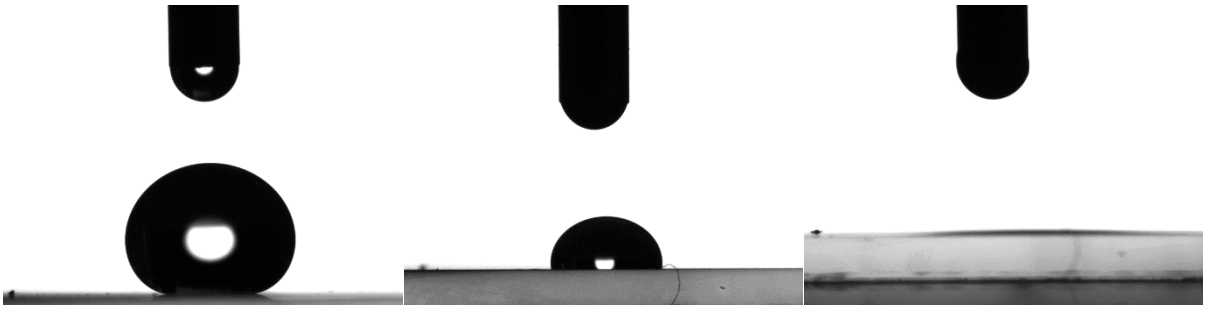

Figure 5.61. Optical contact angle measurements show water, diiodomethane and hexadecane droplets, respectively, deposited on a glass slide coated with soot from Sylgard 184.

The apparent surface energy of the coated glass slide is estimated to be 26.68 mN/m.

Coated Steel Slide

Figure 5.62 shows an electron microscopy image of the coated steel slide. There is a visible thin layer on the steel surface with circular patterns.

The image as was taken with a secondary electron detector, 2000 times magnification and an accelerating voltage of 15.0 kV.

Figure 5.63 shows an elemental analysis of a steel slide coated with soot from Sylgard 184 which indicates the presence of silicon, chromium, oxygen, manganese, iron, molybdenum, copper and nickel. These components may indicate the presence of silicon soot.

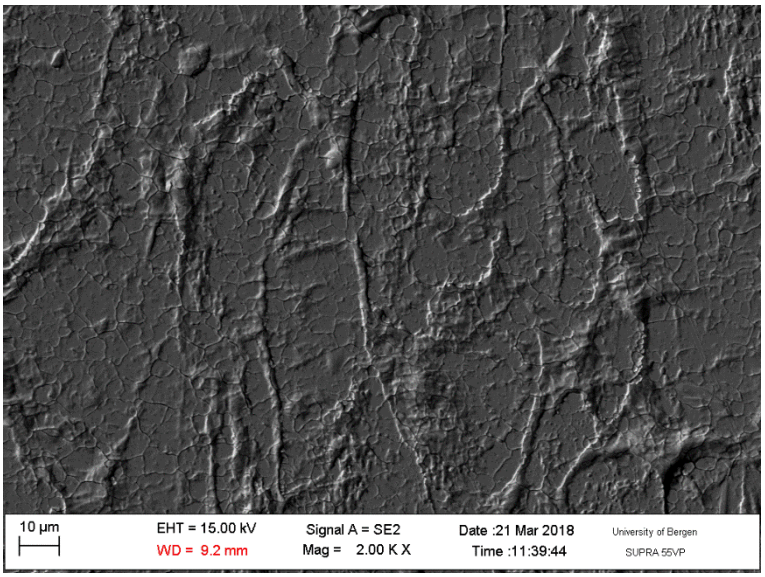

Figure 5.62. Scanning electron microscopy image of a steel slide coated with soot from Sylgard 184.

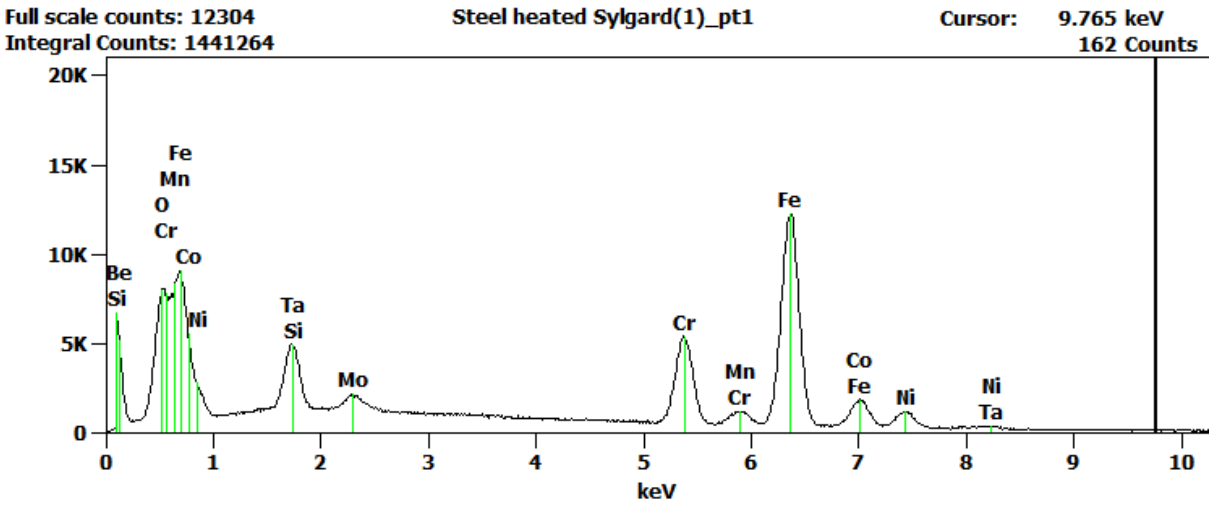

Figure 5.63. Elemental analysis of a steel slide coated with soot from Sylgard 184. The presence of beryllium is probably an instrument error.

Contact angle measurements show that the coated steel surface is partially wetted by water and diiodomethane, and not wetted by hexadecane. Figure 5.64 shows the optical contact angle measurements for water, diiodomethane and hexadecane droplets with contact angles of 82.3°, 40.5° and 14.1°, respectively.

The contact angle hysteresis for water, diiodomethane and hexadecane on the coated steel slide is 19.53°, 20.24° and 7.67°, respectively.

The apparent surface energy of the coated steel slide is estimated to be 35.91 mN/m.

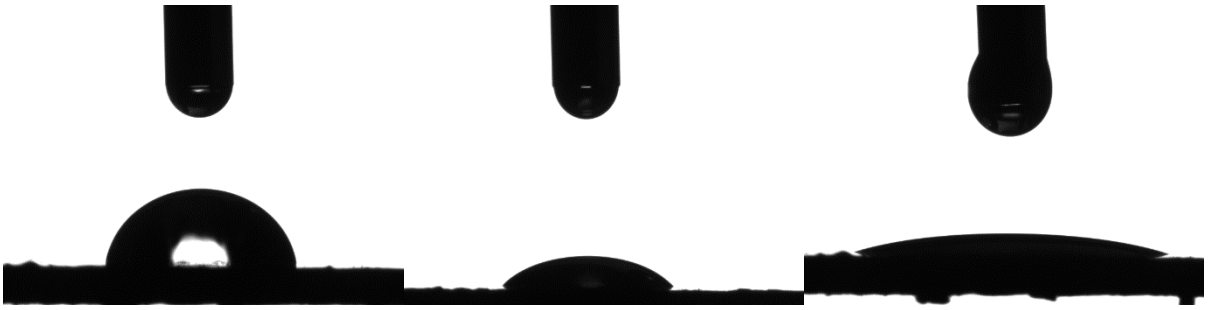

Figure 5.64. Optical contact angle measurements show water, diiodomethane and hexadecane droplets, respectively, on a steel slide coated with soot from Sylgard 184.

5.4 Etched and Coated Aluminum Surfaces

The following etched and coated aluminum slides are characterized by SEM images to investigate surface structure and roughness after treatment. Elemental analysis was performed to identify the composition of the treated slides.

Contact angle measurements with water, diiodomethane and hexadecane were performed on the coated glass and steel surfaces. Contact angle hysteresis was measured for the liquids that did not completely wet the surfaces. Apparent surface energy is calculated for each treated surface.

The aluminum slides were placed vertically in the solutions. Gas bubble appeared from the bottom of the slide, rising up to the surface along the slide.

5.4.1 Etched aluminum slide (10 minutes)

Figure 5.65a shows SEM imaging of an aluminum slide after etching in HCl for 10 minutes to make a micro structured surface. The surface show roughness features of about 1 μm on lager surface features of about 10 μm. The whole surface of the aluminum slide is not etched and the vertical marks from cutting the aluminum are still present.

Figure 5.65b shows SEM imaging of an aluminum slide after etching in HCl for 10 minutes and immersion in HNO_3 + $CuSO_4$ for 6 minutes. The surface has a rougher surface structure and larger features than seen in Figure 5.65a. There are no visible signs of Cu-particles on the surface and the vertical marks from the steel slide are present.

The images are taken with a secondary electron detector, 2000 times magnification and an accelerating voltage of 5.0 kV.

a) b)

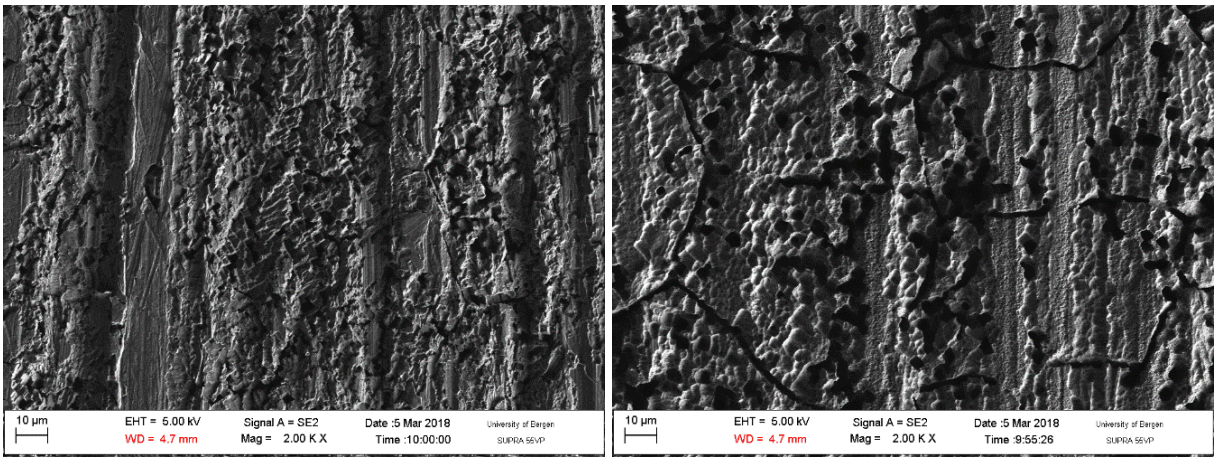

Figure 5.65. Scanning electron microscopy images of a) micro structured aluminum surface from etching in HCl for 10 minutes b) aluminum surface etched in HCl for 10 minutes followed by HNO_3 + $CuSO_4$ for 6 minutes.

Contact angle measurements show that the etched aluminum slide is partially wetted by water and diiodomethane, and completely wetted by hexadecane. Figure 5.66 shows the optical contact angle measurements for water, diiodomethane and hexadecane droplets with contact angles of 32.4°, 21.4° and 6.1°, respectively.

The contact angle hysteresis for water and diiodomethane on the etched aluminum slide is 17.30° and 22.30°, respectively. The contact angle hysteresis for hexadecane was not measured because it completely wetted the etched aluminum surface.

Figure 5.66. Optical contact angle measurements show water, diiodomethane and hexadecane droplets, respectively, deposited on an aluminum slide etched in HCl for 10 minutes followed by immersion in HNO_3 + $CuSO_4$ for 6 minutes.

The apparent surface energy of the etched aluminum surface is estimated to be 53.17 mN/m.

5.4.2 Etched and coated aluminum slide (10 minutes)

Figure 5.67 shows SEM imaging of an aluminum slide after etching in HCl for 10 minutes, immersion in HNO_3 + $CuSO_4$ for 6 minutes, followed by dip-coating in PDES and ethanol. The surface has a rough structure with features of about 2 μm. The image is taken further down at the aluminum slide where more of the surfaces appears to be etched.

The image is taken with a secondary electron detector, 2000 times magnification and an accelerating voltage of 5.0 kV.

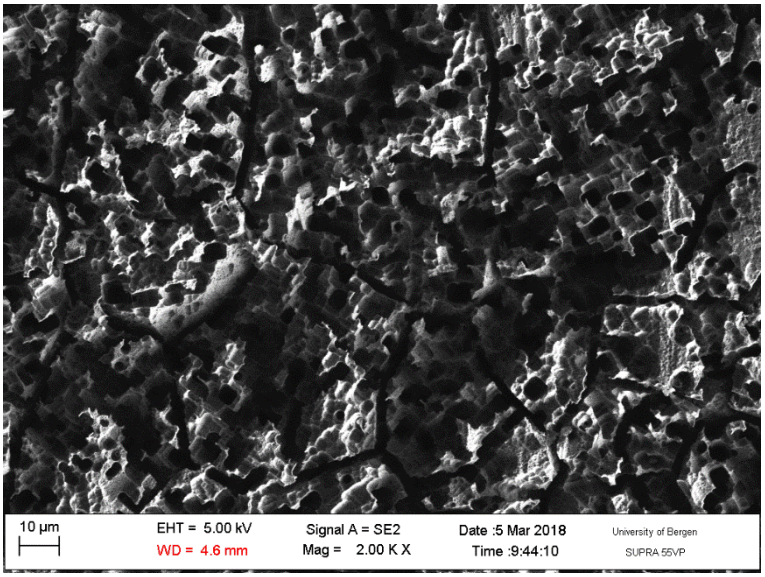

Figure 5.67. Scanning electron microscope image of an aluminum slide etched in HCl for 10 minutes followed by immersion in HNO_3 + $CuSO_4$ for 6 minutes and dip-coated in a solution of PDES and ethanol for 2 hours.

Figure 5.68 shows an elemental analysis of the etched and coated aluminum slide, which indicates the presence of aluminum. These results are similar to the results from the un-treated aluminum slide.

Contact angle measurements show that the etched and coated aluminum slide is not wetted by water or diiodomethane, but completely wetted by hexadecane. Figure 5.69 shows the optical contact angle measurements for water, diiodomethane and hexadecane droplets with contact angles of 150.7°, 137.6° and 10.2°.

The contact angle hysteresis for water and diiodomethane on the etched and coated aluminum slide is 17.95° and 2.51°, respectively. The contact angle hysteresis for hexadecane was not measured because it completely wetted the etched and coated aluminum surface.

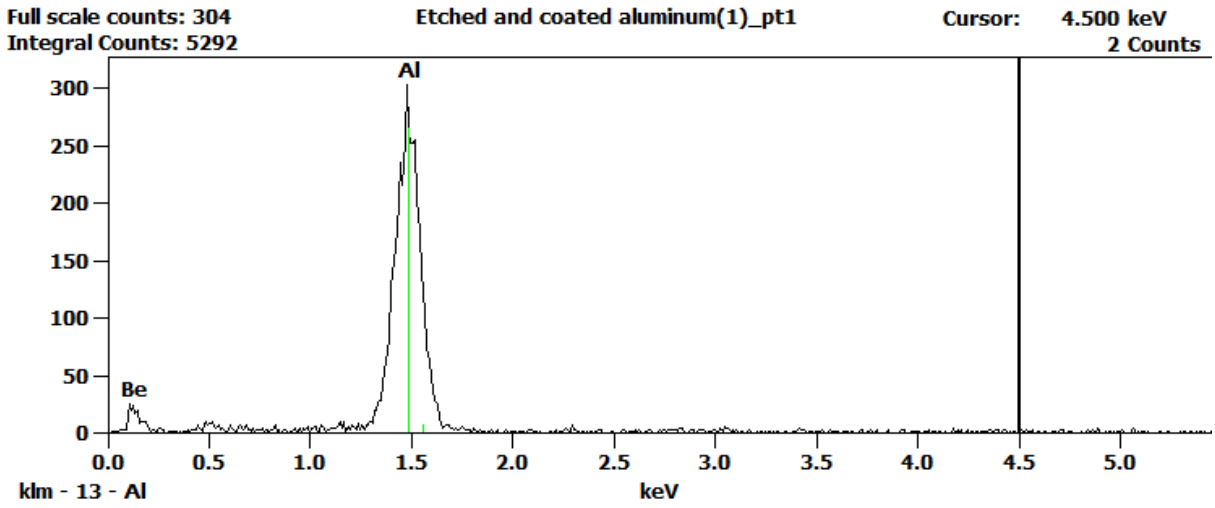

Figure 5.68. Elemental analysis of an aluminum slide etched in HCl for 10 minutes followed by immersion in HNO_3 + $CuSO_4$ for 6 minutes and dip-coated in a solution of PDES and ethanol for 2 hours. The presence of beryllium is probably an instrument error.

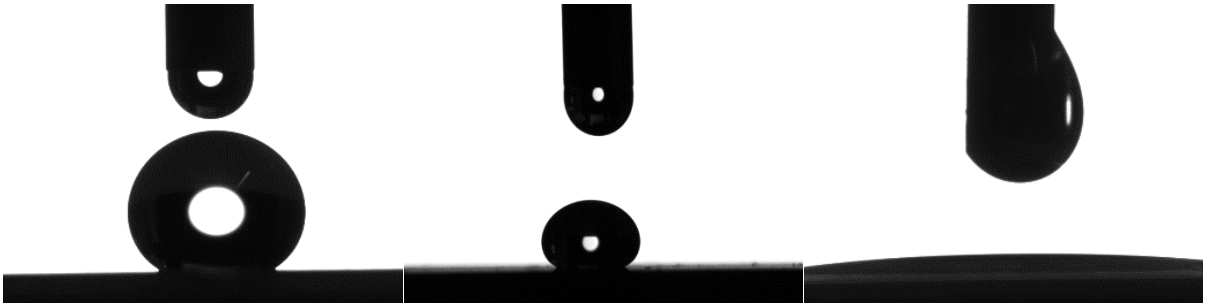

Figure 5.69. Optical contact angle measurements show water, diiodomethane and hexadecane droplets, respectively, deposited on an aluminum slide etched in HCl for 10 minutes followed by immersion in HNO_3 + $CuSO_4$ for 6 minutes and dip-coated in a solution of PDES and ethanol for 2 hours.

The apparent surface energy of the etched and coated aluminum slide is estimated to be 1.98 mN/m. The decrease in apparent surface energy and the contact angles after coating suggest that there are other components on the surface not detected by the elemental analysis in Figure 5.68.

5.4.3 Etched aluminum slide (22 minutes)

Three parallels were tested with the etching time in HCl set to 22 minutes. Variations in etched surface area and malfunctioning with the dip-coater, caused us to repeat the experiment three times. The etching time was increased from the work done by Peng *et al.* [4] in an attempt to fully

etch the aluminum surface, removing the vertical cutting marks. The third parallel was etched in HCl and immersed in the solution of SO_4 and HNO_3 while stirring.

SEM images were taken of these slides in order to compare the surface structure prior to and after coating. No contact angle measurements were performed on the etched but uncoated slides, since work done by Peng *et al.*[4] shows that this hierarchical structure without coating does not sufficiently repel low tension liquids. In addition, we had a limited amount of aluminum slides, and wettability measurements prior to coating would contaminate the surface. If the surface is contaminated, new slides would have to be prepared before coating.

First parallel

The dip-coating instrument did not always function as expected. The aluminum slide for the first parallel was dropped into the solution of PDES and ethanol by the instrument, causing the etched areas described next to have one layer of coating before the elemental analysis was performed and the electron microscopy images were taken.

Figure 5.70a shows an electron microscopy image of the first parallel aluminum slide after etching in HCl for 22 minutes. The surface has a rough structure in some parts, with surface features of about 1 μm on larger surface features of about 10 μm. The vertical marks on the aluminum slide are still present after etching, and the image is taken on the top part of the slide.

Figure 5.70b shows an electron microscopy image of the first parallel aluminum slide after etching in HCl for 22 minutes followed by immersion in HNO_3 + $CuSO_4$ for 6 minutes. The surface has a rougher surface structure and larger features than we see in Figure xa), and the vertical marks on the steel slide are present but not as frequent.

The images in Figure x are taken with a secondary electron detector, 2000 times magnification and an accelerating voltage of 15.0 kV.

Figure 5.71 shows an elemental analysis of the first parallel aluminum slide etched in HCl for 22 minutes followed by immersion in HNO_3 + $CuSO_4$ for 6 minutes. The elemental analysis does not indicate the presence of any other component than aluminum.

a) b)

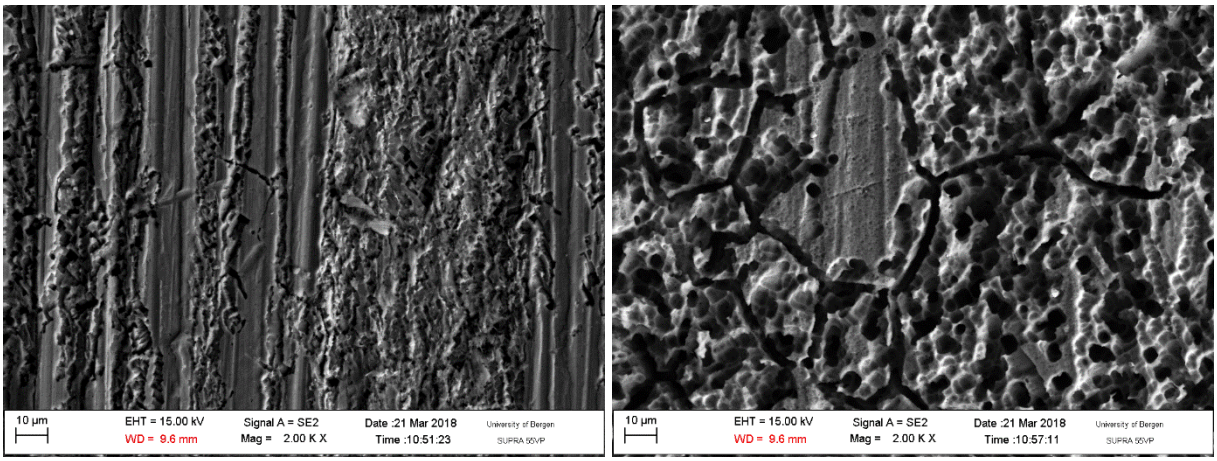

Figure 5.70. Scanning electron microscopy imaging of a) first parallel aluminum slide etched in HCl for 22 minutes b) first parallel aluminum slide etched in HCl for 22 minutes followed by immersion in HNO_3 + $CuSO_4$ for 6 minutes.

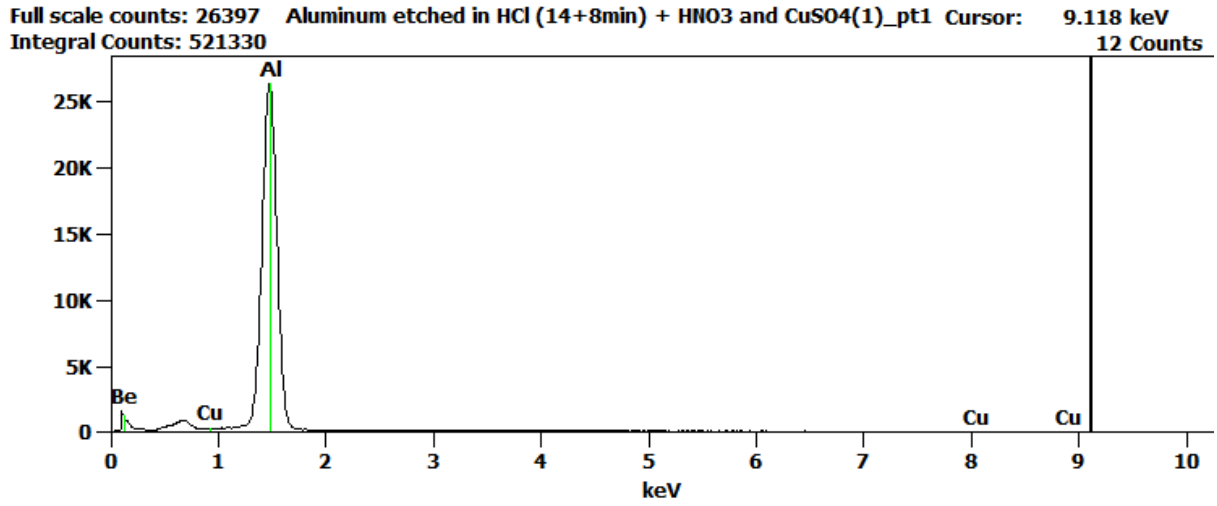

Figure 5.71. Elemental analysis of the first parallel aluminum slide etched in HCl for 22 minutes followed by immersion in HNO_3 + $CuSO_4$ for 6 minutes. There is no indication of copper present in the analysis, and the Cu-signal marks where a peak should show if any copper was detected. The presence of beryllium is probably an instrument error.

Second parallel

The second parallel aluminum slide was kept submerged in the solution of PDES and ethanol twice for uncertain periods due to malfunctioning of the dip-coater. Electron microscopy images and elemental analysis was performed on the etched areas of the second parallel slide prior to coating, so these areas were not affected by the dip-coating errors.

Figure 5.72a shows an electron microscopy image of the second aluminum slide after etching in HCl for 22 minutes. The image is taken at the top part of the slide where the left part of the images shows the untreated aluminum slide. The surface seems to have a rougher surface structure than the first parallel, with surface features of the same size at about 1 μm on larger surface features of about 10 μm. The small bright spots on the image is Cu-particles. This part of the slide was accidentally immersed in HNO_3 + $CuSO_4$ for a few seconds which resulted in relatively pronounced traces of Cu-particles. The vertical marks on the aluminum slide are present on the etched area in a relatively small amount.

Figure 5.72b shows an electron microscopy image of the second aluminum slide after etching in HCl for 22 minutes followed by immersion in HNO_3 + $CuSO_4$ for 6 minutes. The surface shows a rough structure with white spotted areas that are Cu-particles. The surface features seem to be about 2 μm. The bright color of the Cu-particles may indicate that they have weak interactions with the aluminum surface.

The images in Figure 5.72 are taken with a secondary electron detector, 2000 times magnification and an accelerating voltage of 15.0 kV.

a) **b)**

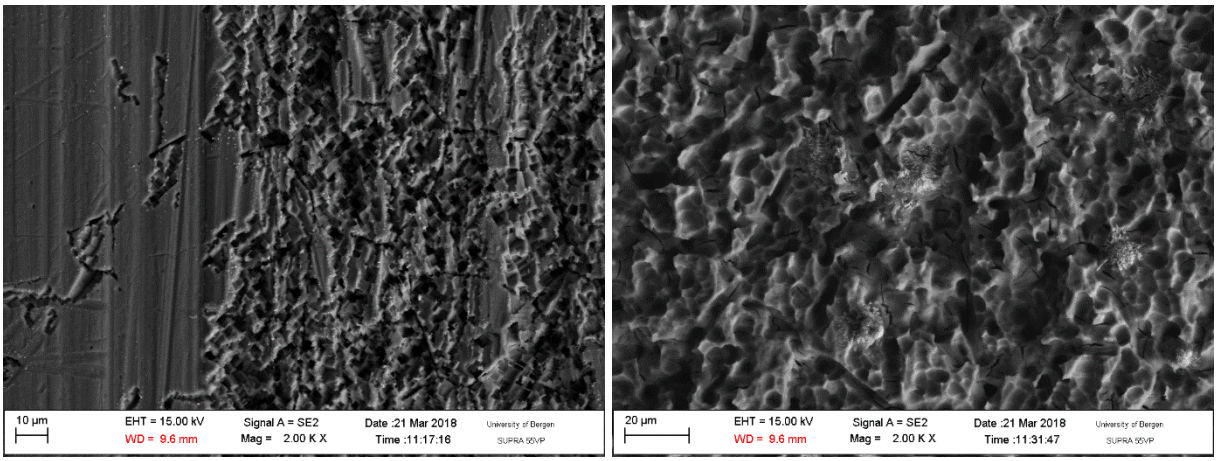

Figure 5.72. Scanning electron microscopy imaging of a) second parallel aluminum slide etched in HCl for 22 minutes b) second parallel aluminum slide etched in HCl for 22 minutes followed by immersion in HNO_3 + $CuSO_4$ for 6 minutes.

Figure 5.73 shows an elemental analysis of the second parallel aluminum slide etched in HCl for 22 minutes followed by immersion in HNO_3 + $CuSO_4$ for 6 minutes. The elemental analysis indicates the presence of chromium, copper, aluminum, sulfur and ruthenium. This implies the presence of copper particles. Chromium and ruthenium may originate from the steel clip

holding the aluminum slide. The clip was in contact with the solution when the set-up was put together.

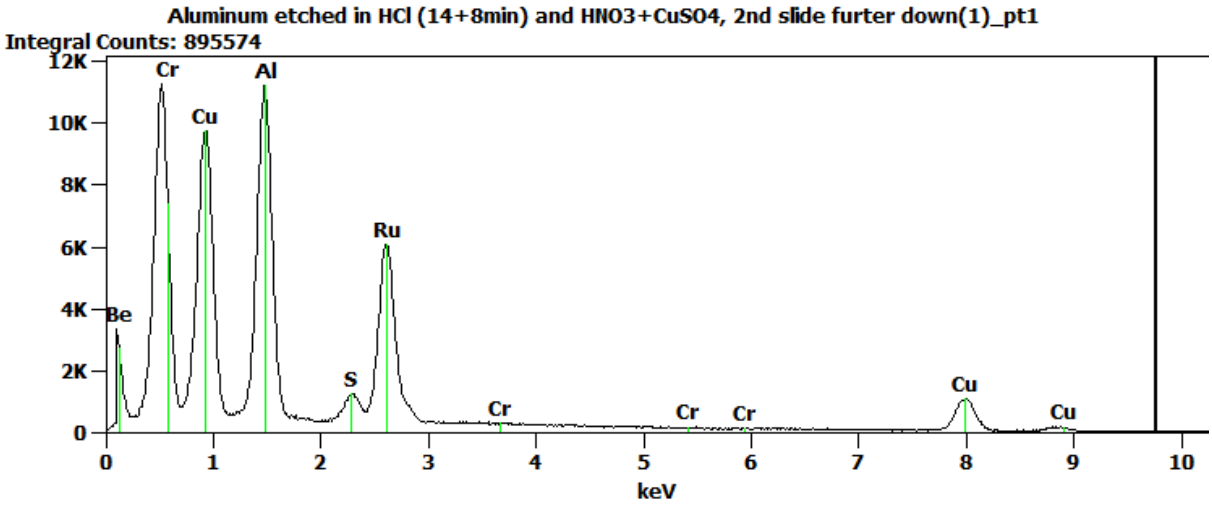

Figure 5.73. Elemental analysis of the second parallel aluminum slide etched in HCl for 22 minutes followed by immersion in HNO_3 + $CuSO_4$ for 6 minutes. The presence of beryllium is probably an instrument error.

Third parallel

The third parallel was also dropped into the solution of PDES and ethanol prior to electron microscopy images and elemental analysis, causing the etched areas described next to have one layer of coating during analysis. The gas bubbles formed at the bottom of the slide were removed due to stirring, causing a greater area of the slide to be etched.

Figure 5.74a shows an electron microscopy image of the third aluminum slide after etching in HCl for 22 minutes while stirring. The image is taken at the upper part of the slide. The surface appears to be completely etched and has a rough surface structure with no noticeable vertical lines. The surface features are about 1 μm.

Figure 5.74b shows an electron microscopy image of the third aluminum slide after etching in HCl for 22 minutes while stirring, followed by immersion in HNO_3 + $CuSO_4$ for 6 minutes while stirring. The surface appears to have a rough structure throughout, with bigger surface features than in Figure 5.74a.

The images in Figure 5.74 are taken with a secondary electron detector and 2000 times magnification. The accelerating voltage used for image a and b was 15.0 kV and 5.0 kV, respectively.

a) b)

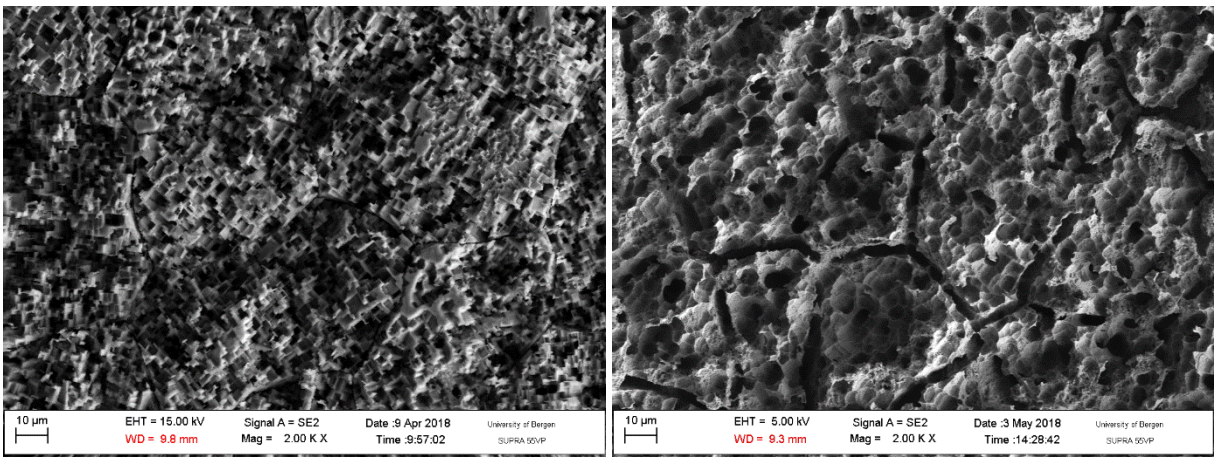

Figure 5.74. Scanning electron microscopy imaging of a) third parallel aluminum slide etched in HCl for 22 minutes while stirring b) third parallel aluminum slide etched in HCl for 22 minutes while stirring, followed by immersion in HNO_3 + $CuSO_4$ for 6 minutes while stirring.

Figure 5.75 shows an elemental analysis of the third parallel aluminum slide etched in HCl for 22 minutes while stirring, followed by immersion in HNO_3 + $CuSO_4$ for 6 minutes while stirring. The elemental analysis does not indicate the presence of any other elements than aluminum.

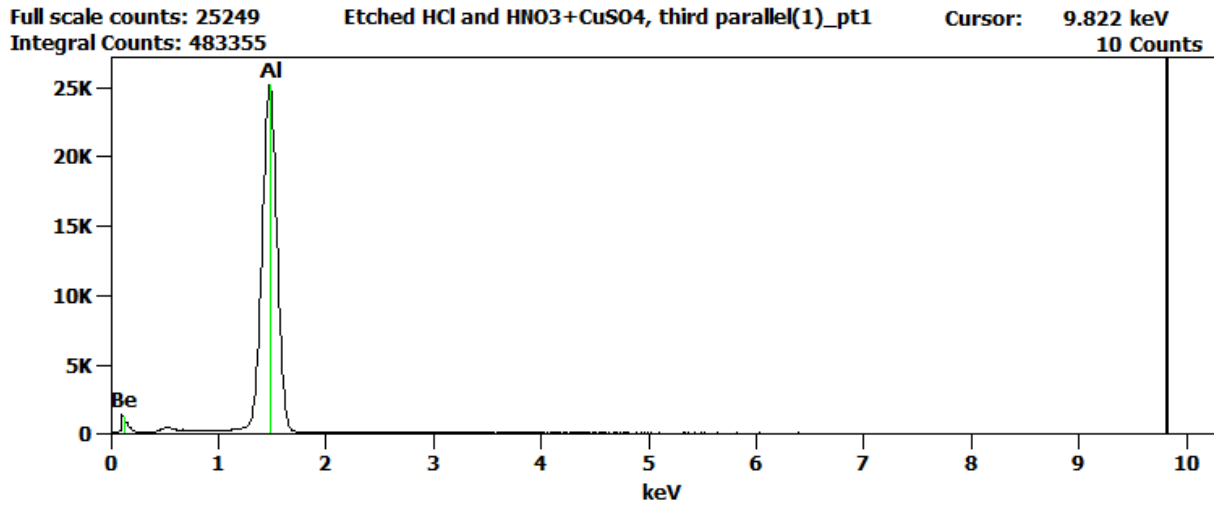

Figure 5.75. Elemental analysis of the third aluminum slide etched in HCl for 22 minutes while stirring, followed by immersion in HNO_3 + $CuSO_4$ for 6 minutes while stirring. The presence of beryllium is probably an instrument error.

The images in Figure 5.70, Figure 5.72, and Figure 5.74a are taken with a secondary electron detector, 2000 times magnification and an accelerating voltage of 15.0 kV. The image in Figure 5.74b is taken with 500 times magnification.

5.4.4 Etched and coated aluminum slide (22 minutes)

During dip-coating the solution of PDES and ethanol was left in an open beaker, causing evaporation of ethanol and a small increase in the concentration of PDES. After dip-coating there were precipitates in the solution from the aluminum slide. These precipitates could be copper particles from the aluminum slides.

First parallel

Figure 5.76 shows an electron microscopy image of the etched and coated first parallel aluminum slide. There are no visible signs of the coating, but the aluminum clearly shows an increase in etched surface further down on the slide.

The image in Figure 5.76 is taken with a secondary electron detector, 200 times magnification and an accelerating voltage of 15.0 kV.

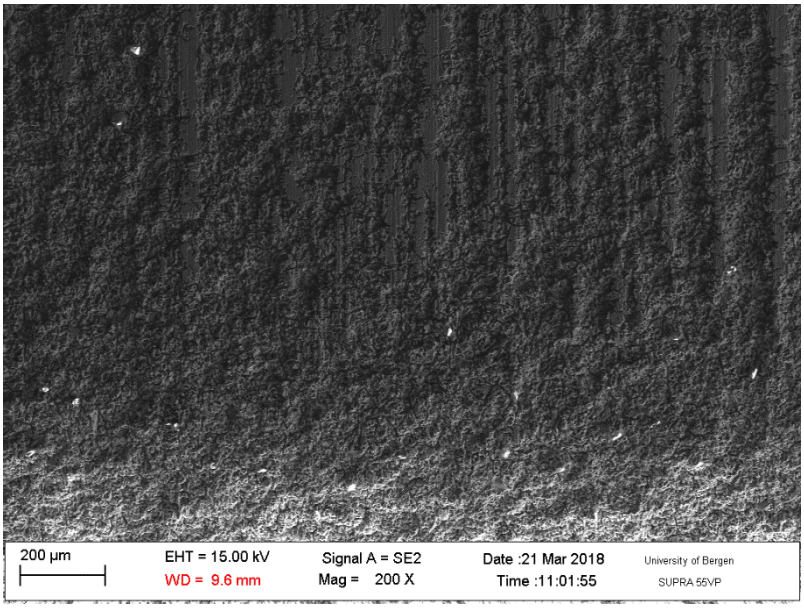

Figure 5.76. Scanning electron microscopy image of the etched and coated first parallel aluminum slide.

Figure 5.77 shows an elemental analysis of the etched and coated first parallel aluminum slide, with presence of aluminum and fluorine.

Contact angle measurements of the etched and coated first parallel aluminum slide shows that the slide is not wetted by water, diiodomethane or hexadecane. Figure 5.78 shows the optical

contact angle measurements for water, diiodomethane and hexadecane droplets with contact angles of 129.5°, 111.5° and 106.3°, respectively.

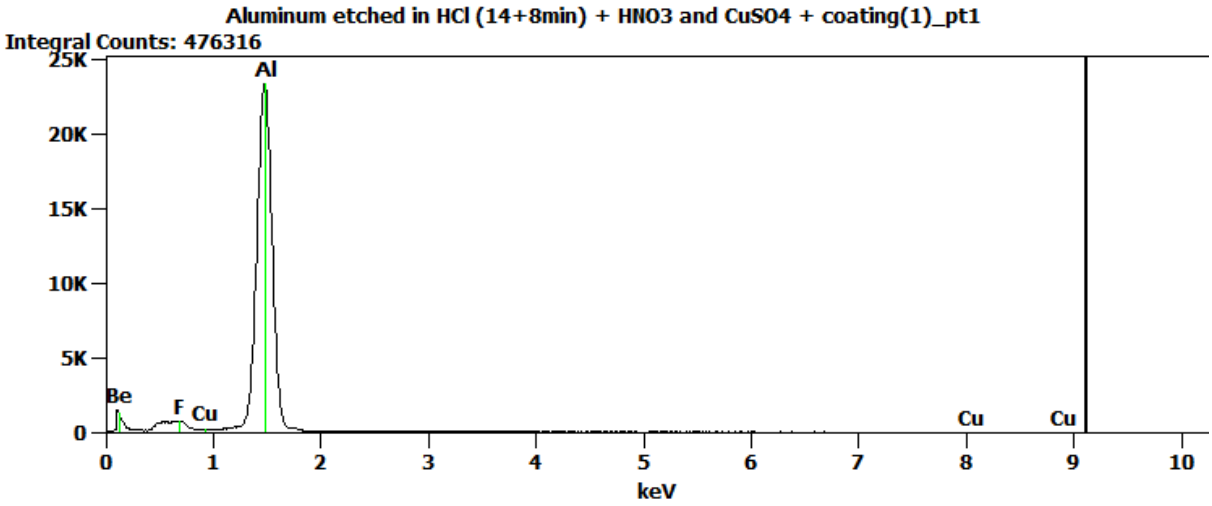

Figure 5.77. Elemental analysis of the etched and coated first parallel aluminum. The presence of beryllium is probably an instrument error.

The contact angle hysteresis for water, diiodomethane and hexadecane on the etched and coated first parallel aluminum slide is 35.04°, 19.21° and 45.71°, respectively.

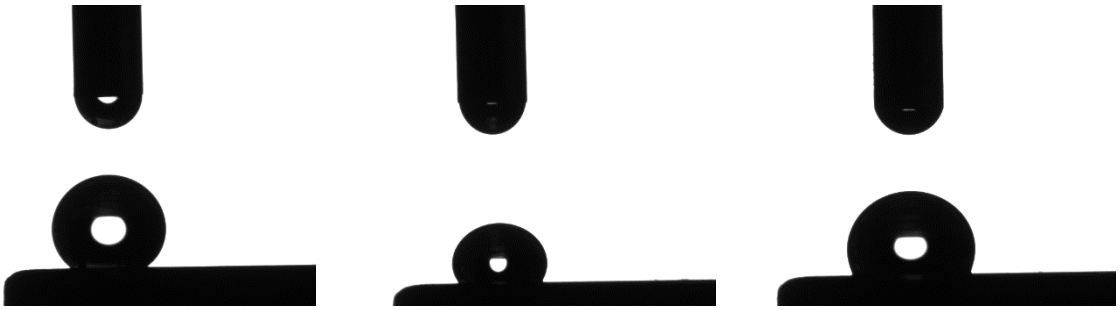

Figure 5.78. Optical contact angle measurements show water, diiodomethane and hexadecane droplets, respectively, deposited on the etched and coated first parallel aluminum slide.

The apparent surface energy of the first parallel etched and coated aluminum slide is estimated to be 4.47 mN/m.

Second parallel

Figure 5.79 shows an electron microscopy image of the etched and coated second parallel aluminum slide. The coated area looks smoother and there are no visible Cu-particles.

The image in Figure 5.79a is taken with a secondary electron detector, 200 times magnification and an accelerating voltage of 15.0 kV. Figure 5.79b is taken with 2000 times magnification.

a) **b)**

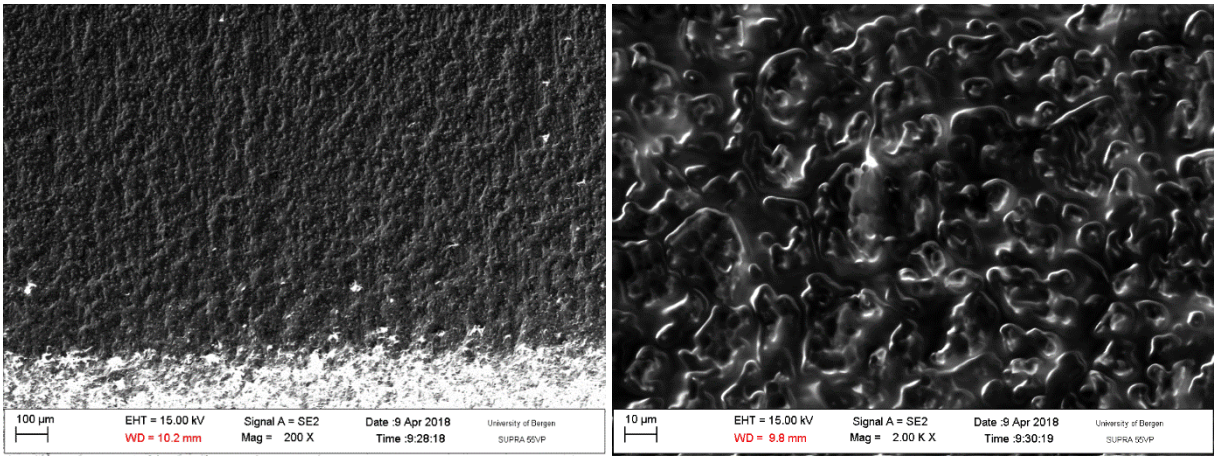

Figure 5.79. Scanning electron microscopy imaging of the etched and coated second parallel aluminum. Image is taken with a) 200 times magnification b) 2000 times magnification.

Figure 5.80 shows an elemental analysis of the etched and coated second parallel aluminum slide, with indicates the presence of silicon, chlorine, oxygen, carbon, fluorine and aluminum. This may imply the presence of PDES on the aluminum slide.

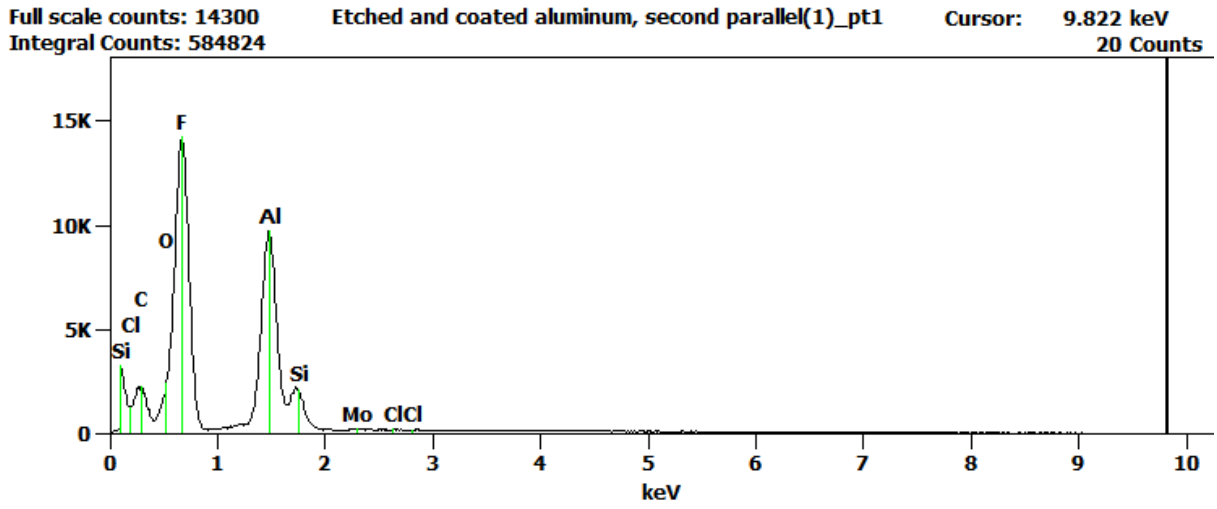

Figure 5.80. Elemental analysis of the etched and coated second parallel aluminum. The presence of beryllium is probably an instrument error.

Contact angle measurements of the etched and coated second parallel aluminum slide shows that the slide is not wetted by water, diiodomethane or hexadecane. Figure 5.81 show the optical

contact angle measurements for water, diiodomethane and hexadecane droplets with contact angles of 153.4°, 119.2° and 105.8°, respectively.

The contact angle hysteresis for water, diiodomethane and hexadecane on the etched and coated second parallel aluminum slide is 21.69°, 48.44° and 26.61°, respectively.

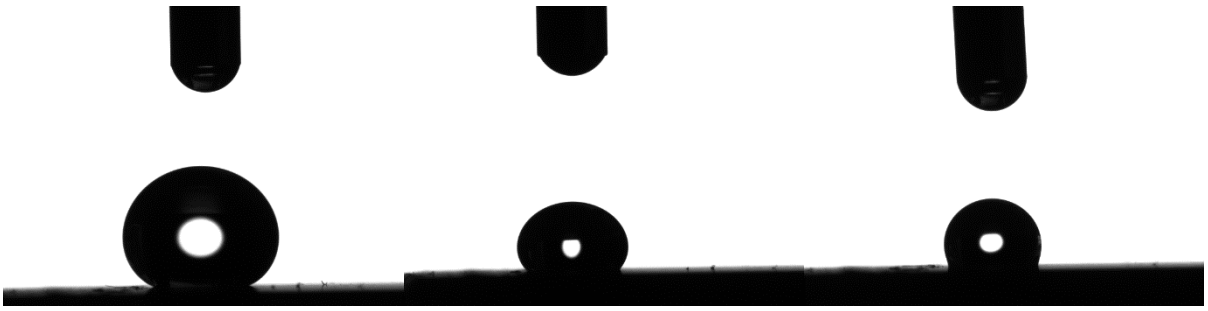

Figure 5.81. Optical contact angle measurements show water, diiodomethane and hexadecane droplets, respectively, deposited on the etched and coated second parallel aluminum slide.

The apparent surface energy of the etched and coated second parallel aluminum slide is estimated to be 4.85 mN/m.

Third parallel

Figure 5.82 shows an electron microscopy image of the third etched and coated aluminum slide. The brighter areas near the bottom of the image are caused by weak interactions between the platform conduction electrons in the instrument. The surface has a rough structure and there are no visible signs of the coating.

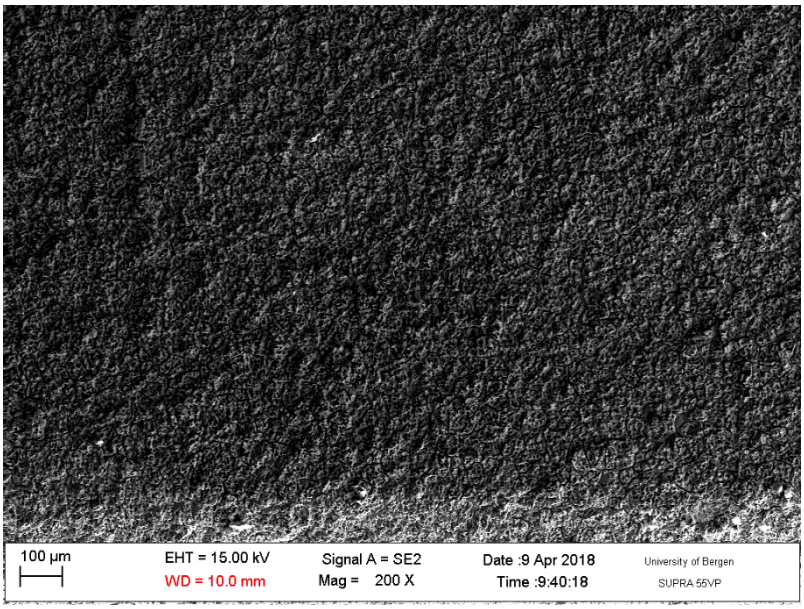

Figure 5.82. Scanning electron microscopy imaging of the etched and coated third parallel aluminum slide.

Figure 5.83 shows an elemental analysis of the etched and coated third parallel aluminum slide, which indicates the presence of silicon, fluorine and aluminum. This may imply the presence of PDES on the surface.

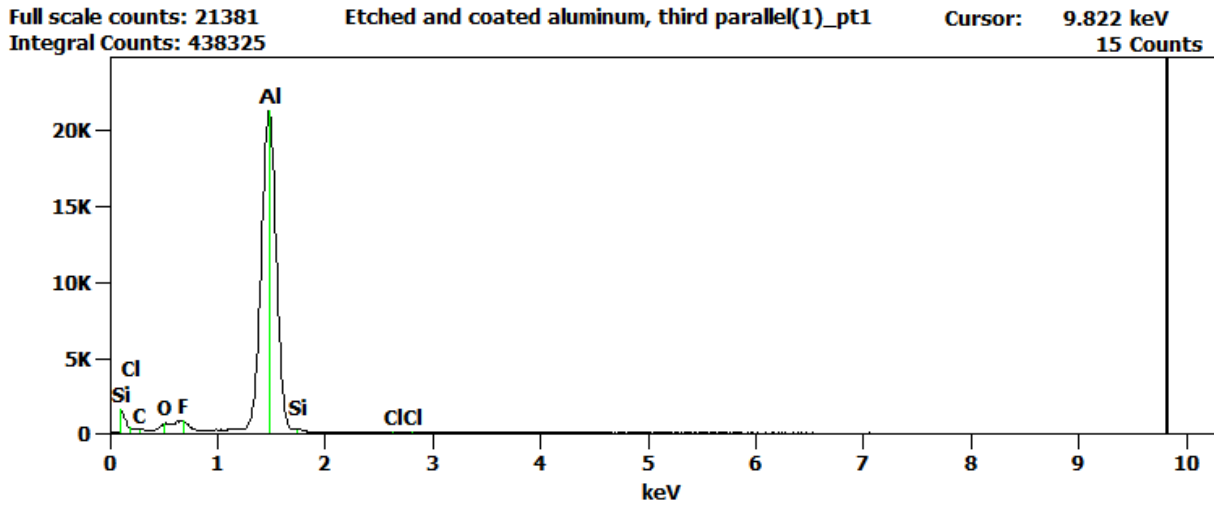

Figure 5.83. Elemental analysis of the etched and coated third parallel aluminum slide.

Contact angle measurements of the etched and coated third aluminum slide shows that the slide is not wetted by water or diiodomethane, and partially wetted by hexadecane. Figure 5.84 show the optical contact angle measurements with contact angles of 155.7°, 120.2° and 67.6°, respectively.

The contact angle hysteresis for water, diiodomethane and hexadecane for the etched and coated third parallel is 52.10°, 18.18° and 31.86°, respectively.

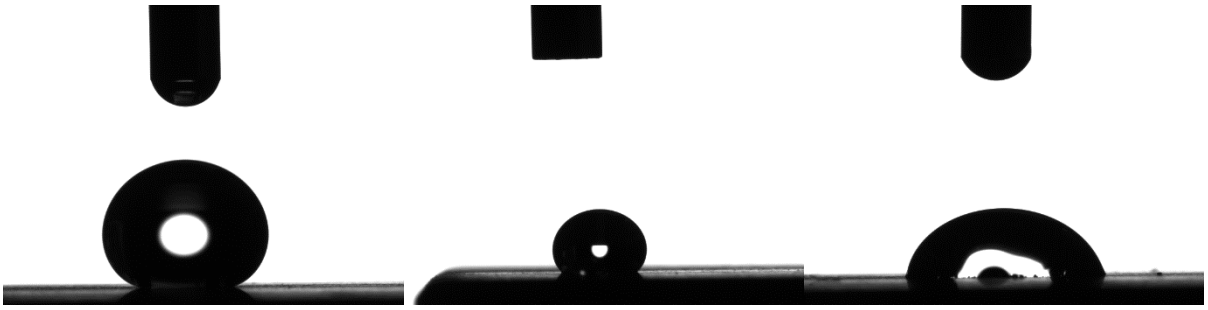

Figure 5.84. Optical contact angle measurements show water, diiodomethane and hexadecane, respectively, deposited on the etched and coated third parallel aluminum slide.

The apparent surface energy of the etched and coated third aluminum slide is estimated to be 11.66 mN/m.

6 Discussion

In the following chapter selected results from Chapter 5 are discussed. It begins by discussing the most repellent coatings made by the colloidal suspensions, followed by further analysis of the soot from heating silicon oil. Finally, the most successful treatments of aluminum (with regard to superamphiphobicity) are discussed. A table with the overview of the discussed findings is given at the end of the chapter.

6.1 Substrates Coated by Colloidal Suspensions

Based on work done by Zhou *et al.* [2], the suspensions were prepared using silica particles, since teflon particles were not available. This also lead to a lower amount of fluorine present. We investigated if it was possible to make a stable homogeneous suspension for dip-coating, and if the coating would be hierarchically structured. The aim was to let PDES/POCS bond/react with the silica particles. These particles would in turn interact with the diluted Capstone ST-110/100 and be stabilized, before deposition on the dip-coated substrates

From the results in chapter 5.2 we find that some of the suspensions show higher stability and the coatings present high contact angles. We choose to focus on these suspensions in the discussion. Other suspensions are unstable and the coatings give relatively low contact angles. Possible mechanisms for the formulation of the suspensions will be presented.

The same amount of silica particles was used in this experiment, as the amount of teflon particles used by Zhou *et al.*[2] This presented an obstacle when mixing the particles and PDES/POCS, because the volume of PDES/POCS was too small to mix with all the silica particles. This leaves us to assume that some particles probably never were in contact with PDES/POCS, others were partially in contact, and some were in complete contact with PDES/POCS.

All eight colloidal suspensions were non-optimal (i.e. of poor quality) regarding homogeneity and stability. The samples containing Capstone ST-100 gave more homogenous suspensions with both PDES and POCS, than Capstone ST-110. The combination of hydrophilic silica particles and Capstone ST-100 gave the most homogenous and stable suspension, for both POCS and PDES.

Zhou *et al.*[9] suggested a possible mechanism for the syntheses of the suspension (see Figure 6.1). We may assume that our synthesis had more or less a similar reaction, substituting teflon particles with silica particles.

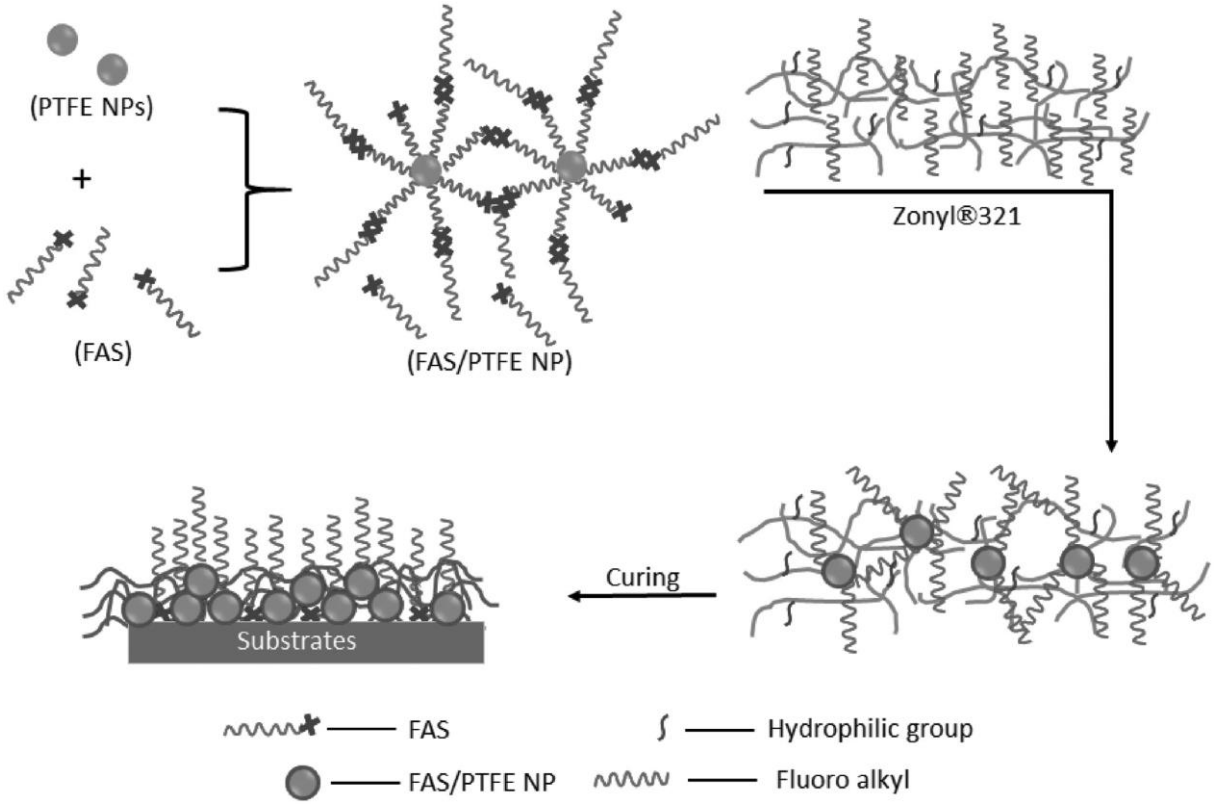

Figure 6.1. Illustration of possible interaction. We substituted teflon with silica particles, and Zonyl®321 with Capstone. Figure reprinted from Zhou *et al.*[2]

According to the data sheets[34-35], both Capstone ST-100 and ST-110 are sustainable replacements for Zonyl®321. They are based on short-chain molecules that cannot break down to toxic compounds like Zonyl®321 can. Zonyl®321's possible chemical structure is found in Figure 6.2. It is a fluorinated co-polymer comprising a fluoropolymer core and a polyurethane shell[2]. The structure or composition of the Capstone fluorochemicals are not given, but we may assume they have a structure similar to that of Zonyl321 (see Figure 6.2).

The visible observations and SEM imaging show that the coated layers have various thicknesses. This is understandable from the instability of the suspensions. They would either precipitate, or a layer of foam would cover the suspension during immersion of the substrates. Particles from the foam-layer is left on the substrates when they are withdrawn. Substrates that are dip-coated in the suspensions with precipitation obtained thinner coatings due to less particles in the suspension.

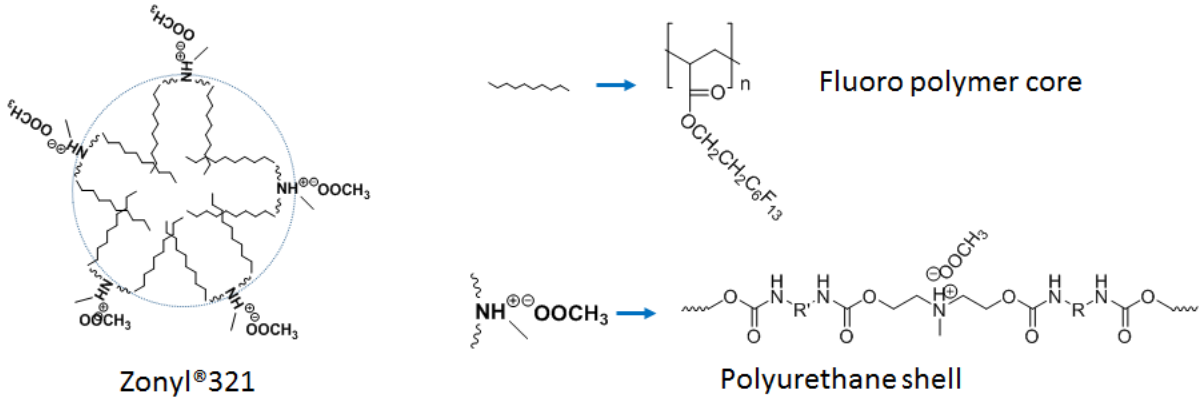

Figure 6.2. Illustration of the possible chemical structure of Zonyl®321. It consists of a fluorinated co-polymer comprising fluoropolymer core and polyurethane shell. Figure reprinted from Zhou *et al.*[2]

White areas in the SEM imaging show that the interactions between the substrate and some of the thicker coatings were too weak to get proper images. This may suggest that some of the coating adheres poorly to the substrates[36]. This was not seen with the coated steel, which implies a higher affinity for the coatings on steel substrates. On the substrates with thin coatings, both areas without detectable particles and areas of randomly scattered particles were observed.

PDES (1H, 1H, 2H, 2H-perfluorodecyl-triethoxysilane)

The system based on hydrophilic silica particles,100-OX50(PDES), is the most stable and homogenous of the PDES suspensions. The coating shows higher affinity to the steel substrate compared to the glass substrate, resulting in greater amounts of fluorine present on steel. Never the less, both coated substrates presents a low apparent surface energy, and hydrophobicity and oleophobicity for the tested liquids. The lack of fluorine present in Figure 5.21 may suggest that the coated layer is relatively thin, hence causing it to be neglected when displaying the results. The elemental analysis is estimated to penetrate 2 μm in to the sample, and a relatively big amount of glass substrate will be detected.

High contact angle hysteresis for the coated substrates suggests a surface structure where the liquids can partially penetrate the surface. This may imply relatively large spacing between the peaks (pitch value) on the surface. This can be described by Cassie wetting regime. The steel surface has a rougher surface structure, as seen in Figure 5.3, which will increase the contact area with the liquids. This could explain why the coated steel substrates give higher contact angle hysteresis than the same coating on glass substrates.

The rest of the suspensions show more precipitation, and less suspended particles. Some of the coatings show high values of fluorine, which may be from Capstone in the suspension that has adhered directly on the substrates. The steel substrates typically show more fluorine present from elemental analysis, though this does not give a higher contact angle than for coatings on glass substrates. The apparent surface energies for the coated steel surfaces are lower than for the respective coated glass substrates. This is likely caused by higher amount of fluorine present.

The findings discussed may suggest that the suspension with PDES does not provide a hierarchical surface structure that promotes superamphiphobicity. The relatively large contact angles may occur because of the coatings roughness and low apparent surface energy due to the presence of fluorine. It is not clear whether PDES and the silica particles has reacted in the desirable manner, but the contact angles do not suggest this.

POCS (1H, 1H, 2H, 2H-perfluorooctyl-trichlorosilane)

The system based on hydrophilic silica particles, 100-OX50(POCS), is the most stable and homogenous suspension, yet this coating presents lower contact angles and higher apparent surface energies than the other suspensions with POCS. The coatings based on this system were thick due to foam formation, showing superhydrophobicity and oleophobicity for diiodomethane on both substrates and the presence of fluorine. The high contact angle hysteresis suggests that the surface structures are not hierarchical.

The system based on hydrophilic silica particles, 110-OX50(POCS), and hydrophobic silica particles, 100-R972(POCS), showed superhydrophobicity and low contact angle hysteresis on the glass substrate, implying that water could follow Cassie-Baxter wetting regime and give self-cleaning properties. Low contact angle hysteresis is not observed for the same coatings on steel substrates, indicating a different wetting regime. Both coatings have low apparent surface energies and shows the presence of fluorine, which is likely to contribute to the high contact angles. The rough structures on the steel surfaces may contribute to give the coatings larger pitch values and higher contact angle hysteresis.

The findings above suggest that the contact angles are dependent on the coatings apparent surface energy, which may be assumed to be more or less inversely proportional to the amount of fluorine present. We see no evidence that the most stable and homogenous suspensions returned coatings with hierarchical surface structure. This suggests that the suspension did not react as described in Figure 6.1, and that the fluorine present mainly originates from Capstone.

6.2 Silicon Soot Coated Substrates

Based on work done by Long *et al.*[3] we used one-step thermal treatment of silicon oil and Sylgard 184 to deposit soot directly on glass and steel substrates. We investigated the possibility for making a coating with the same type of topography as Long *et al.*[3], by using simple laboratory equipment and identical parameters for heating oil. Pending the arrival of Sylgard 184, we used Silicon Oil DC 200 to make the soot coatings. Silicon Oil DC 200 has a viscosity of 30 000 mPas, while Sylgard 184 has a viscosity of 4000 – 6500 mPas. Both compounds have the same monomers, but based on the viscosity assessments, we may assume that Sylgard 184 consists of shorter polymers.

Long *et al.*[3] presents results showing the temperature dependence of the soot structure. Temperatures below 300°C leaves the soot loosely packed with large gaps among the particles. This caused a liquid with surface tension of 48.4 mN/m to easily penetrate the structure similar to a Wenzel wetting regime. Heating temperatures of 300°C-400°C increase the decomposition rate of the silicon oil, resulting in denser deposition of soot. Therefore, the gaps among the soot particles becomes much narrower. This may cause a re-entrant geometry that traps air under the droplet, and it prevents liquids with a minimal surface tension of 48.4 mN/m from penetrating the structure. This can be described by a Cassie-Baxter wetting regime. No liquids with surface tension lower than 48.4 mN/m was repelled by the soot presented by Long e*t al.*[3] Therefore, this coating is not expected to show oleophobicity towards hexadecane.

A tube furnace was used in our experiment. When a sample is placed inside the furnace it is not possible to determine the exact location, nor to repeat the same position for the following samples. Differences of 1 cm may cause visible changes in the amount of heat a sample has been exposed to. This can be observed since oils with more heat exposure turn solid, while at lower temperatures it remains liquid and little soot is formed. This leaves the samples heating to be unprecise, and we can assume that the experiments were performed at different temperatures than intended.

Silicon oil DC 200

Figure 5.54 shows the soot particles on the glass slide. The size and density of the particles appears to be similar to the superhydrophobic and superoleophobic (for liquids with a surface tension of 48.4 mN/m and higher) soot presented by Long *et al.*[3] While it was not possible to detect soot particles on the steel substrate from visible observations or SEM imaging, both

coated substrates show superhydrophobicity with a low contact angle hysteresis and a high apparent surface energy (but lower than waters' surface tension). This suggest that the soot deposited on the steel substrate has a similar structure, and Cassie-Baxter wetting regime may describe waters behavior on the soot.

Contact angle measurements for diiodomethane on both coated substrates indicates that the pitch value in the soot is too large, so it will not trap enough air to repel liquids with surface energies close to 48.4 mN/m. This may indicate that the oil did not reach temperatures above 300°C, and diiodomethane follow a Wenzel wetting regime.

The findings indicate that Silicon Oil DC 200 has similar behavior as the oil used by Long *et al.*[3], Sylgard 184, and that type of substrate does not affect the behavior of the soot. The soot may not have been heated at high enough temperatures to create a surface structure that sufficiently traps air and repels lower surface tension liquids, without further decreasing the apparent surface energy.

Sylgard 184

Electron microscopy imaging of soot from heating Sylgard 184 on glass and steel substrates did not have sufficient quality to return any information about the soot particles. However, contact angle measurements reveal superhydrophobicity and low contact angle hysteresis on soot deposited on the glass slide, indicating similar particle structure as for Silicon Oil DC 200. The apparent surface energy of the soot is about 50 mN/m lower than for water, and is likely contributing to the superhydrophobicity of the surface.

Soot deposited on the steel substrate did not show superhydrophobicity, indicating that the heating did not reach sufficiently high temperatures.

These findings indicate the same behavior as for Silicon Oil DC 200, suggesting that polymer length does not substantially affect the wetting properties on the soot surface.

6.3 Etched Aluminum Slides

Based on work done by Peng *et al.*[4] we used $CuSO_4$ and HNO_3 for making nanostructures after etching in HCl. Although copper sulfate was used instead of copper nitrate, we assume this will have a negligible influence on the accumulation of copper particles on to the aluminum surface.

We found that an increased etching period in HCl to 22 minutes while stirring, was most sufficient in order to achieve a homogenous micro structured surface.

The visible copper particles on the second parallel aluminum slide disappeared after coating, which suggests that they are poorly adhered to the surface. The change in surface structure after immersion in PDES and ethanol for an uncertain period of time, may be caused by a reaction between aluminum and PDES, or absorption of PDES to the aluminum surface. The high amounts of fluorine present contribute to the low apparent surface energy. The surface is superhydrophobic and oleophobic, with high contact angle hysteresis. This suggests that there is no hierarchical structure present, which is expected after the apparent loss of copper particles. These findings suggest that the surface fits a Cassie impregnated wetting regime.

The third aluminum parallel shows presence of fluorine and hence a low apparent surface energy. The contact angle measurements show that the surface is superhydrophobic with a high contact angle hysteresis. This suggests that there is a roughness in the structure, but it does not imply a hierarchical structure. The lack of traceable copper particles supports this assumption. Waters wetting regime on this substrate can be described by Cassie impregnated, because of the high contact angles and high contact angle hysteresis.

The findings above suggest that the copper-particles adheres too poorly to the aluminum surface for a hierarchical structure to be made. Without a hierarchical structure, liquids with low surface tension can wet the surface structure. The coating with fluorine promotes superhydrophobicity because of a low apparent surface energy, but the lack of low contact angle hysteresis prevents self-cleaning properties.

Table 6.1. Overview of the discussed findings.

Method	**Substrate**		**Superamphiphobicity observed?**	**Superhydrophobicity observed?**
Fluorinated silica particle coating	Glass		No	Yes (POCS), no (PDES)
	Steel		No	Yes (POCS), no (PDES)
Soot formation silicon oil	Silicon Oil DC 200	Glass	No	Yes
		Steel	No	Yes
	Sylgard 184	Glass	No	Yes
		Steel	No	No
Etching/cupper NP deposition	Aluminum		No	Yes, no (first parallel)

7 Conclusions and Future Work

In this thesis we have explored three different methods for providing superamphiphobic surfaces on various substrates. The aim was to investigate whether the methods were applicable to more substrate types than used in the original works, and whether the superamphiphobic properties could be retained if fluorinated compounds were excluded from the coating formulations.

Glass and steel substrates were dip-coated in a waterborne coating system consisting of fluorinated compounds and silica particles (replacing Teflon nanoparticles in the original work), in order to investigate if this system could provide a hierarchically structured superamphiphobic coating. We found that neither PDES (1H, 1H, 2H, 2H-perfluorodecyl-triethoxysilane) nor POCS (1H, 1H, 2H, 2H-perfluorooctyl-trichlorosilane) provided stable colloidal suspensions with silica particles, and no indication of hierarchical surface structures was found from the coatings. The ratio between silica particles and volume of PDES and POCS was not optimal for making suspensions. This should be adjusted in order to identify whether the challenge in making these suspensions lay with the lack of contact between all particles and PDES/POCS, or that the silica particles will not be stabilized by these components.

Two types of silicon oil with different viscosity underwent similar thermal treatment to deposit soot with intend to induce superamphiphobic properties on different substrates. The soot was characterized with respect to surface structure and wetting properties, and compared. There are no indications that the substrate material or oil viscosity affects the properties of the deposited soot. We were not able to replace the results from the original work, the wetting behavior suggests that the spacing we achieved between the soot particle are too large in order to gain superamphiphobicity. The spacing may be reduced with higher temperatures, and superamphiphobicity may be achieved. For further experiments, efforts should be made to have a stricter temperature control during the heating/deposition process. Variations in temperature and time can be used to investigate any difference in behavior for the different viscosity oils.

Aluminum were etched in HCl and copper particles subsequently deposited onto the aluminum in order to investigate if this would provide a hierarchical surface structure. The surface was coated to lower the surface energy. Poor adhesion of the copper particles to the aluminum surface seemed to prevent the formation of a hierarchical surface structure. Comparing SEM

images from our work with the original work we find indications that copper particles were lost during coating. Further investigation into the effect of using $CuSO_4$ instead of $Cu(NO_3)_2$ as the source for copper particles may be pursued.

To summarize, we conclude that in order to fabricate hierarchical surface structures, all parameters must be carefully controlled throughout the process. Without fluorinated compounds for giving a sufficiently low surface energy of the material in contact with liquids, superamphiphobicity seems to be an almost impossible task.

8 Bibliography

1. Bhushan, B., *Biomimetics - Bioinspired Hierarchical-Structured Surfaces for Green Science and Technology*. Springer: 2012a; p 23-24.
2. Zhou, H.; Wang, H. X.; Niu, H. T.; Zhao, Y.; Xu, Z. G.; Lin, T., A Waterborne Coating System for Preparing Robust, Self-healing, Superamphiphobic Surfaces. *Adv Funct Mater* **2017,** *27* (14).
3. Long, M. Y.; Peng, S.; Yang, X. J.; Deng, W. S.; Wen, N.; Miao, K.; Chen, G. Y.; Miao, X. R.; Deng, W. L., One-Step Fabrication of Non-Fluorinated Transparent Super Repellent Surfaces with Tunable Wettability Functioning in Both Air and Oil. *Acs Appl Mater Inter* **2017,** *9* (18), 15857-15867.
4. Peng, S.; Bhushan, B., Mechanically durable superoleophobic aluminum surfaces with microstep and nanoreticula hierarchical structure for self-cleaning and anti-smudge properties. *J Colloid Interf Sci* **2016,** *461*, 273-284.
5. Neinhuis, C.; Barthlott, W., Characterization and distribution of water-repellent, self-cleaning plant surfaces. *Ann Bot-London* **1997,** *79* (6), 667-677.
6. Bhushan, B., *Biomimetics - Bioinspired Hierarchical-Structured Surfaces for Green Science and Technology*. Springer: 2012i; p 27-60.
7. Bhushan, B., *Biomimetics - Bioinspired Hierarchical-Structured Surfaces for Green Science and Technology*. Springer: 2012b; p 28.
8. Bhushan, B., *Biomimetics - Bioinspired Hierarchical-Structured Surfaces for Green Science and Technology*. Springer: 2012c; p 247-252.
9. Yang, J.; Zhang, Z. Z.; Xu, X. H.; Zhu, X. T.; Men, X. H.; Zhou, X. Y., Superhydrophilic-superoleophobic coatings. *J Mater Chem* **2012,** *22* (7), 2834-2837.
10. Berg, J. C., *An Introduction to Interfaces & Colloids, The Bridge to Nanoscience*. World Scientific Publishing Co. Pte. Ltd: 2010a; p 218-227.
11. Squadrone, S.; Ciccotelli, V.; Prearo, M.; Favaro, L.; Scanzio, T.; Foglini, C.; Abete, M. C., Perfluorooctane sulfonate (PFOS) and perfluorooctanoic acid (PFOA): emerging contaminants of increasing concern in fish from Lake Varese, Italy. *Environ Monit Assess* **2015,** *187* (7).
12. Guan, K. H., Relationship between photocatalytic activity, hydrophilicity and self-cleaning effect of TiO2/SiO2 films. *Surf Coat Tech* **2005,** *191* (2-3), 155-160.
13. Tourkine, P.; Le Merrer, M.; Quere, D., Delayed Freezing on Water Repellent Materials. *Langmuir* **2009,** *25* (13), 7214-7216.
14. Zhao, K.; Liu, K. S.; Li, J. F.; Wang, W. H.; Jiang, L., Superamphiphobic CaLi-based bulk metallic glasses. *Scripta Mater* **2009,** *60* (4), 225-227.
15. Liu, Y.; Cao, H. J.; Chen, S. G.; Wang, D. A., Ag Nanoparticle-Loaded Hierarchical Superamphiphobic Surface on an Al Substrate with Enhanced Anticorrosion and Antibacterial Properties. *J Phys Chem C* **2015,** *119* (45), 25449-25456.
16. Fujii, T.; Aoki, Y.; Habazaki, H., Fabrication of Super-Oil-Repellent Dual Pillar Surfaces with Optimized Pillar Intervals. *Langmuir* **2011,** *27* (19), 11752-11756.
17. Berg, J. C., *An Introduction to Interfaces & Colloids, The Bridge to Nanoscience*. World Scientific Publishing Co. Pte. Ltd: 2010b; p 26-42.
18. contributors, W. C. File:WassermoleküleInTröpfchen.svg. https://commons.wikimedia.org/w/index.php?title=File:Wassermolek%C3%BCleInTr%C3%B6pfchen.svg&oldid=71884170 (accessed 12 December 2017 12:32 UTC).

19. Bhushan, B., *Biomimetics - Bioinspired Hierarchical-Structured Surfaces for Green Science and Technology*. Springer: 2012d; p 247.
20. Krüss, So You Want to Measure Surface Energy? , 8.
21. K. J. Owens, D.; Wendt, R. C. J., *Owens, D. K. & Wendt, R. C. Estimation of the surface free energy of polymers. J. Appl. Polym. Sci. 13, 1741-1747*. 1969; Vol. 13, p 1741-1747.
22. Bhushan, B., *Biomimetics - Bioinspired Hierarchical-Structured Surfaces for Green Science and Technology*. Springer: 2012e; p 42.
23. Bhushan, B., *Biomimetics - Bioinspired Hierarchical-Structured Surfaces for Green Science and Technology*. Springer: 2012f; p 35-37.
24. Bhushan, B., *Biomimetics - Bioinspired Hierarchical-Structured Surfaces for Green Science and Technology*. Springer: 2012g; p 44.
25. Bhushan, B., *Biomimetics - Bioinspired Hierarchical-Structured Surfaces for Green Science and Technology*. Springer: 2012h; p 37-60.
26. Berg, J. C., *An Introduction to Interfaces & Colloids, The Bridge to Nanoscience*. World Scientific Publishing Co. Pte. Ltd: 2010c; p 223-227.
27. Bhushan, B., Theme issue 'Bioinspired hierarchically structured surfaces for green science' compiled and edited by Bharat Bhushan Preface. *Philos T R Soc A* **2016,** *374* (2073).
28. Bhushan, B., *Biomimetics - Bioinspired Hierarchical-Structured Surfaces for Green Science and Technology*. Springer: 2012j; p 250-252.
29. Brown, P. S.; Bhushan, B., Designing bioinspired superoleophobic surfaces. *Apl Mater* **2016,** *4* (1).
30. GmbH, D. I., Operating manual OCA 15Pro. 2013.
31. Schmitt, M.; Heib, F., High-precision drop shape analysis on inclining flat surfaces: Introduction and comparison of this special method with commercial contact angle analysis. *J Chem Phys* **2013,** *139* (13).
32. Bergen, U. o. Skanningelektronmikroskop. http://www.uib.no/elmi/56375/skanningelektronmikroskop.
33. Cras, J. J.; Rowe-Taitt, C. A.; Nivens, D. A.; Ligler, F. S., Comparison of chemical cleaning methods of glass in preparation for silanization. *Biosens Bioelectron* **1999,** *14* (8-9), 683-688.
34. DuPont, Capstone ST-100. In *Penetrating Sealer For Porous Surfaces, Technical Information*, 2009.
35. DuPont, Capstone ST-110. In *Penetrating Sealer For Porous Surfaces*, 2010.
36. JEOL, A Guide To Scanning Microscope Observation. 25.01.2018 ed.; 2018; p 36.

Appendix A

Images of treated substrates

A.1 PDES coated substrates

Figure A.1. 110-OX50(PDES) coatings.

Figure A.2. 110-R972(PDES) coatings.

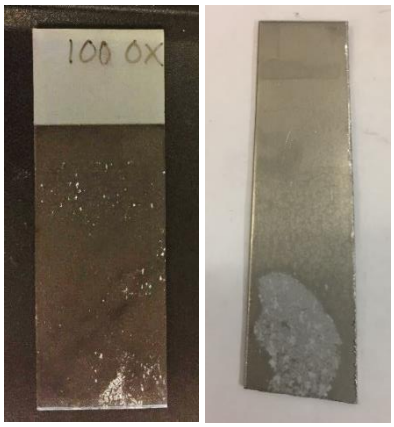

Figure A.3. 100-OX(PDES) coatings.

Figure A.4. 100-R972(PDES) coatings.

A.2 POCS coated substrates

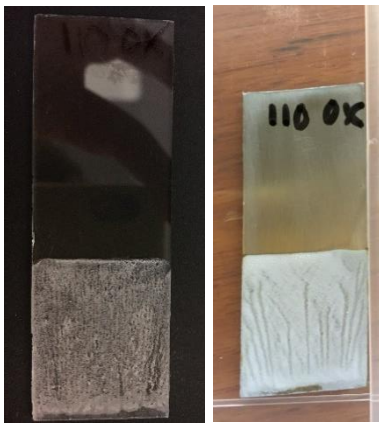

Figure A.5. 110-OX50(POCS) coatings

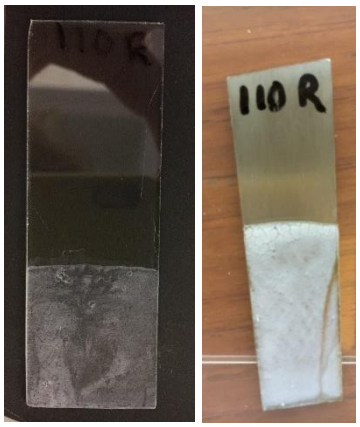

Figure A.6. 110-R972(POCS) coatings

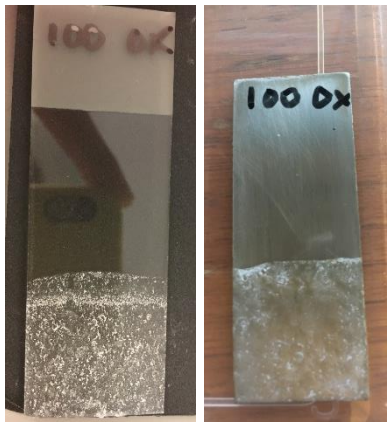

Figure A.7. 100-OX50(POCS) coatings.

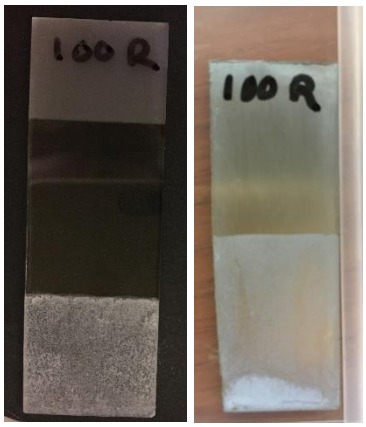

Figure A.8. 100-R972(POCS) coatings.

A.3 Soot deposition

Figure A.9. Silicon oil DC 200 coating.

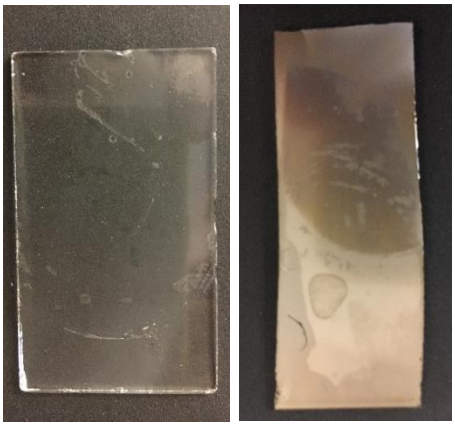

Figure A.10. Sylgard 184 coating.

A.4 Treated aluminum slides

Figure A.11. Aluminum slide etched 10 minutes in and 6 minutes in HNO_3 + $CuSO_4$ followed by coating in a solution of PDES and ethanol.

Figure A.12. Aluminum slide parallels one, two and three, respectively, etched 22 minutes in HCl and 6 minutes in HNO_3 + $CuSO_4$, followed by coating in a solution of PDES and ethanol.

Appendix B

Contact angle hysteresis graphs

B.1 Substrates

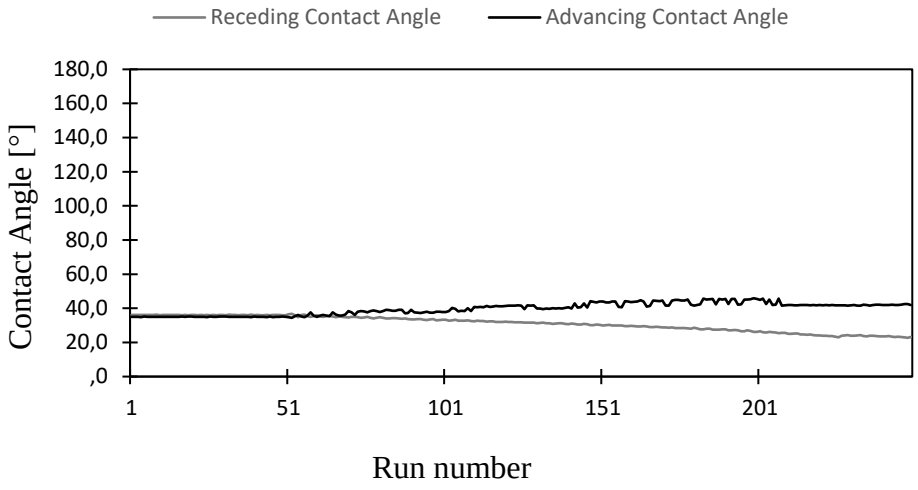

Figure B.1. Tilted glass slide with diiodomethane droplet.

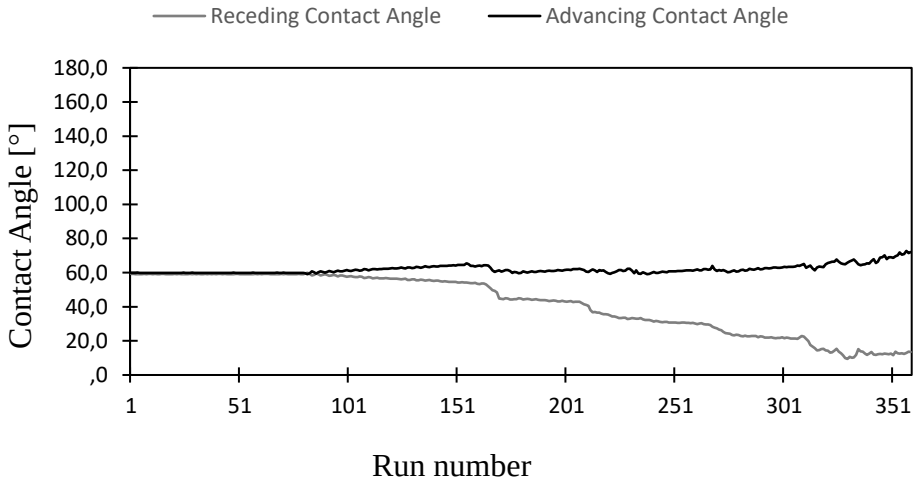

Figure B.2. Tilted steel slide with diiodomethane droplet.

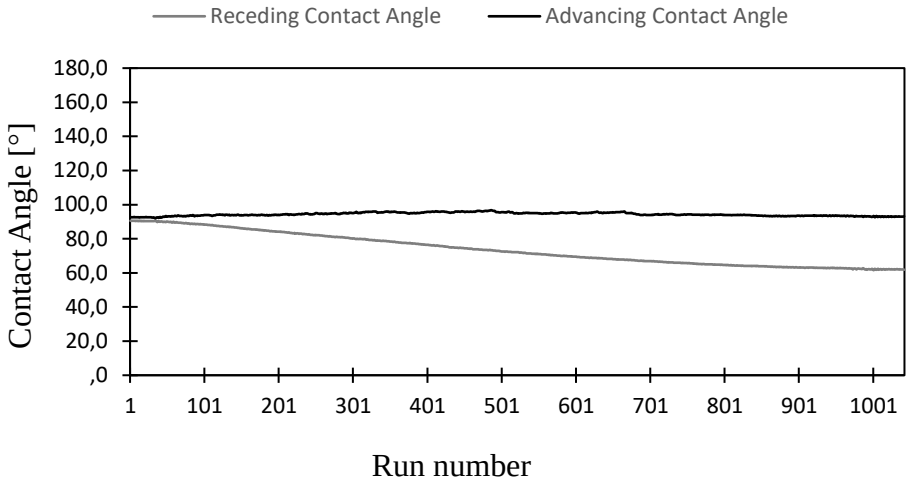

Figure B.3. Tilted steel slide with water droplet.

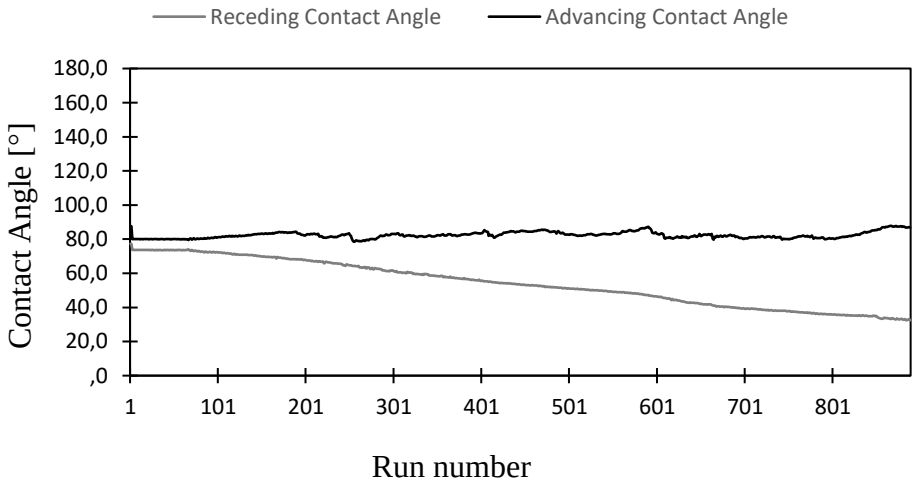

Figure B.4. Tilted aluminum slide with water droplet.

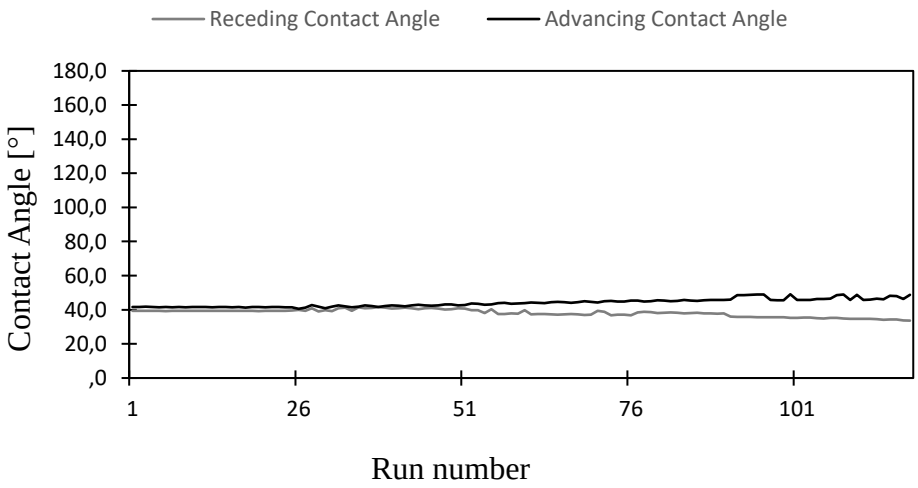

Figure B.5. Tilted aluminum slide with diiodomethane droplet.

B.2 PDES

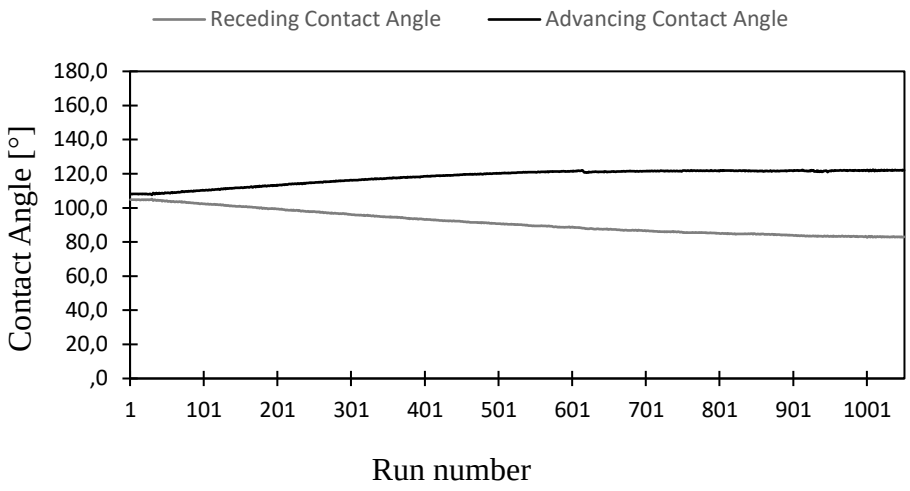

Figure B.6. Tilted 110-OX50(PDES) coated glass slide with water droplet.

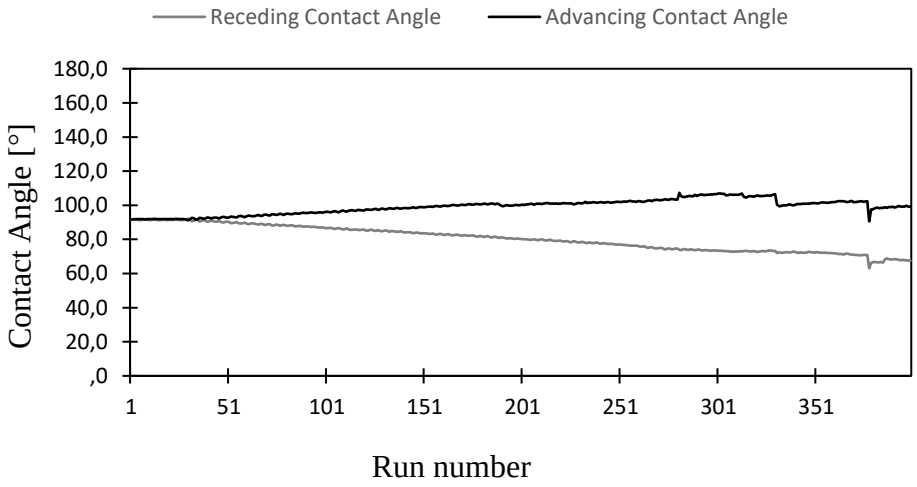

Figure B.7. Tilted 110-OX50(PDES) coated glass slide with diiodomethane droplet.

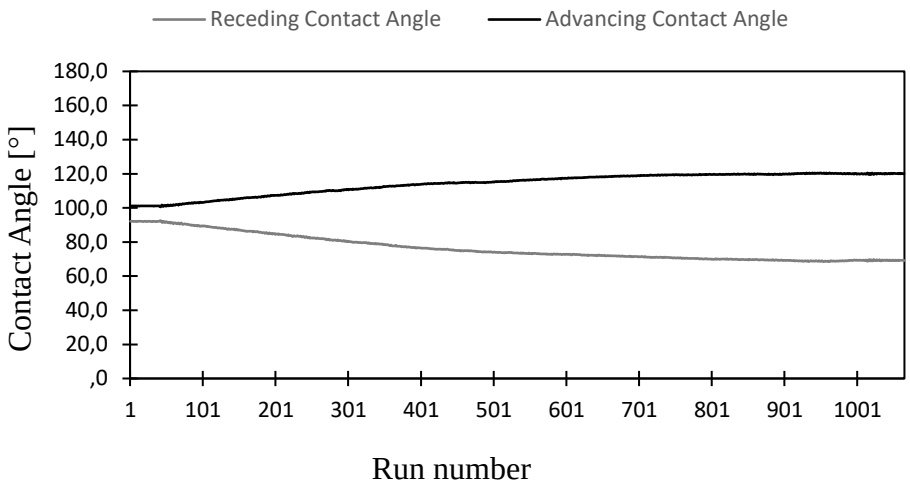

Figure B.8. Tilted 110-OX50(PDES) coated glass slide with hexadecane droplet.

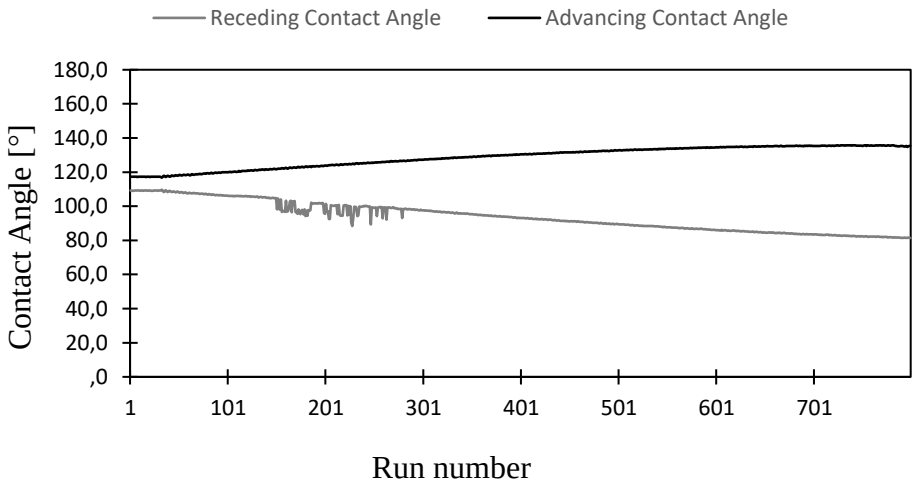

Figure B.9. Tilted 110-OX50(PDES) coated steel slide with water droplet.

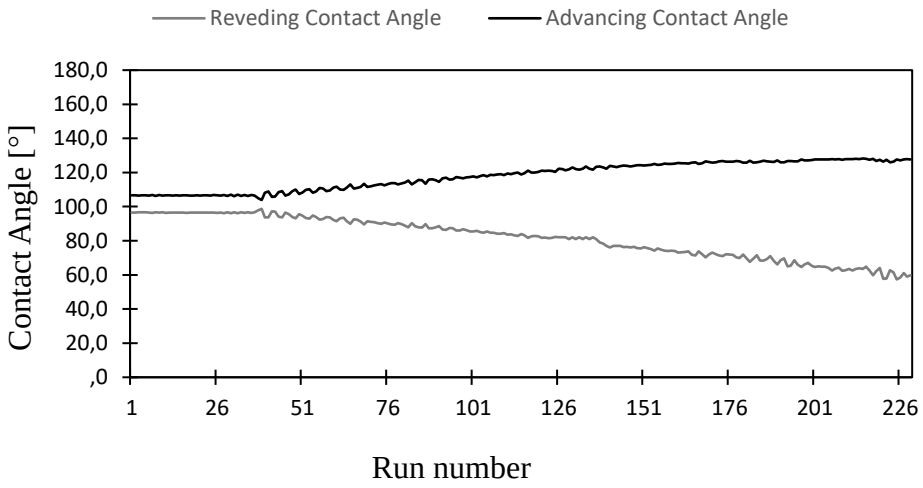

Figure B.10. Tilted 110-OX50(PDES) coated steel slide with diiodomethane droplet.

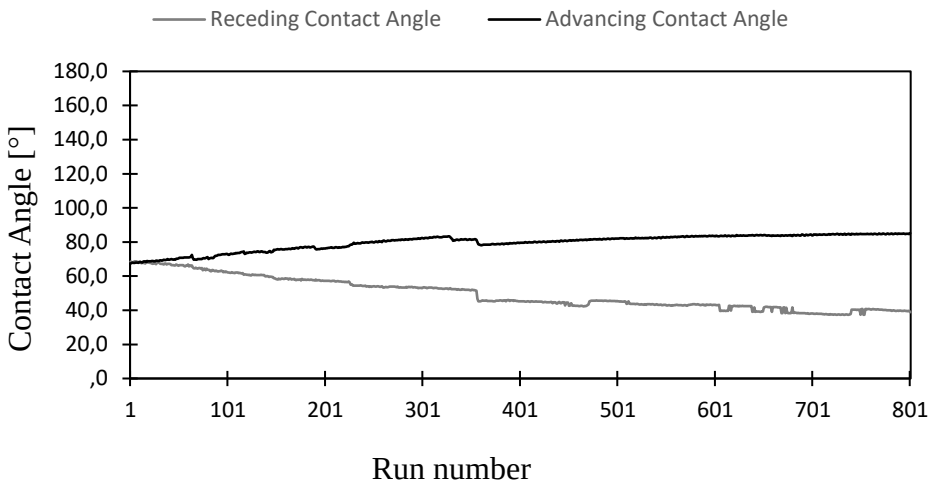

Figure B.11. Tilted 110-OX50(PDES) coated steel slide with hexadecane droplet.

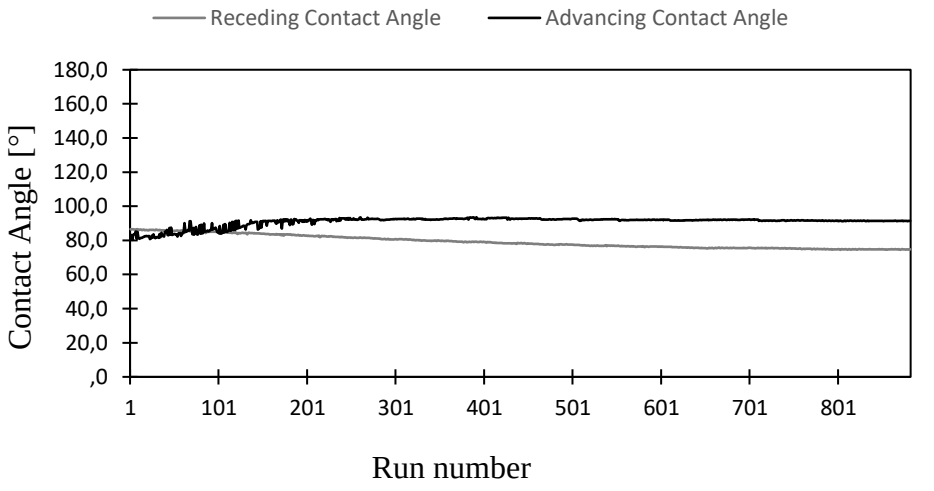

Figure B.12. Tilted 110-R972(PDES) coated glass slide with water droplet.

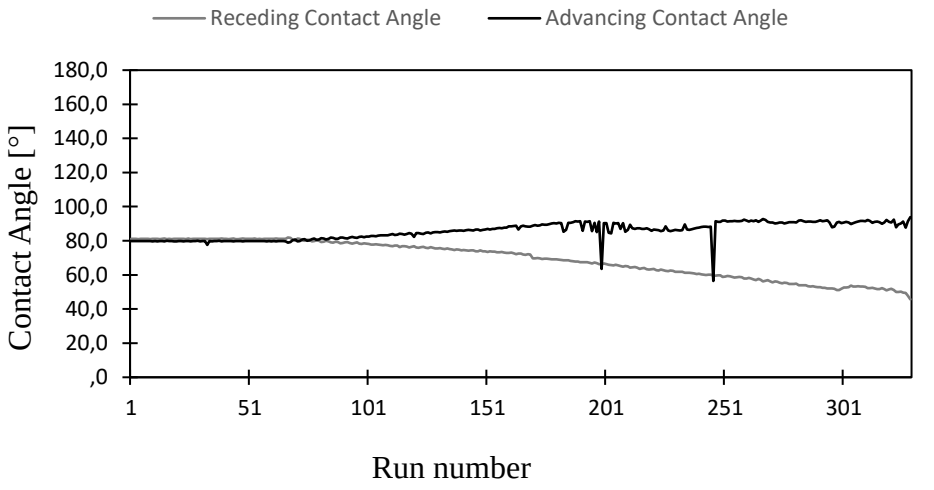

Figure B.13. Tilted 110-R972(PDES) coated glass slide with diiodomethane droplet.

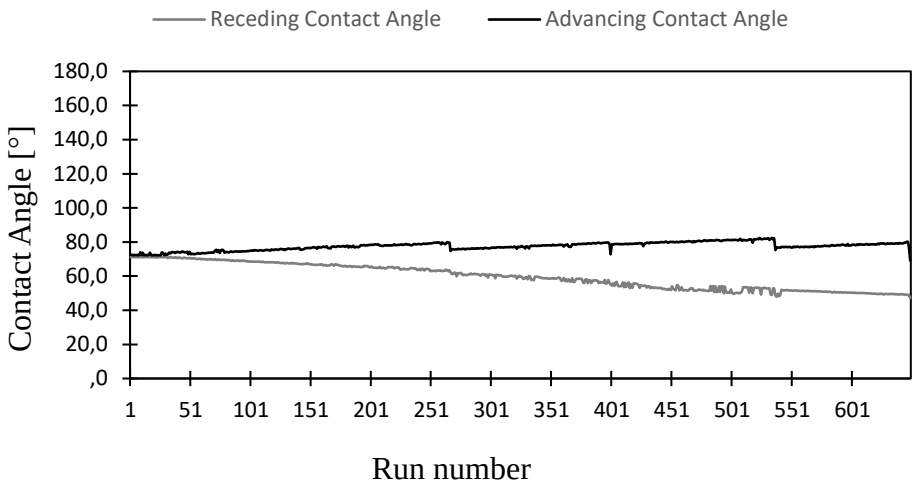

Figure B.14. Tilted 110-R972(PDES) coated glass slide with hexadecane droplet.

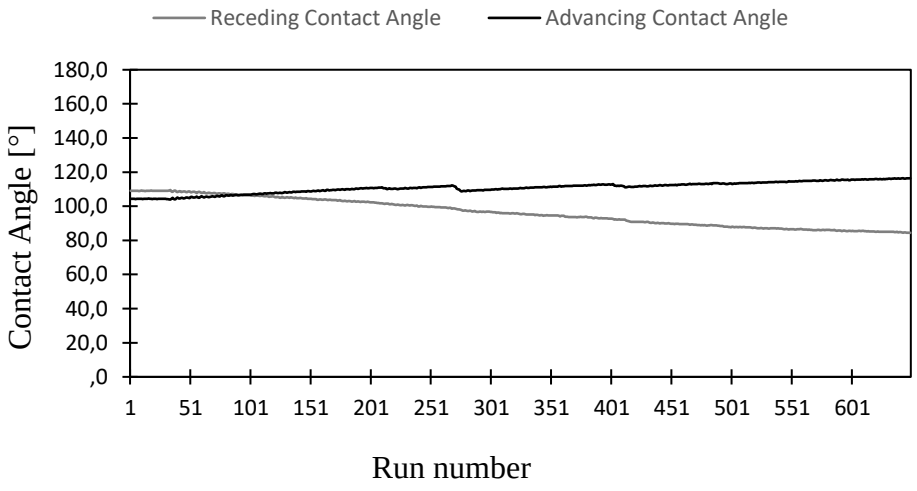

Figure B.15. Tilted 110-R972(PDES) coated steel slide with water droplet.

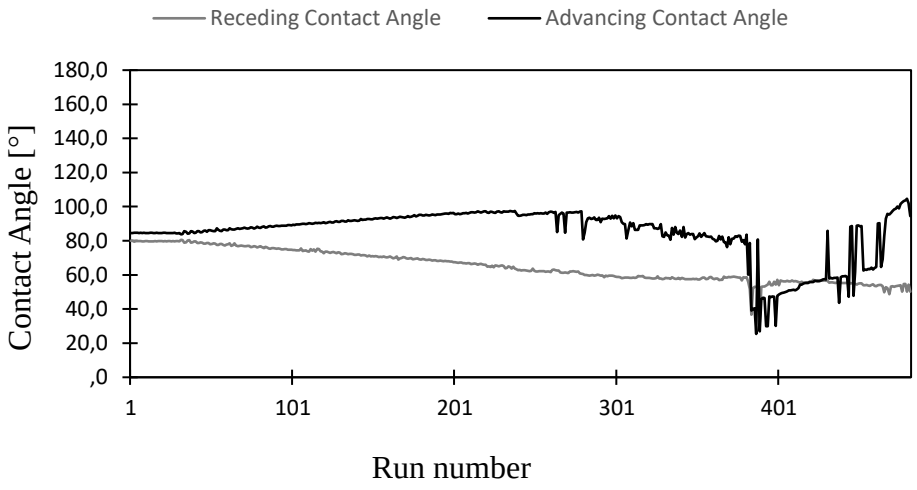

Figure B.16. Tilted 110-R972(PDES) coated steel slide with diiodomethane droplet.

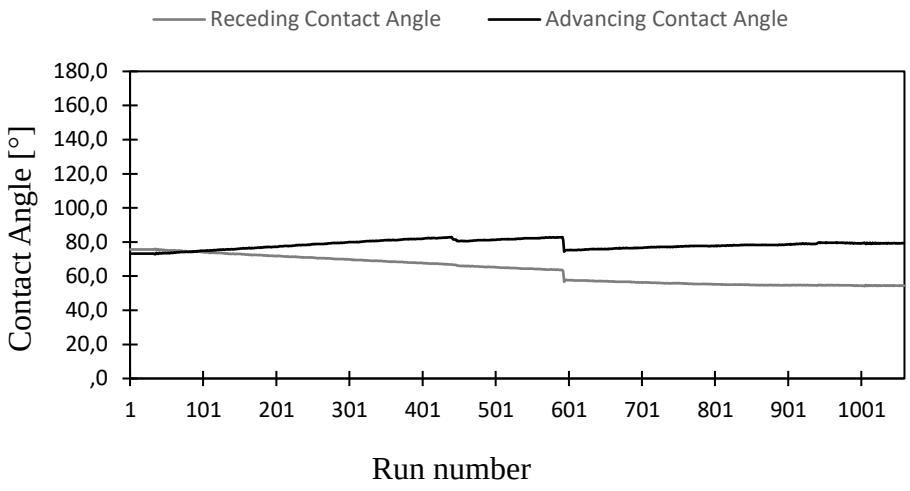

Figure B.17. Tilted 110-R972(PDES) coated steel slide with hexadecane droplet.

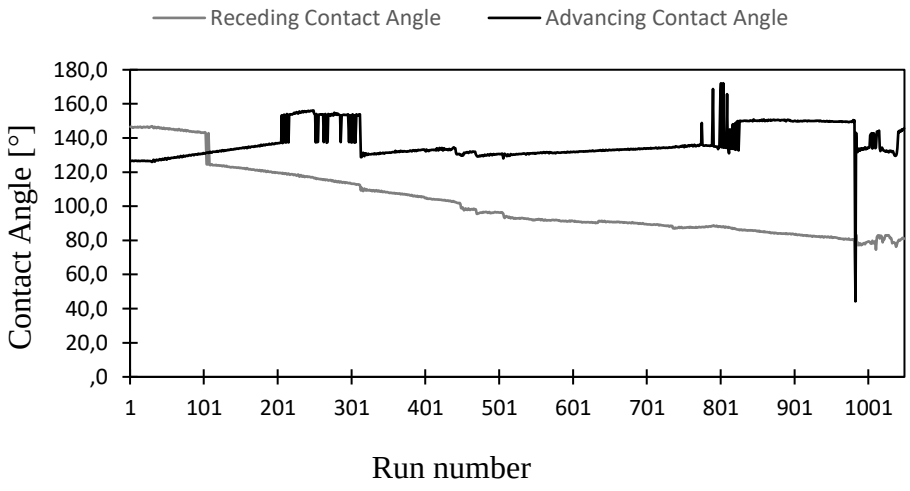

Figure B.18. Tilted 100-OX50(PDES) coated glass slide with water droplet.

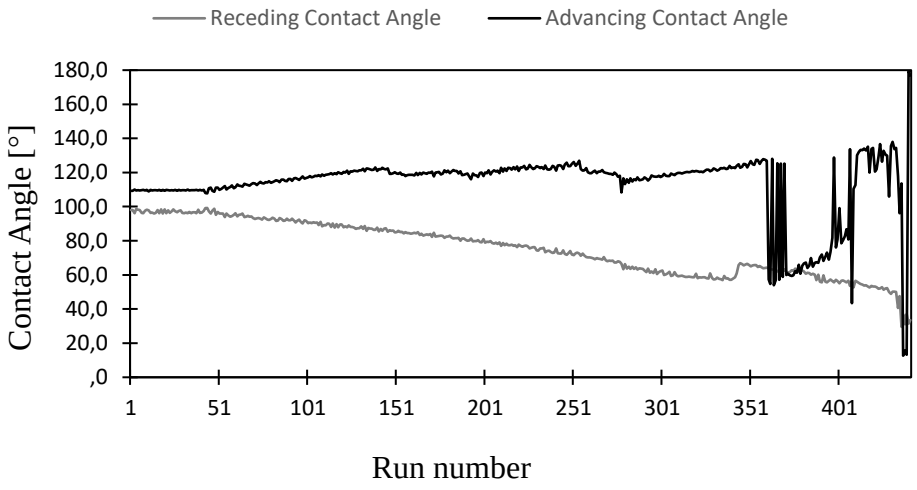

Figure B.19. Tilted 100-OX50(PDES) coated glass slide with diiodomethane droplet.

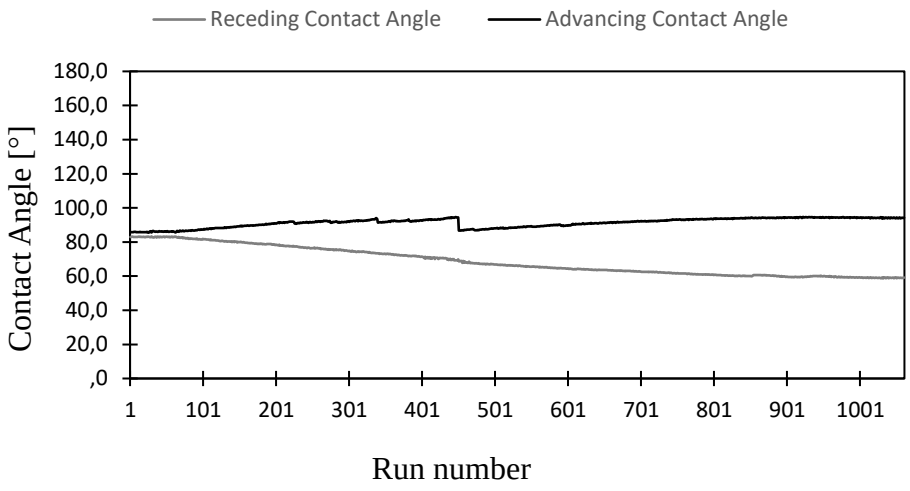

Figure B.20. Tilted 100-OX50(PDES) coated glass slide with hexadecane droplet.

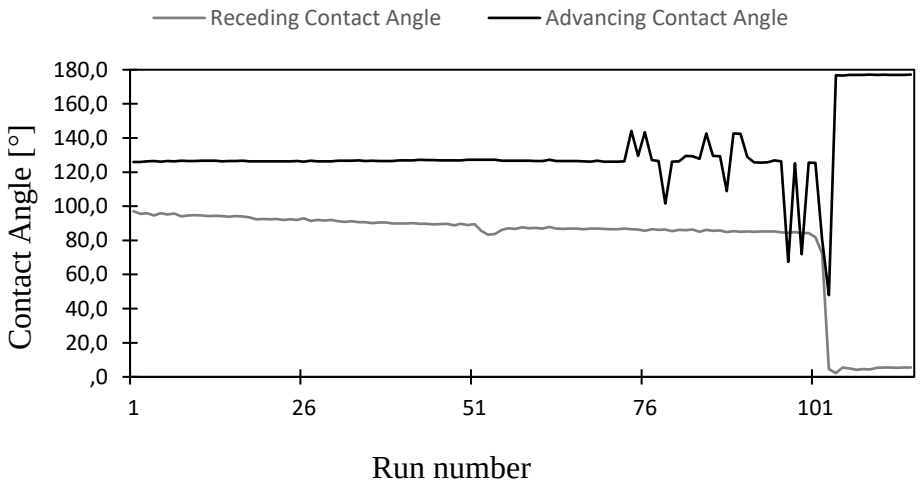

Figure B.21. Tilted 100-OX50(PDES) coated steel slide with water droplet.

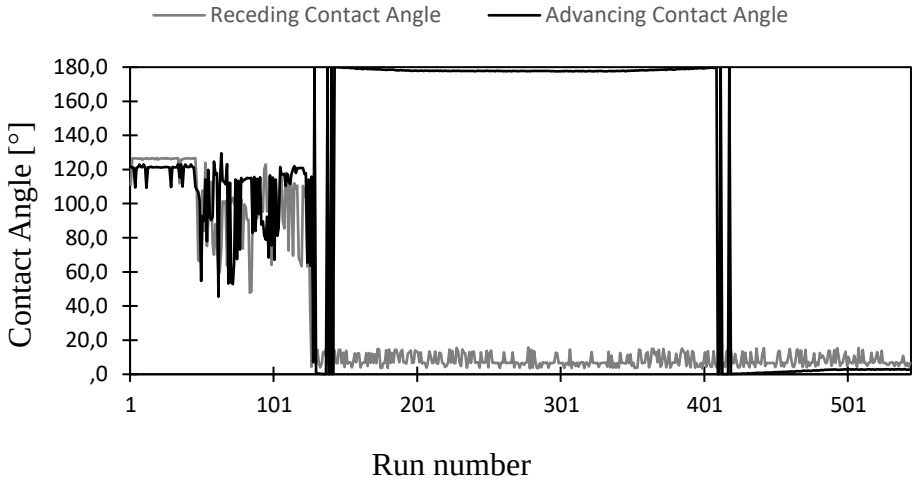

Figure B.22. Tilted 100-OX50(PDES) coated steel slide with diiodomethane droplet.

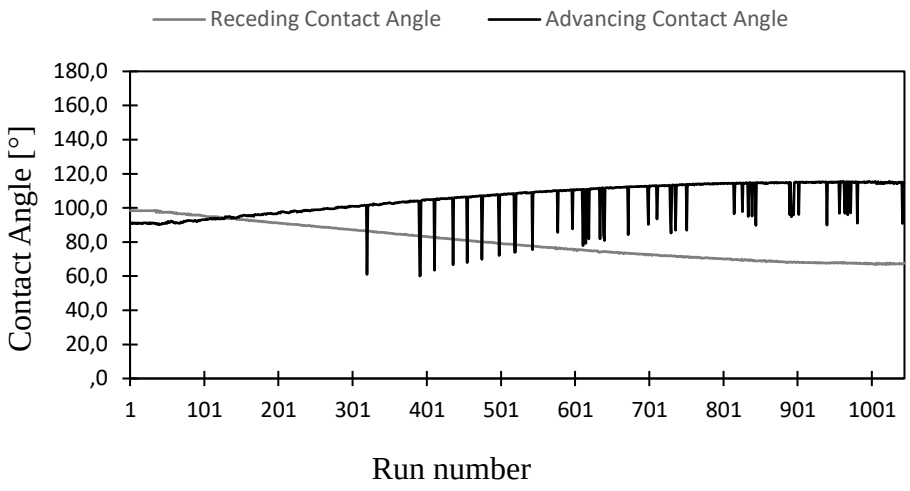

Figure B.23. Tilted 100-OX50(PDES) coated steel slide with hexadecane droplet.

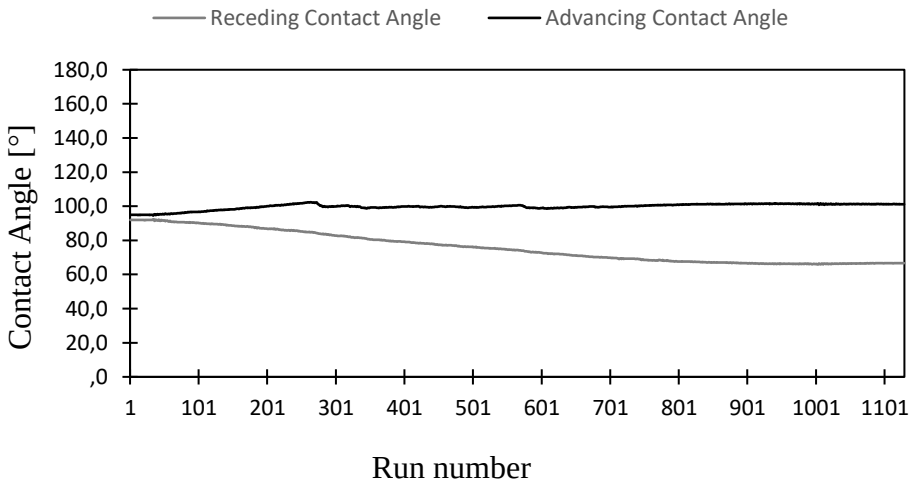

Figure B.24. Tilted 100-R972(PDES) coated glass slide with water droplet.

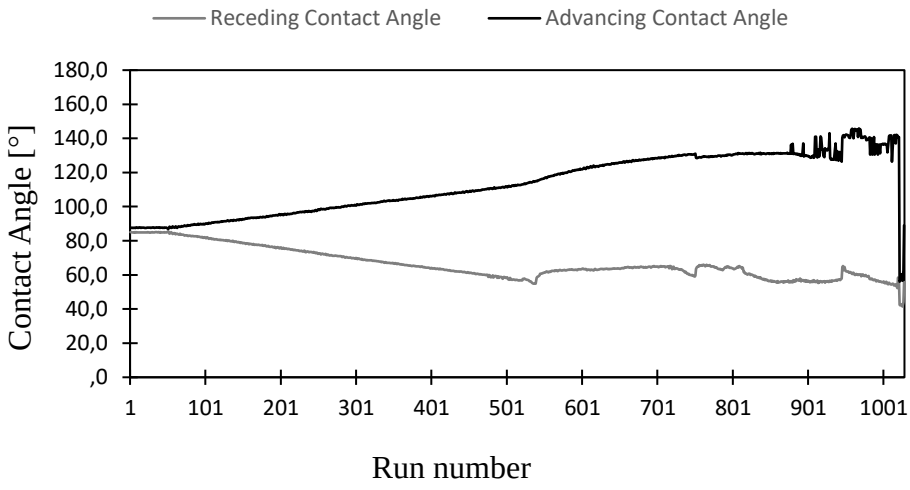

Figure B.25. Tilted 100-R972(PDES) coated glass slide with diiodomethane droplet.

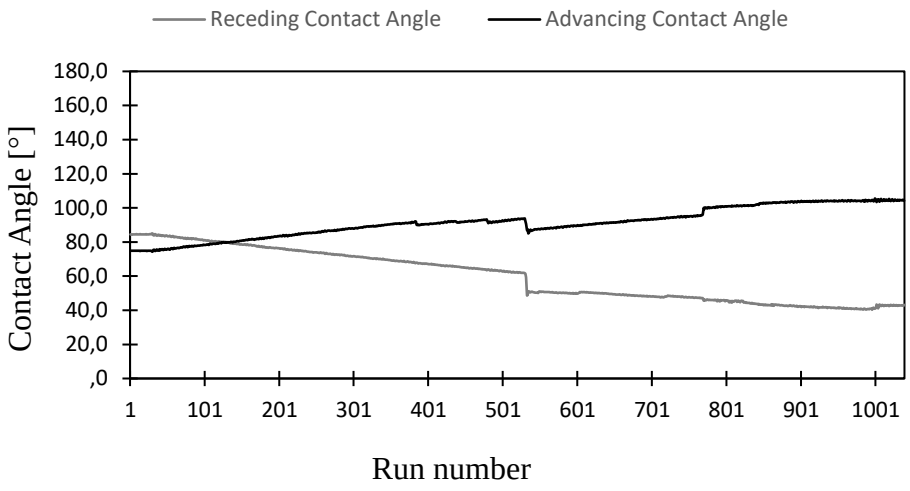

Figure B.26. Tilted 100-R972(PDES) coated glass slide with hexadecane droplet.

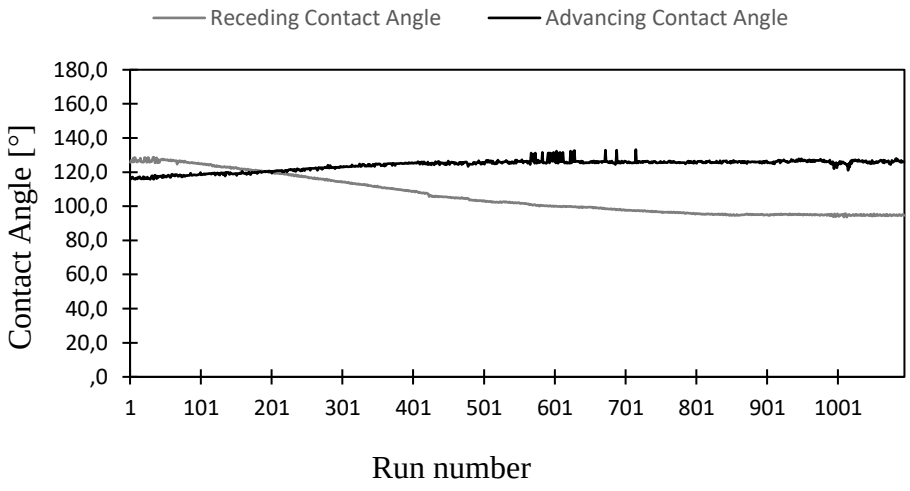

Figure B.27. Tilted 100-R972(PDES) coated steel slide with water droplet.

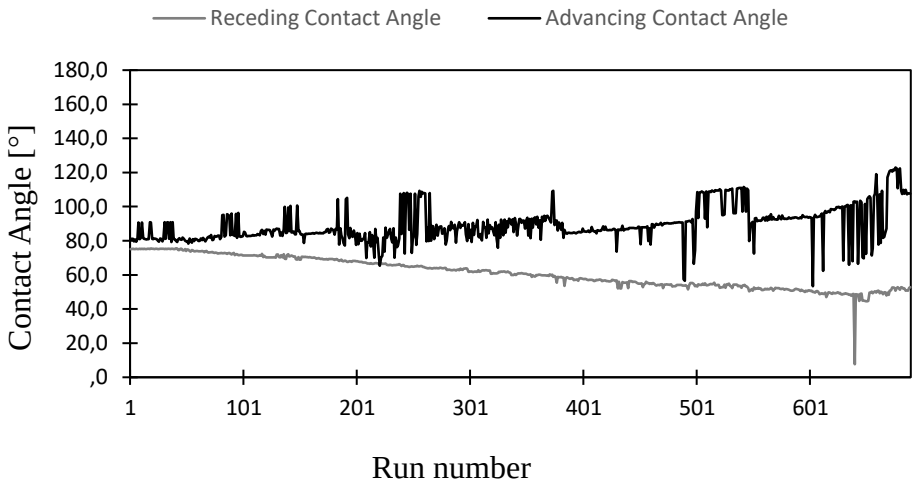

Figure B.28. Tilted 100-R972(PDES) coated steel slide with diiodomethane droplet.

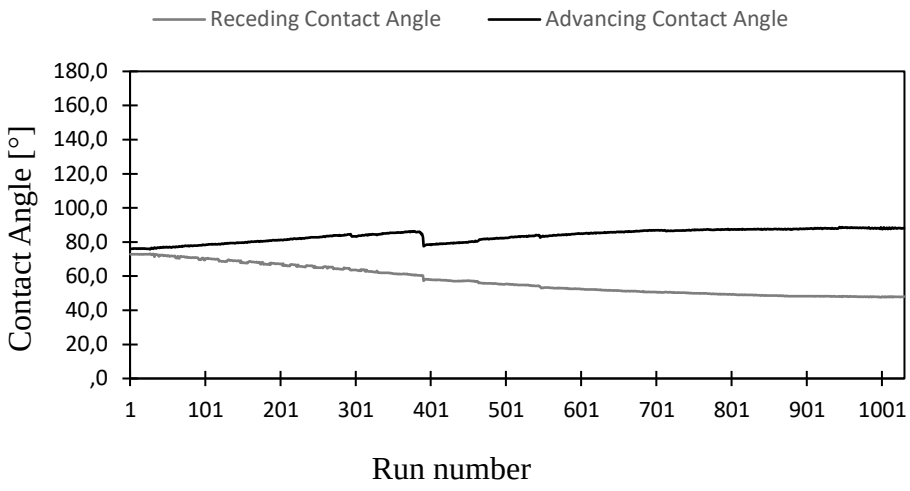

Figure B. 29. Tilted 100-R972(PDES) coated steel slide with hexadecane droplet.

B.3 POCS

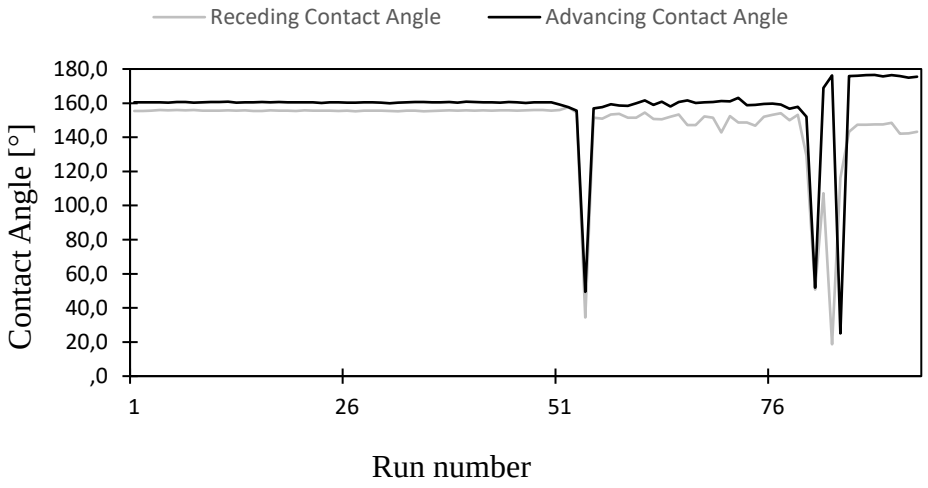

Figure B.30. Tilted 110-OX50(POCS) coated glass slide with water droplet.

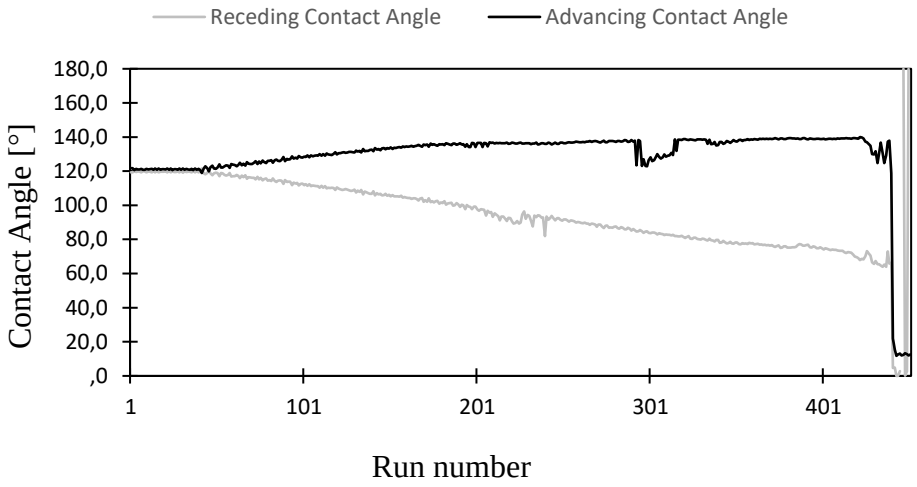

Figure B.31. Tilted 110-OX50(POCS) coated glass slide with diiodomethane droplet.

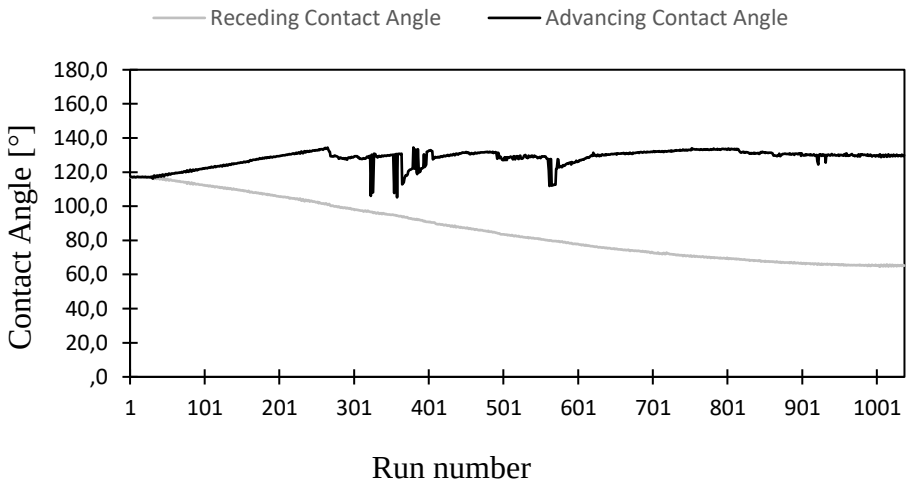

Figure B.32. Tilted 110-OX50(POCS) coated glass slide with hexadecane droplet.

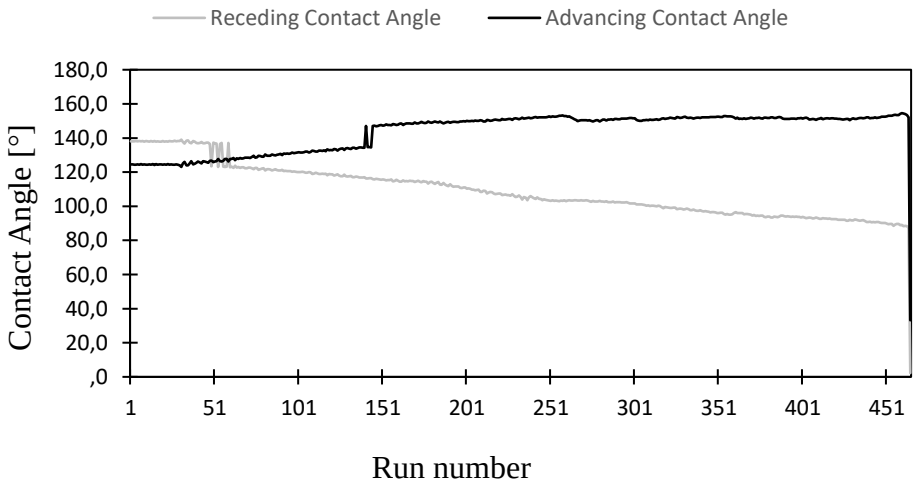

Figure B.33. Tilted 110-OX50(POCS) coated steel slide with water droplet.

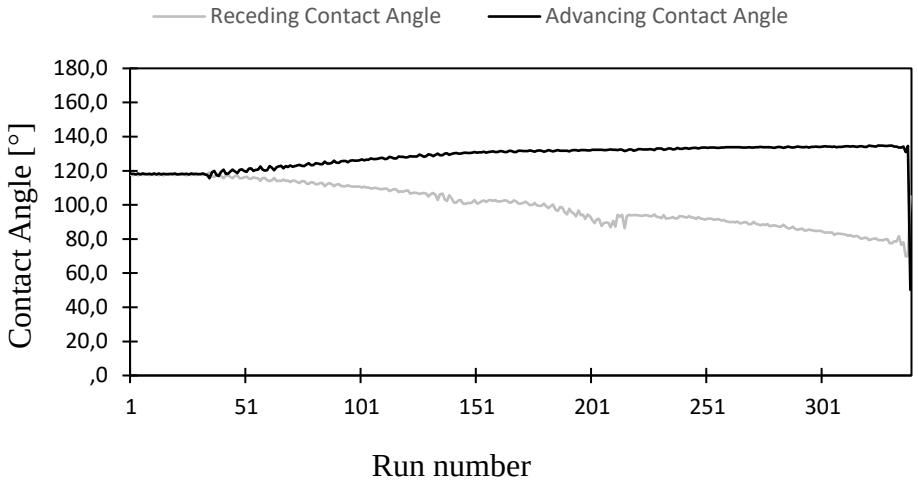

Figure B.34. Tilted 110-OX50(POCS) coated steel slide with diiodomethane droplet.

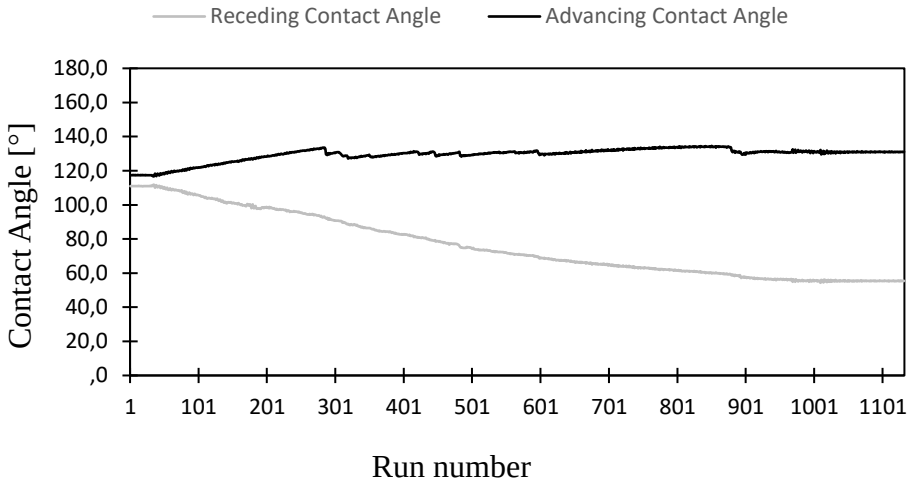

Figure B.35. Tilted 110-OX50(POCS) coated steel slide with hexadecane droplet.

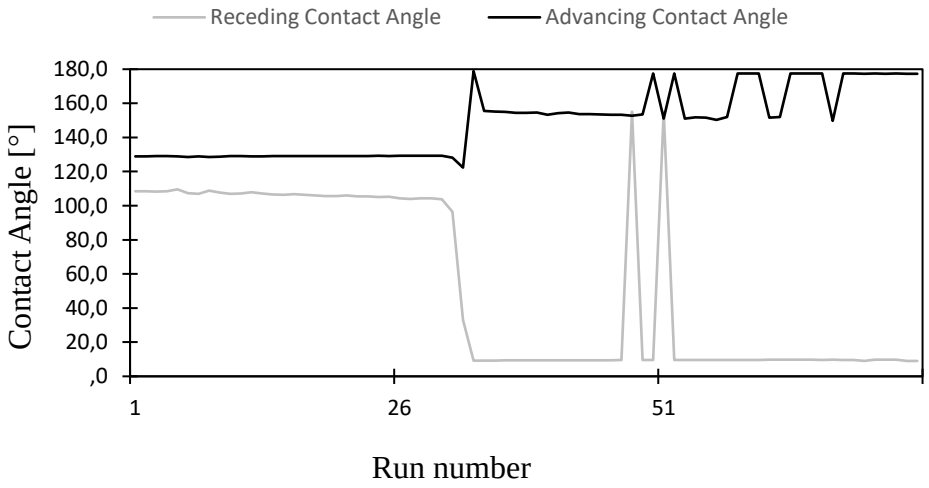

Figure B.36. Tilted 110-R972(POCS) coated glass slide with diiodomethane droplet.

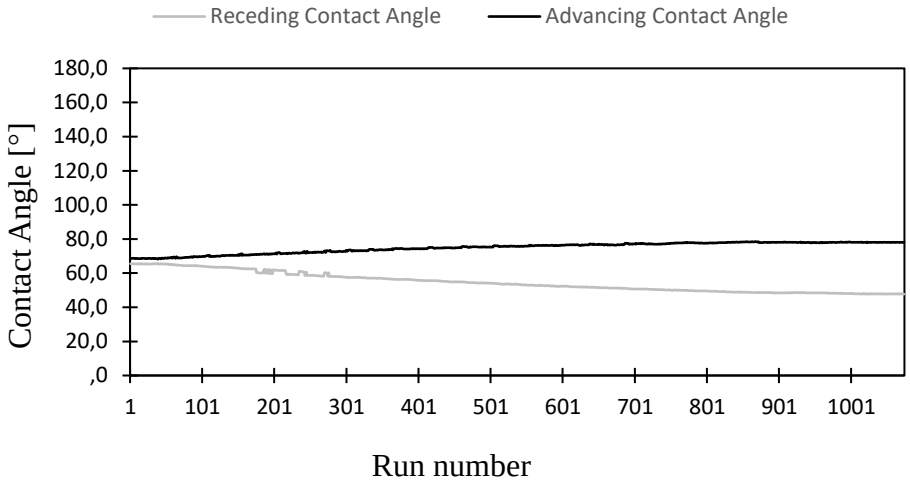

Figure B.37. Tilted 110-R972(POCS) coated glass slide with hexadecane droplet.

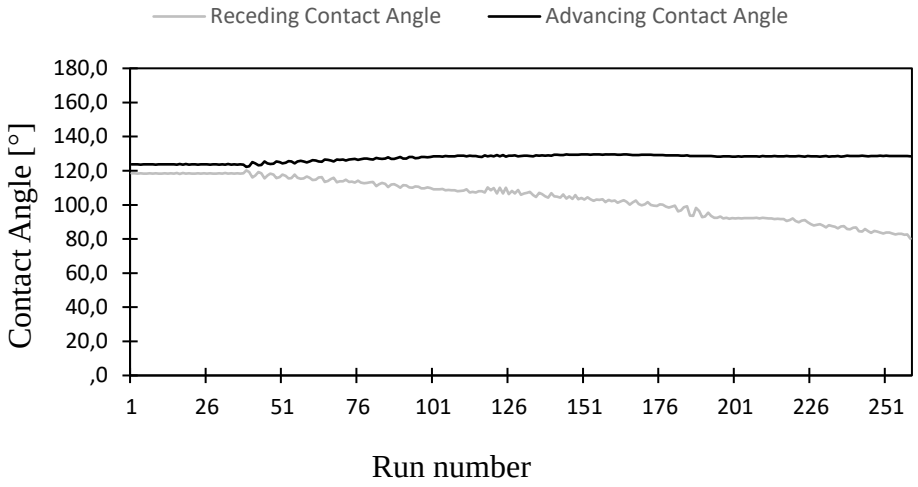

Figure B.38. Tilted 110-R972(POCS) coated steel slide with diiodomethane droplet.

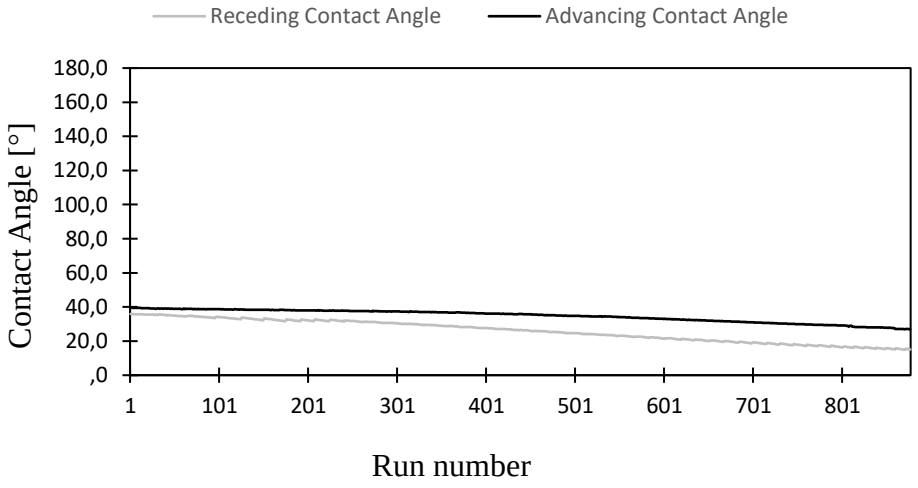

Figure B.39. Tilted 110-R972(POCS) coated steel slide with hexadecane droplet.

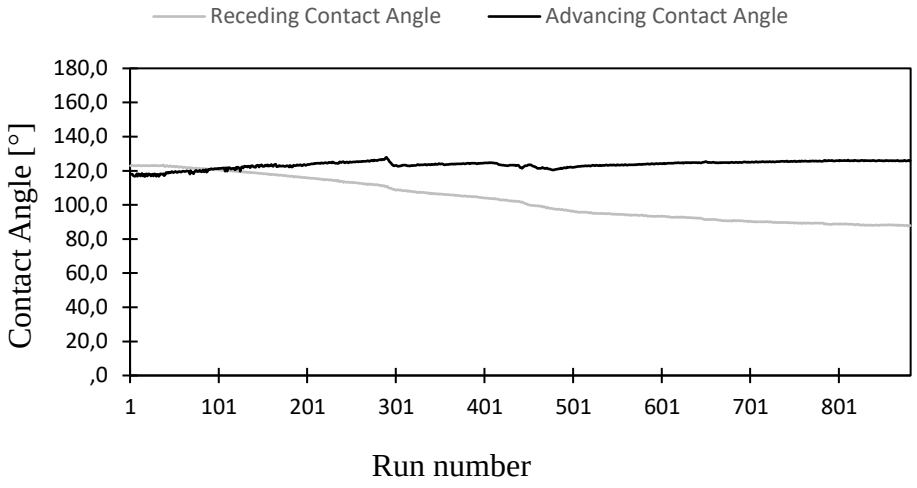

Figure B.40. Tilted 100-OX50(POCS) coated glass slide with water droplet.

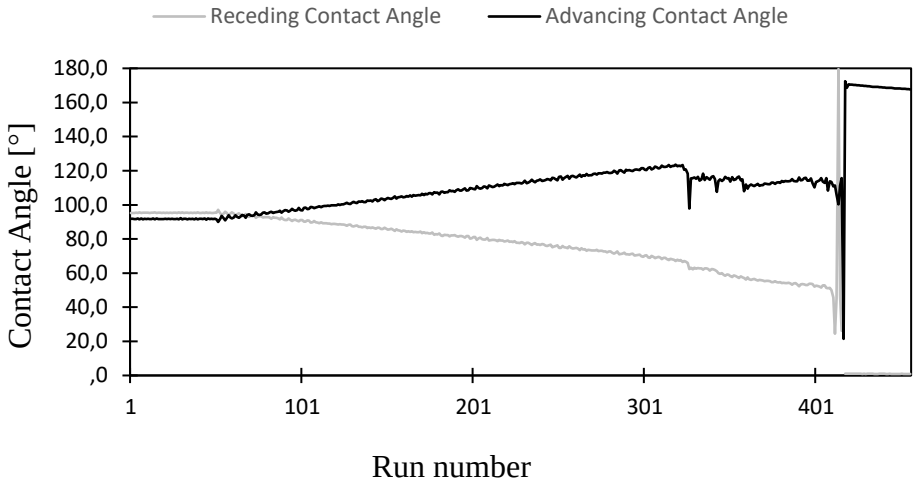

Figure B.41. Tilted 100-OX50(POCS) coated glass slide with diiodomethane droplet.

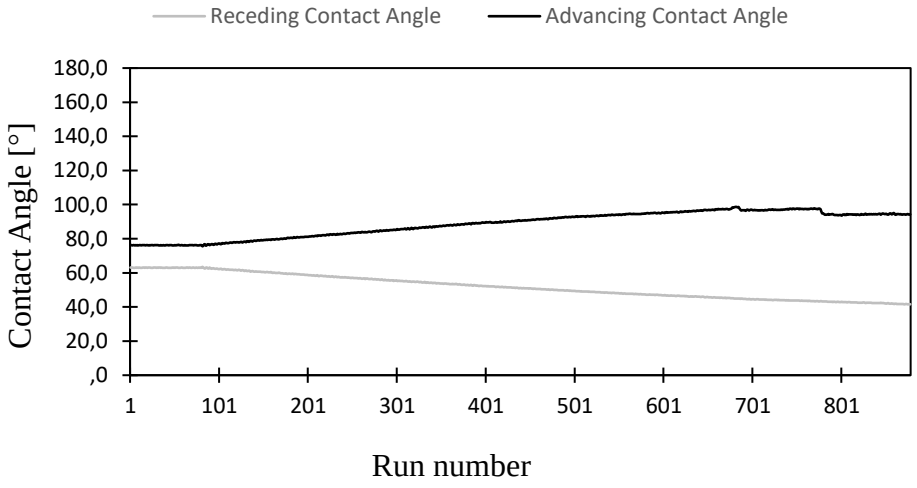

Figure B.42. Tilted 100-OX50(POCS) coated glass slide with hexadecane droplet.

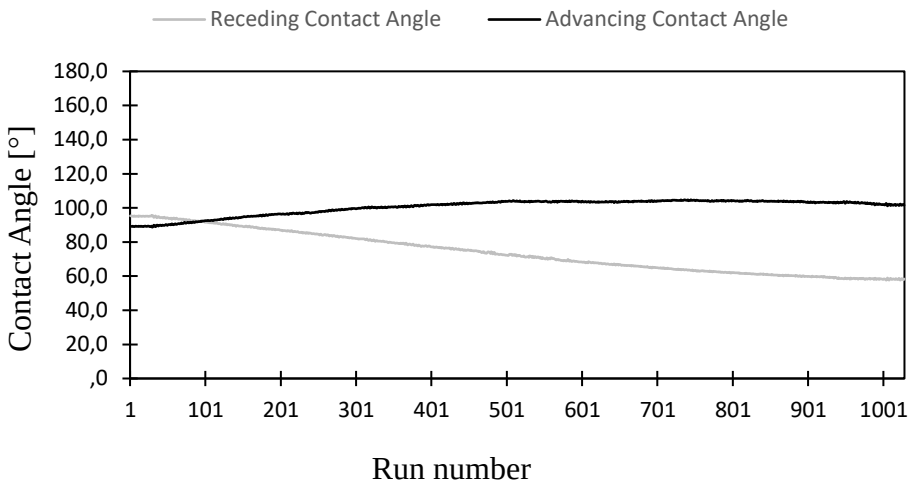

Figure B.43. Tilted 100-OX50(POCS) coated steel slide with water droplet.

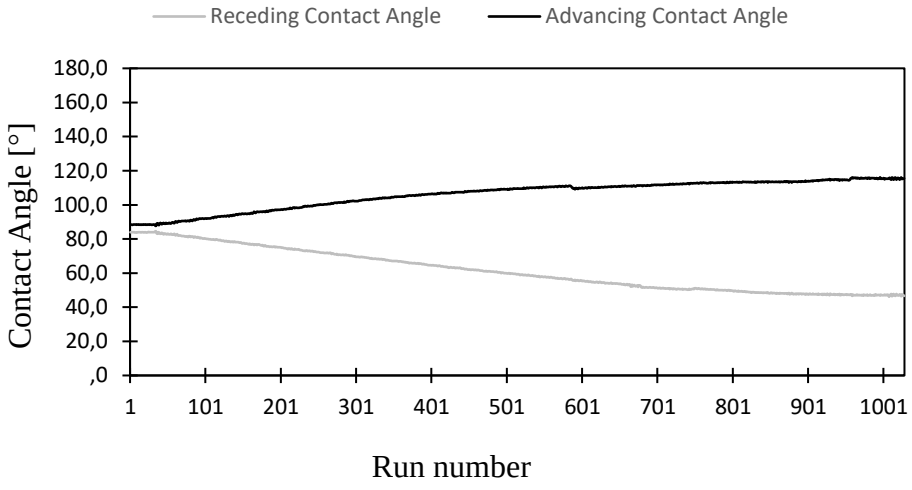

Figure B.44. Tilted 100-OX50(POCS) coated steel slide with diiodomethane droplet.

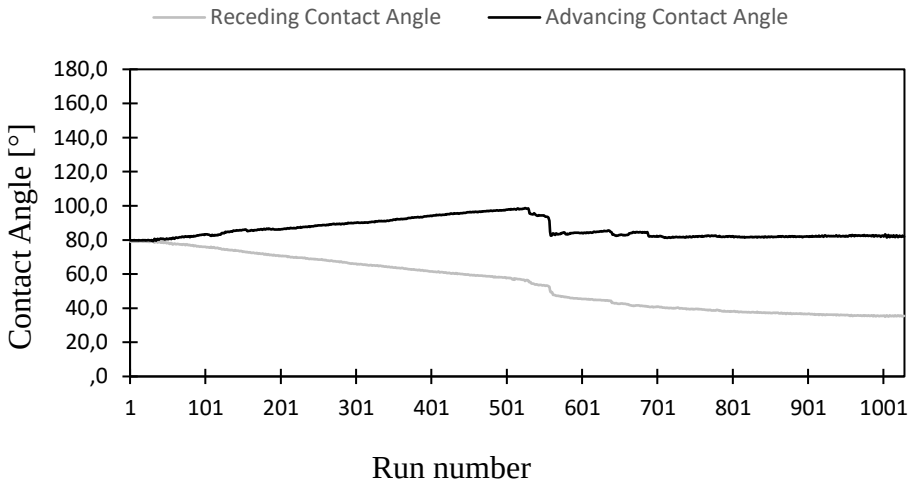

Figure B.45. Tilted 100-OX50(POCS) coated steel slide with hexadecane droplet.

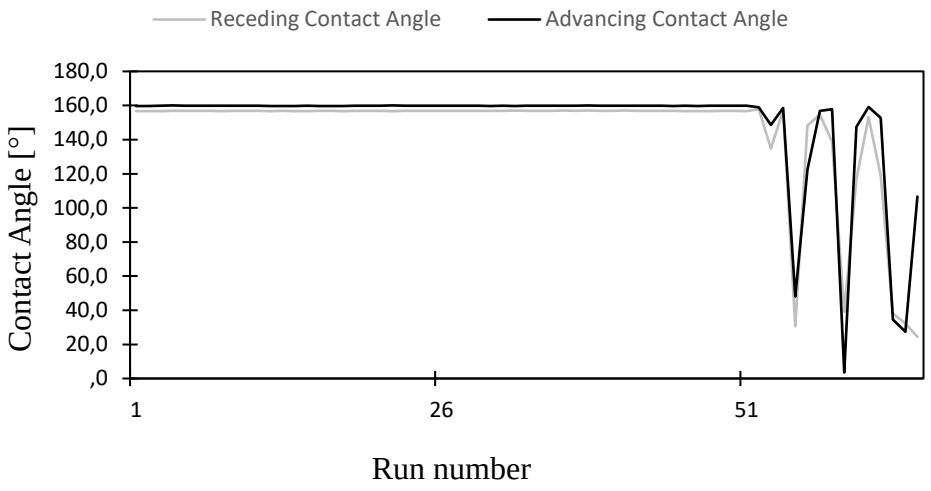

Figure B.46. Tilted 100-R972(POCS) coated glass slide with water droplet.

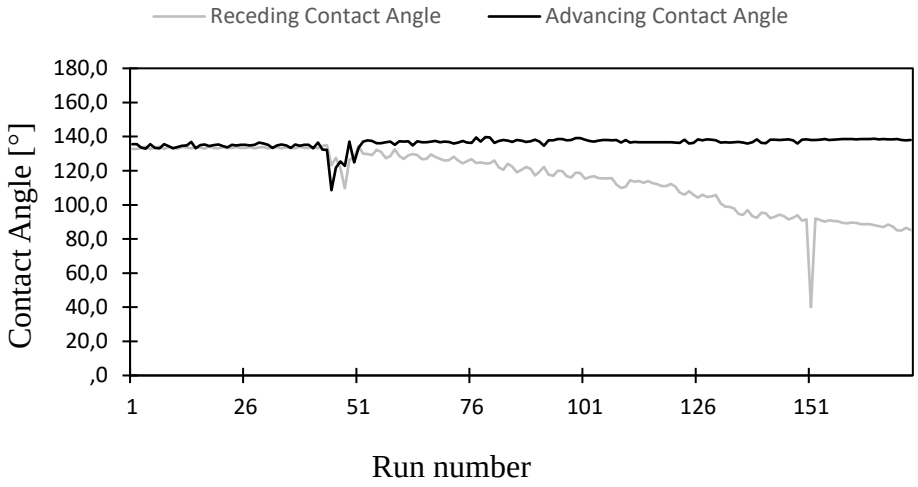

Figure B.47. Tilted 100-R972(POCS) coated glass slide with diiodomethane droplet.

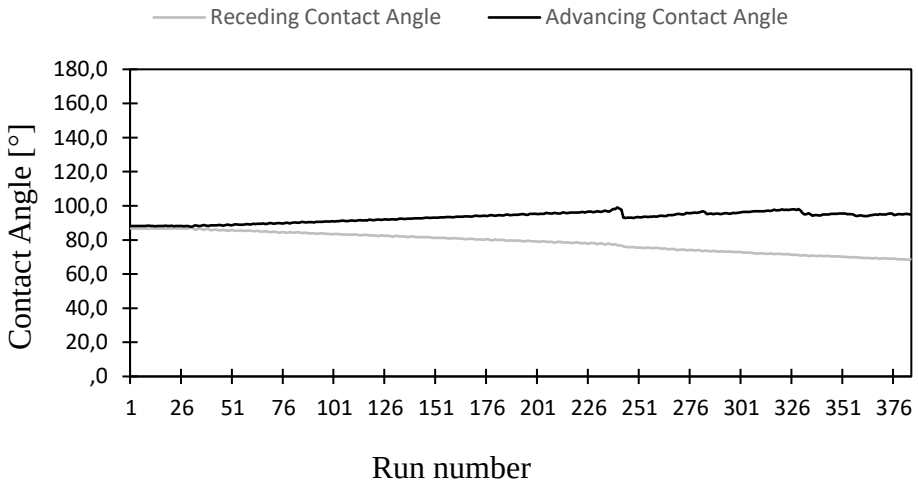

Figure B.48. Tilted 100-R972(POCS) coated glass slide with hexadecane droplet.

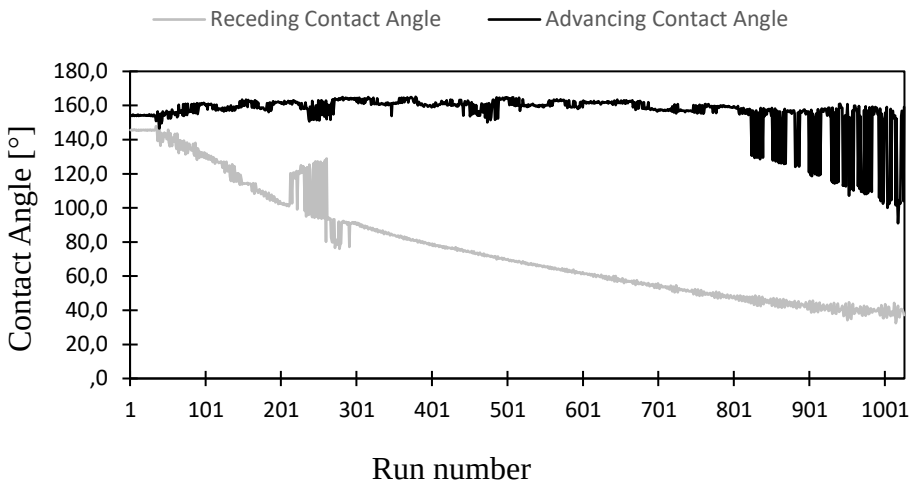

Figure B.49. Tilted 100-R972(POCS) coated steel slide with water droplet.

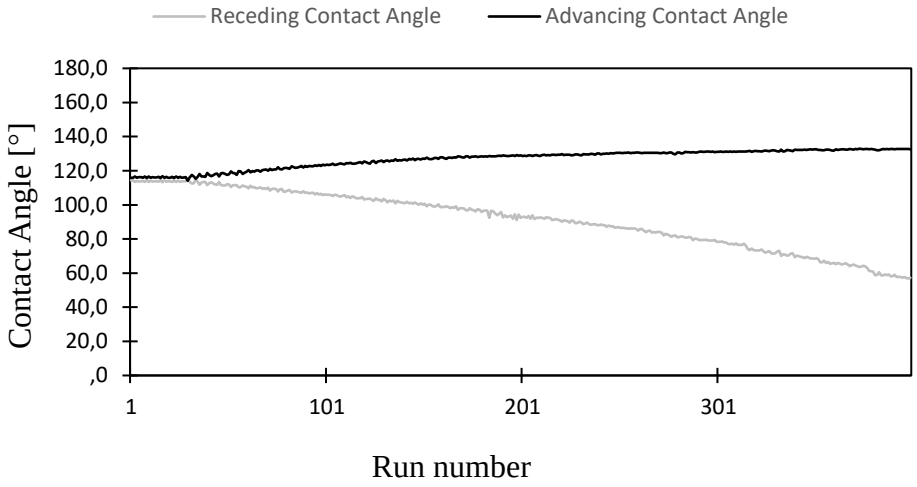

Figure B.50. Tilted 100-R972(POCS) coated steel slide with diiodomethane droplet.

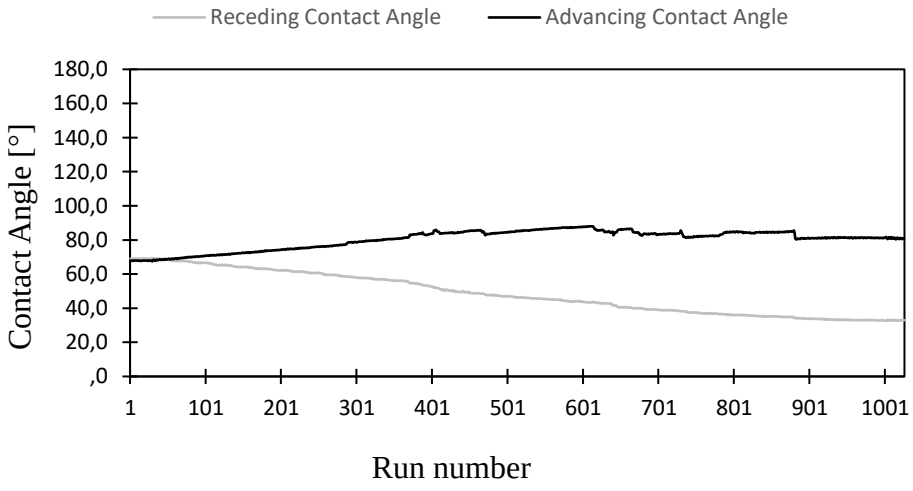

Figure B.51. Tilted 100-R972(POCS) coated steel slide with hexadecane droplet.

B.4 Silicon Oil DC 200

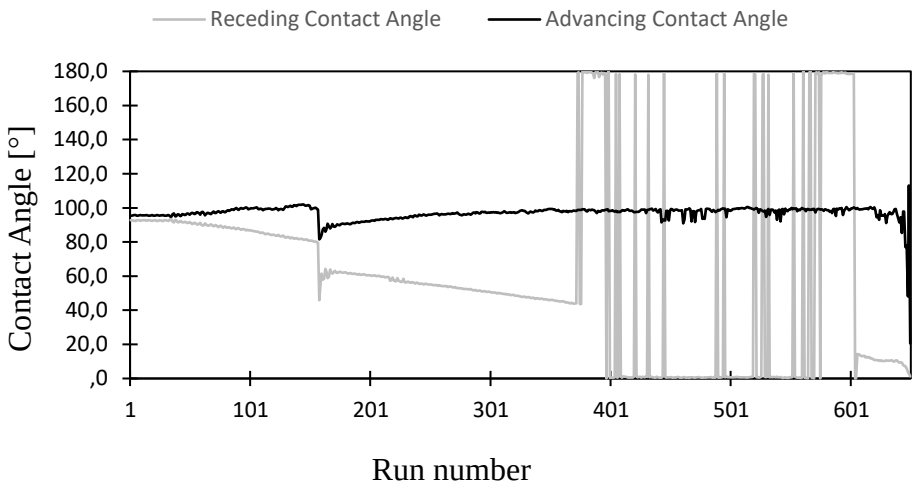

Figure B.52. Tilted glass slide coated with heated Silicon Oil DC 200 with a diiodomethane droplet.

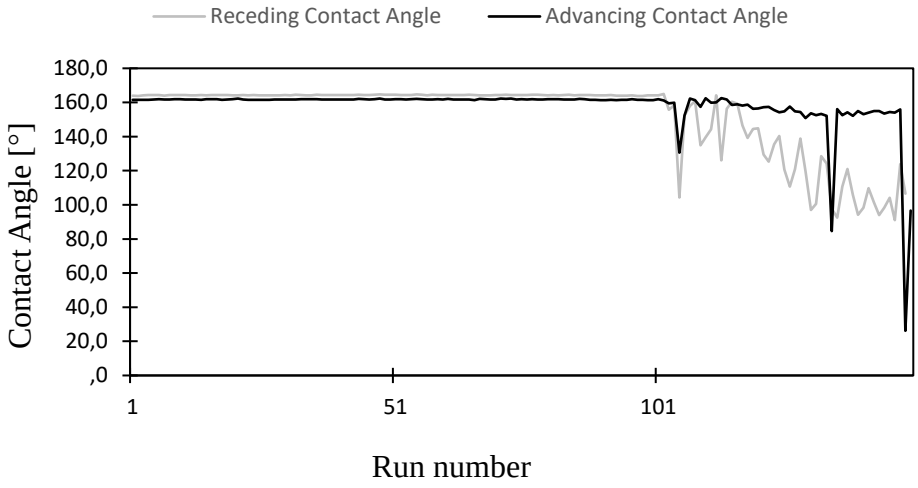

Figure B.53. Tilted steel slide coated with heated Silicon Oil DC 200 with a water droplet.

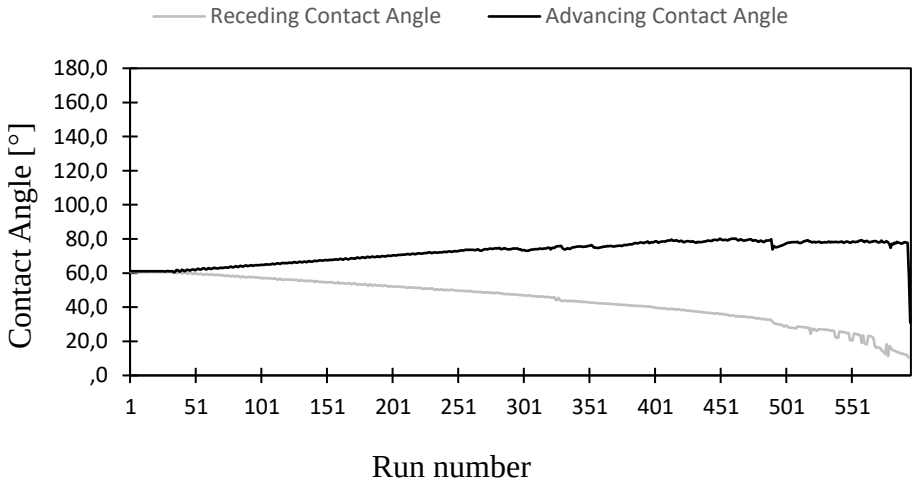

Figure B.54. Tilted steel slide coated with heated Silicon Oil DC 200 with a diiodomethane droplet.

B.5 Sylgard 184

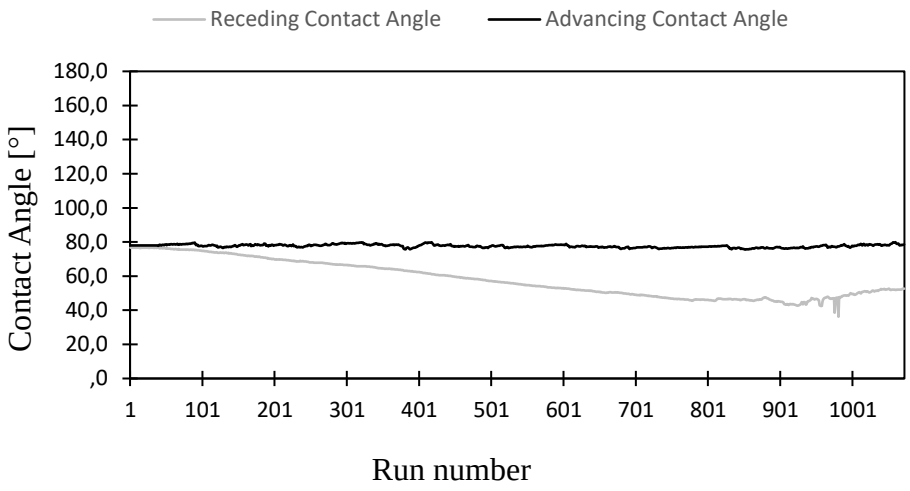

Figure B.55. Tilted Sylgard 184 coated steel slide with water droplet.

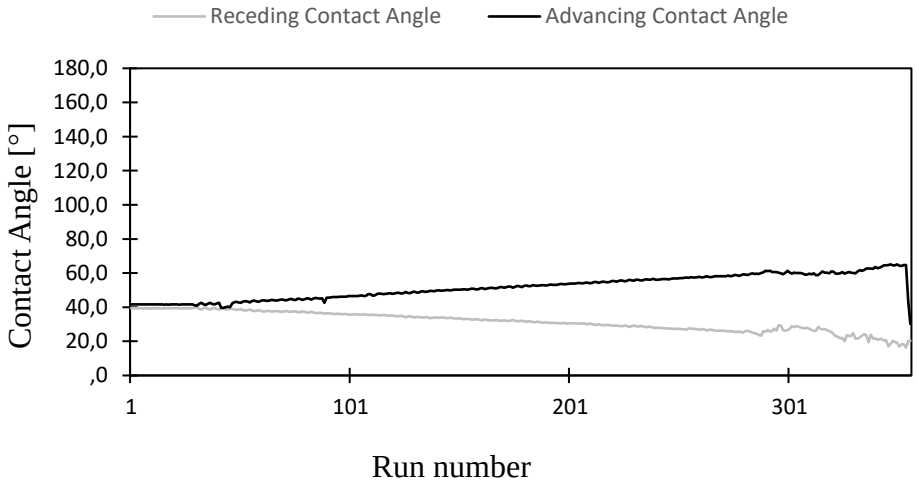

Figure B.56. Tilted Sylgard 184 coated steel slide with diiodomethane droplet.

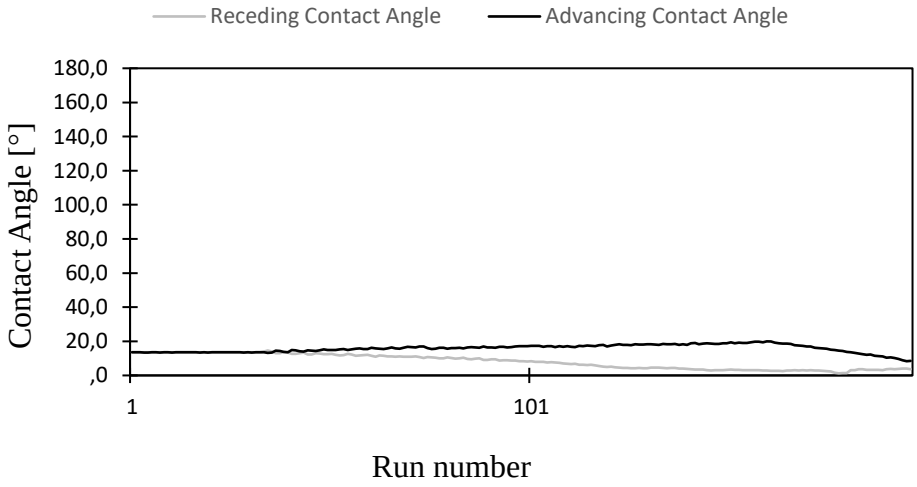

Figure B.57. Tilted Sylgard 184 coated steel slide with hexadecane droplet.

B.6 Etched aluminum surface

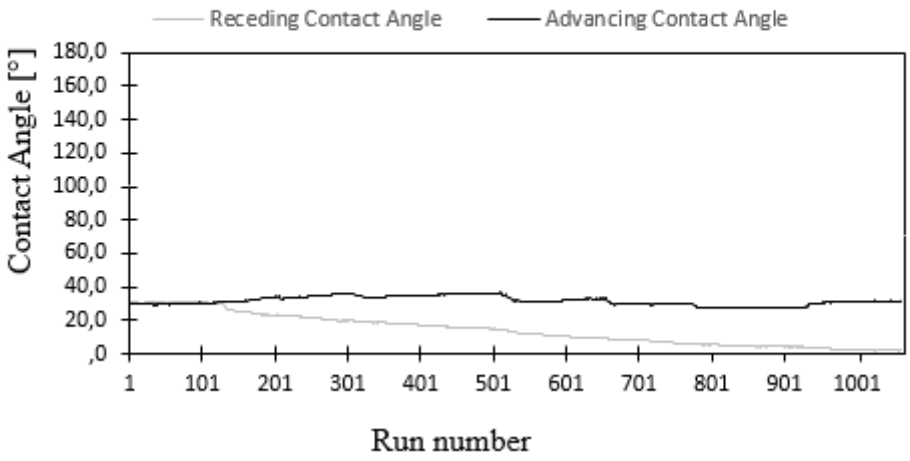

Figure B.58. Tilted aluminum etched in HCl (10 minutes) and immersed HNO_3+$CuSO_4$ with water droplet.

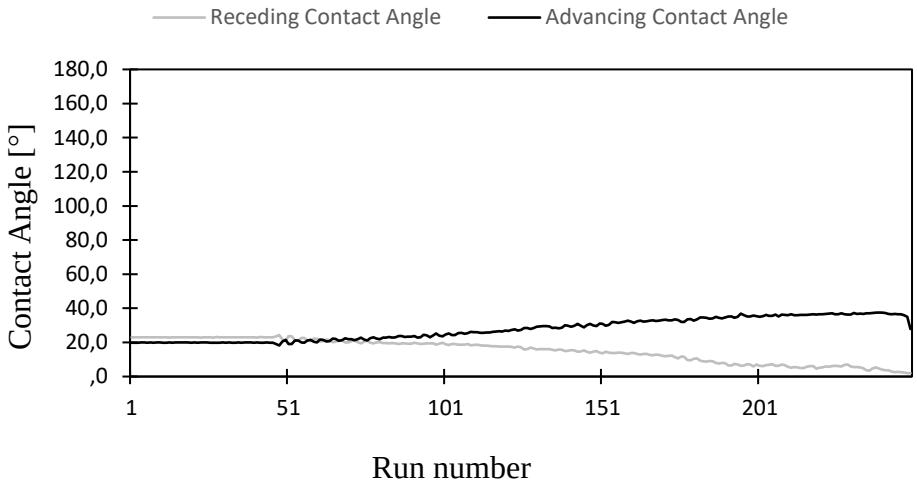

Figure B.59. Tilted etched aluminum slide HCl (10 minutes) and immersed in HNO_3+$CuSO_4$ with diiodomethane droplet.

B.7 Etched and coated aluminum surface (10 minutes)

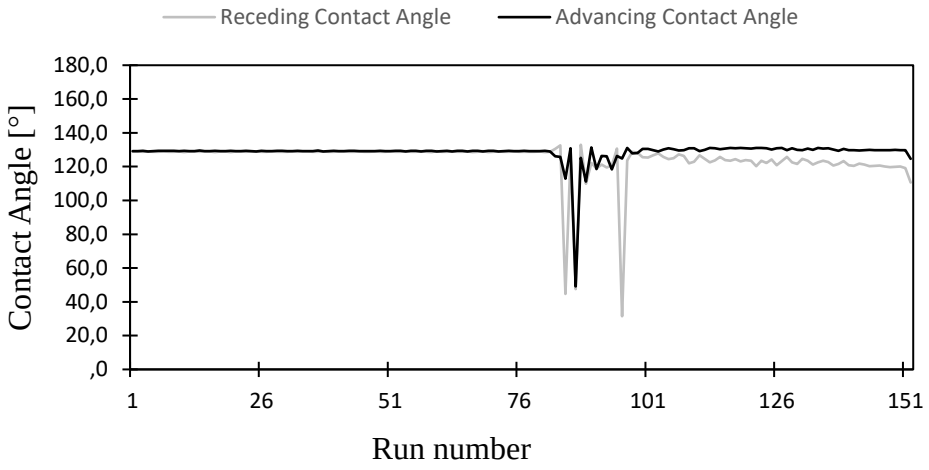

Figure B.60. Tilted etched and coated aluminum surface with diiodomethane droplet.

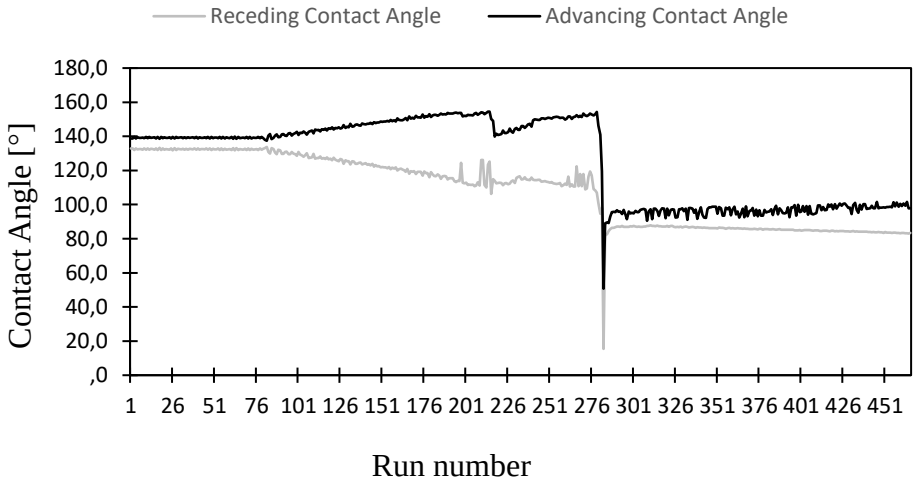

Figure B.61. Tilted etched and coated aluminum surface with water droplet.

B.8 Etched and coated aluminum slide (22 minutes)

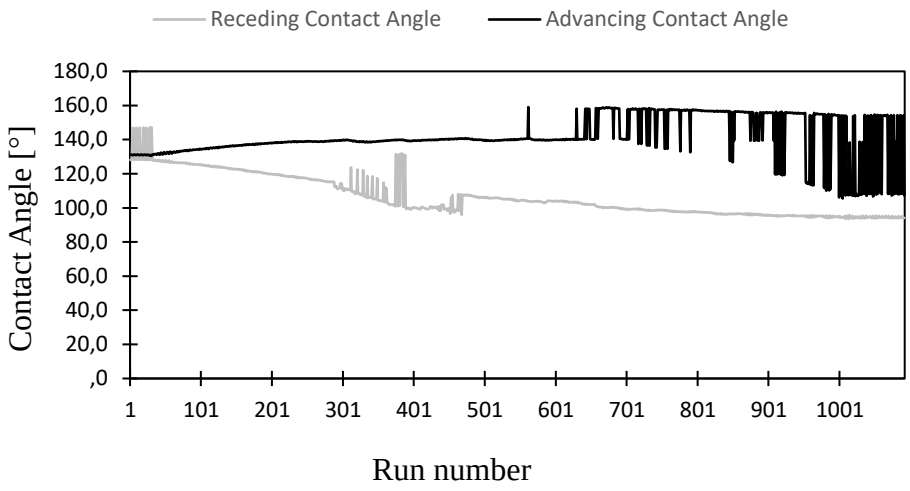

Figure B.62. Tilted first parallel aluminum slide etched and coated with water droplet.

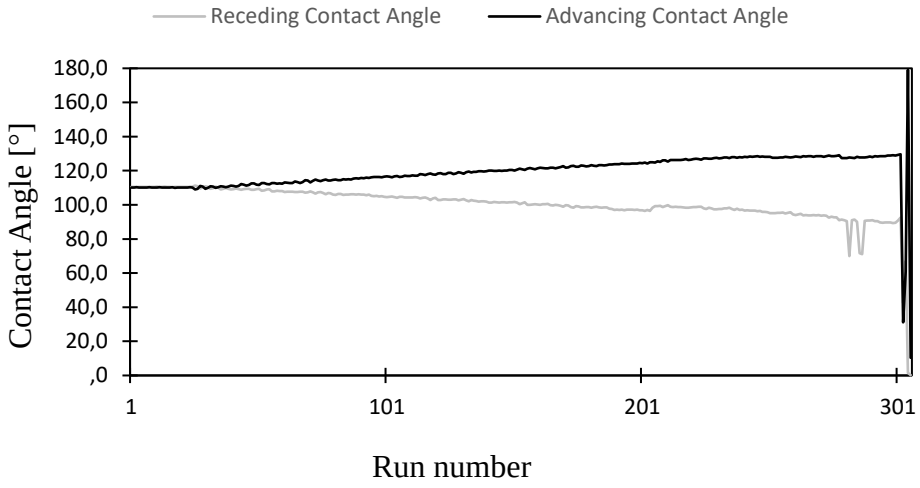

Figure B.63. Tilted first parallel aluminum slide etched and coated with a diiodomethane droplet.

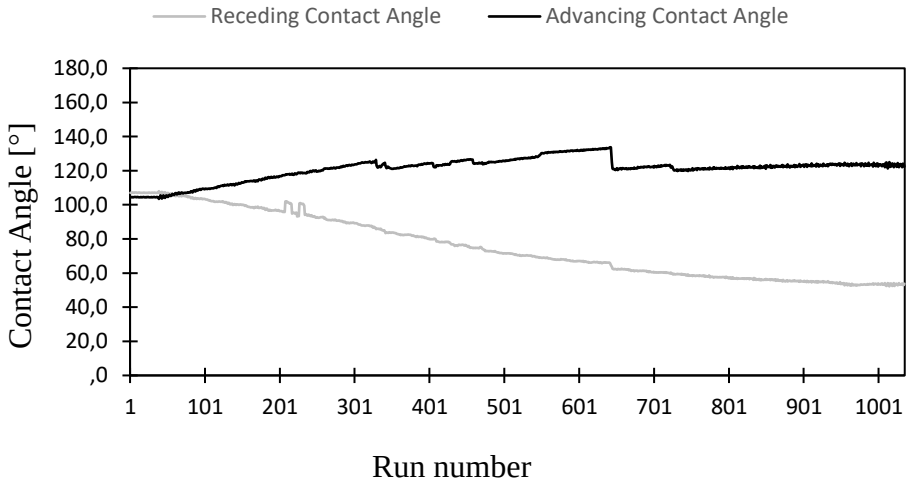

Figure B.64. Tilted first parallel aluminum slide etched and coated with a hexadecane droplet.

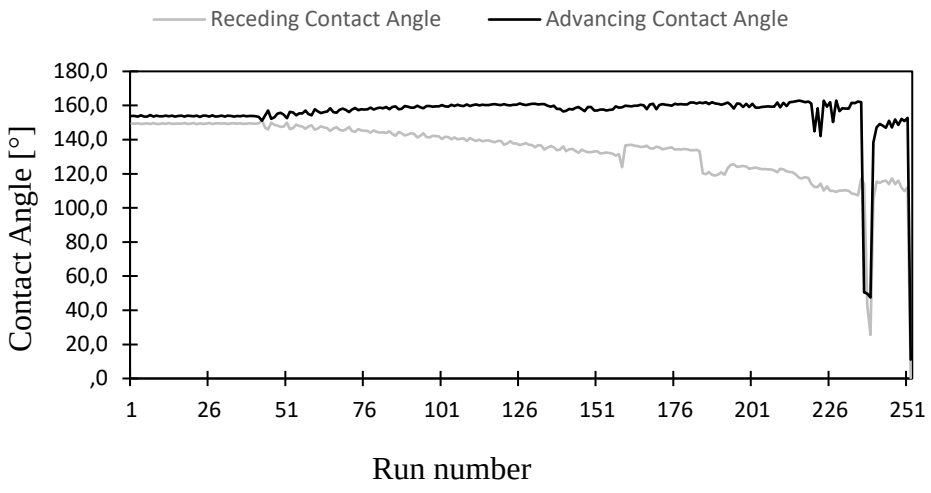

Figure B.65. Tilted second parallel aluminum slide etched and coated with water droplet.

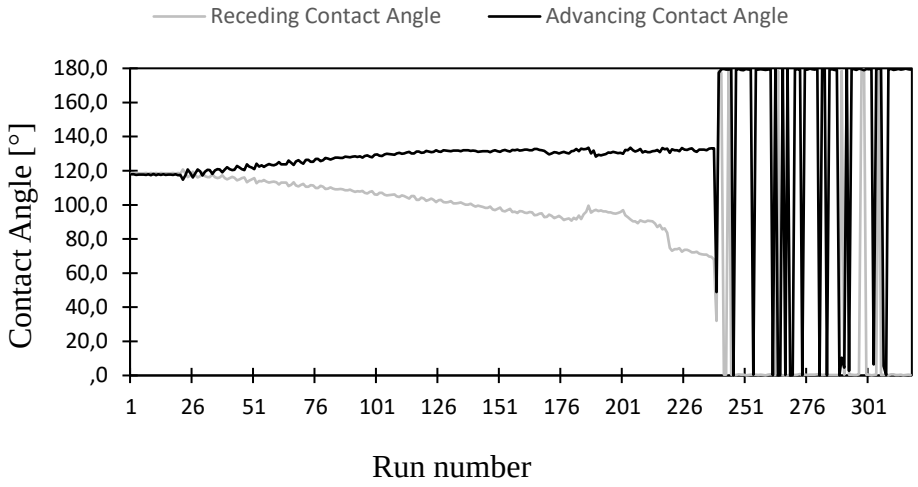

Figure B.66. Tilted second parallel aluminum slide etched and coated with diiodomethane droplet.

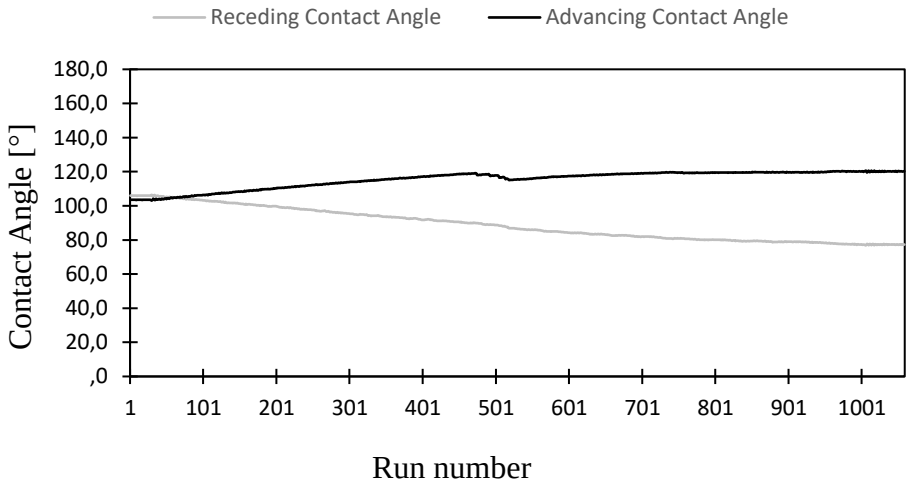

Figure B.67. Tilted second parallel aluminum slide etched and coated with hexadecane droplet.

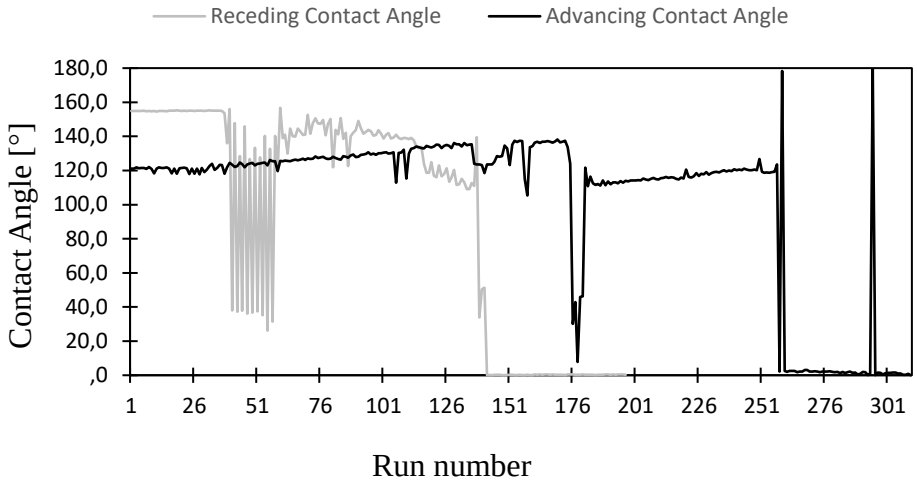

Figure B.68. Tilted third parallel aluminum slide etched and coated with water droplet.

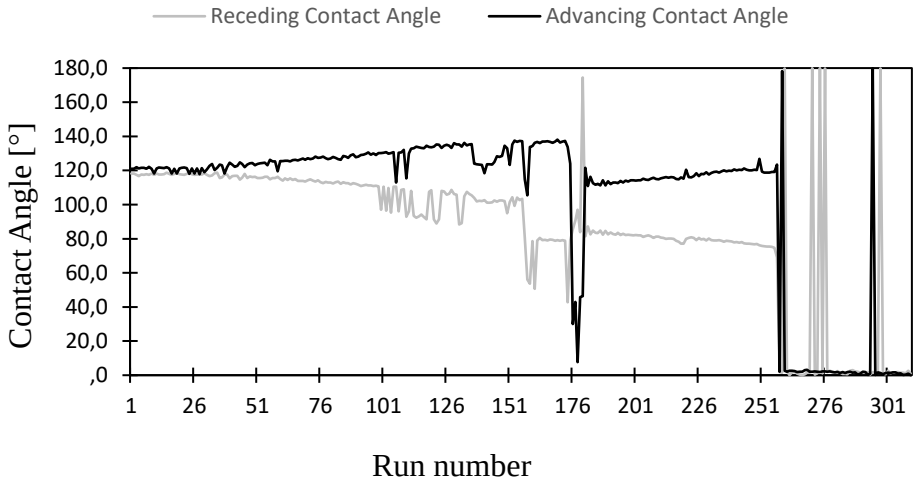

Figure B.69. Tilted third parallel aluminum slide etched and coated with diiodomethane droplet.

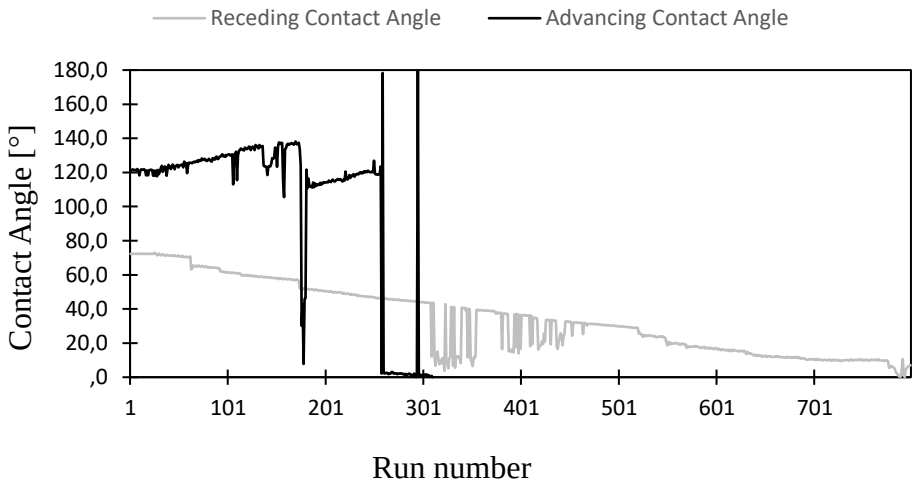

Figure B.70. Tilted third parallel aluminum slide etched and coated with hexadecane droplet.

Appendix C

Surface energy graphs

C.1 Substrates

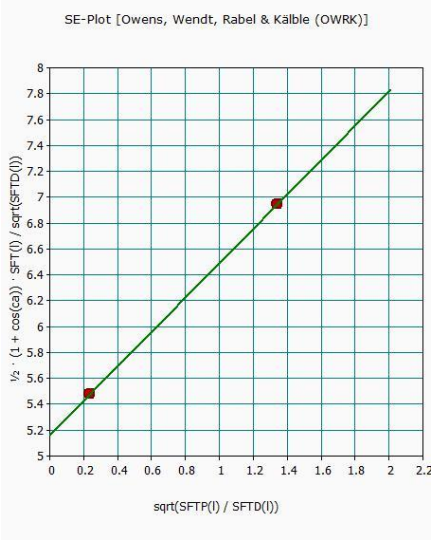

Figure C.1. Steel slide

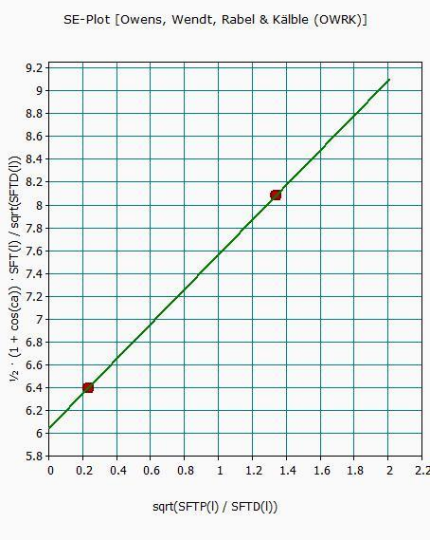

Figure C.2. Aluminum slide

C.2 PDES

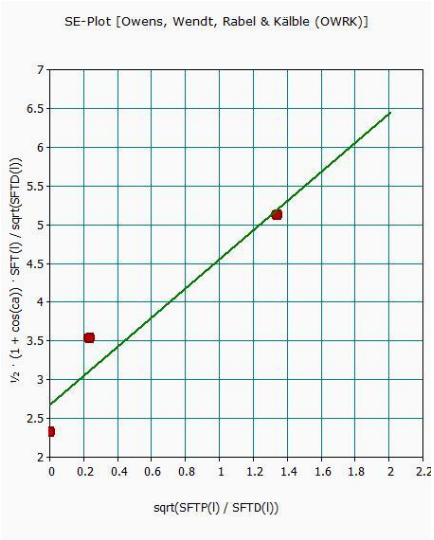

Figure C.3. Glass coated with 110-OX50(PDES)

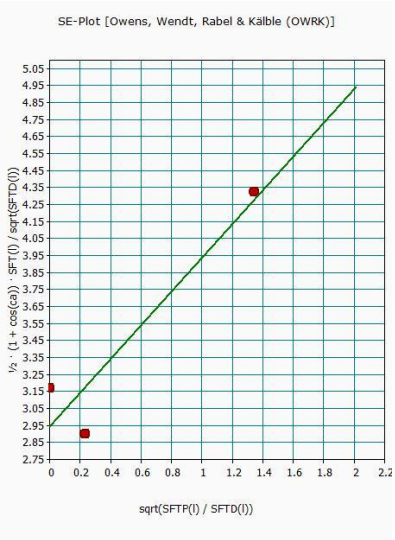

Figure C.4. Steel coated with 110-OX50(PDES)

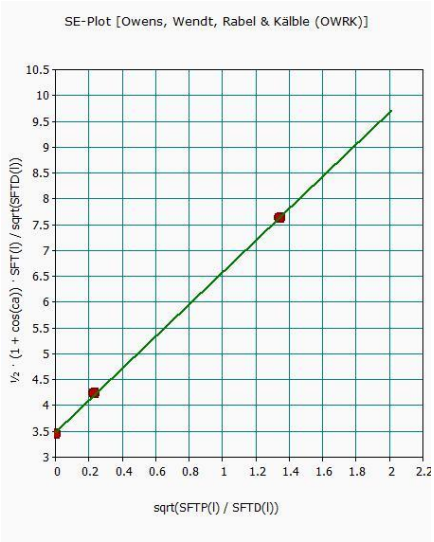

Figure C.5. Glass coated with 110-R972(PDES)

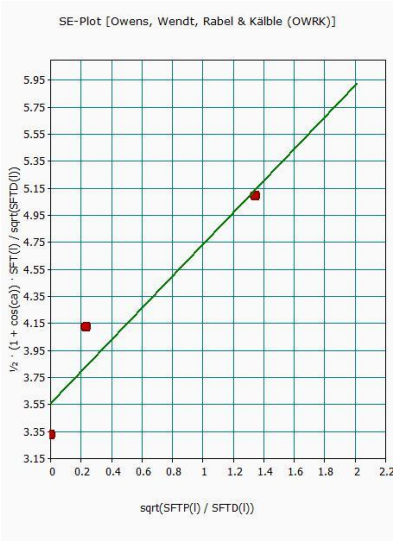

Figure C.6. Steel coated with 110-R972(PDES)

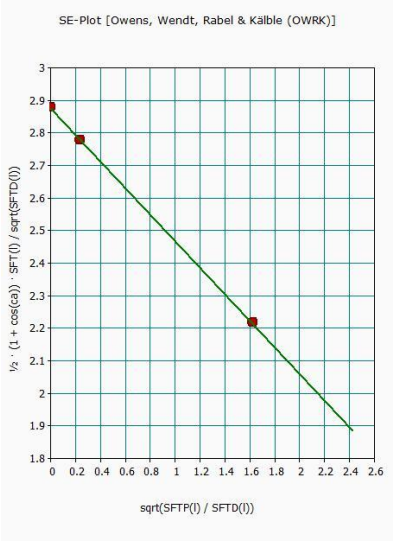

Figure C.7. Glass coated with 100-OX50(PDES)

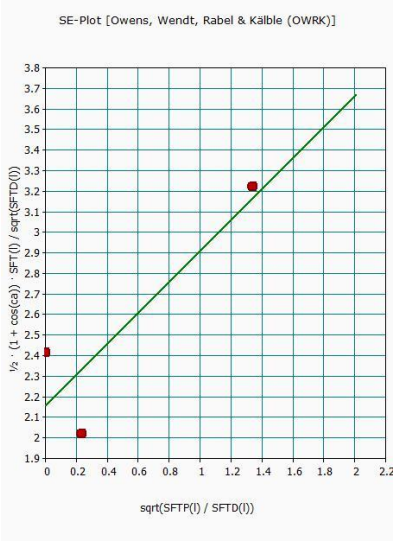

Figure C.8. Steel coated with 100-OX50(PDES)

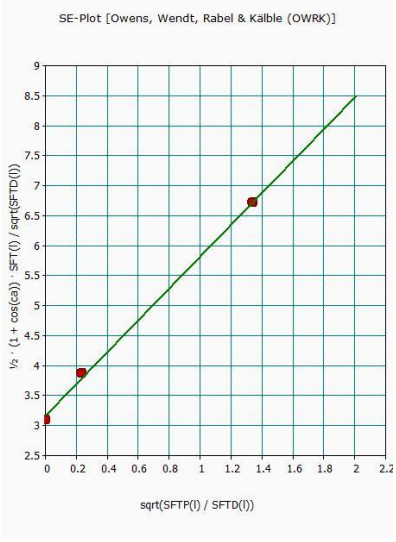

Figure C.8. Glass coated with 100-R972(PDES)

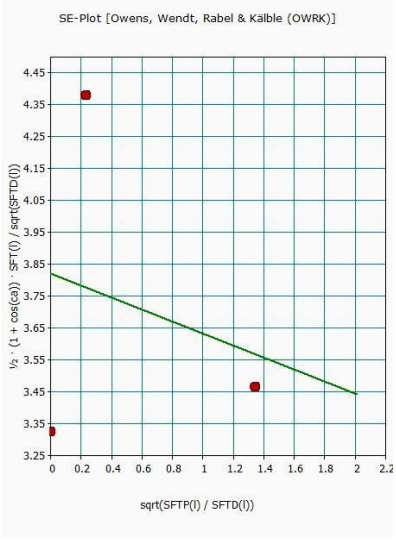

Figure C.9. Steel coated with 100-R972(PDES)

C.3 POCS

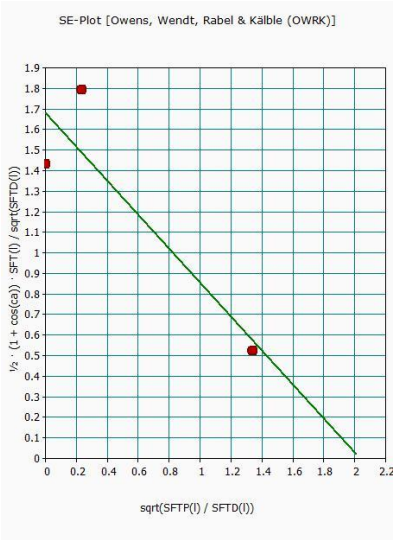

Figure C.10. Glass coated with 110-OX50(POCS)

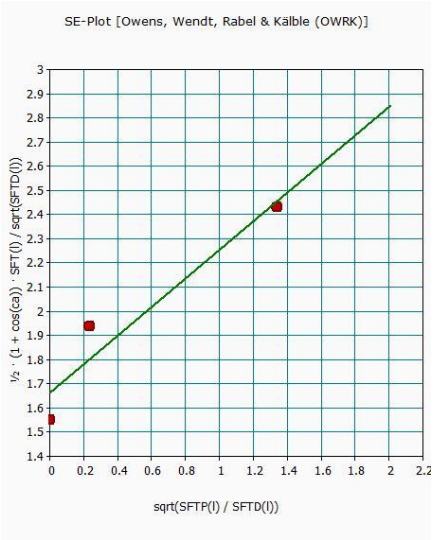

Figure C.11. Steel coated with 110-OX50(POCS)

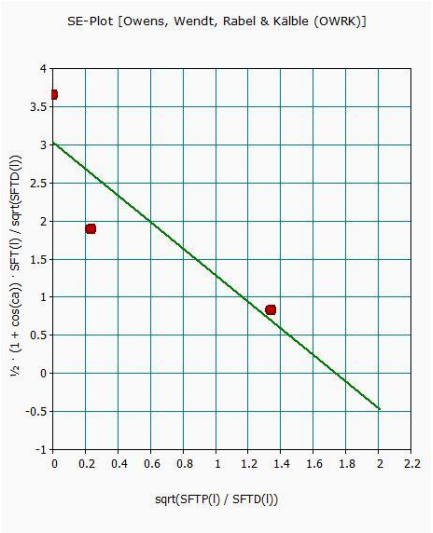

Figure C.12. Glass coated with 110-R972(POCS)

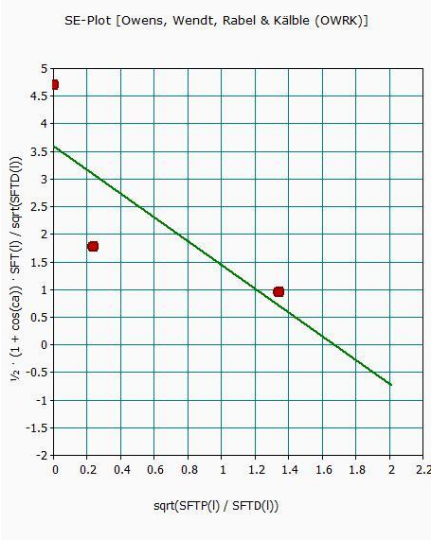

Figure C.13. Steel coated with 110-R972(POCS)

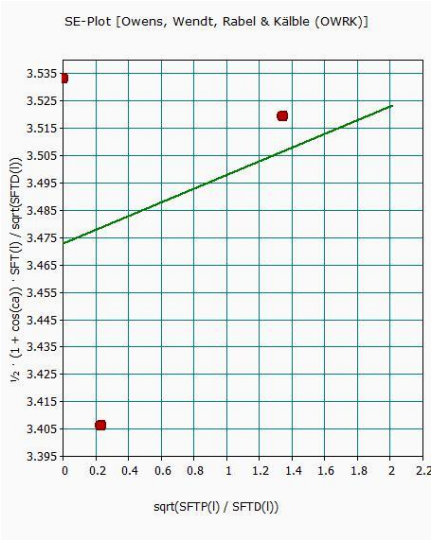

Figure C.14. Glass coated with 100-OX50(POCS)

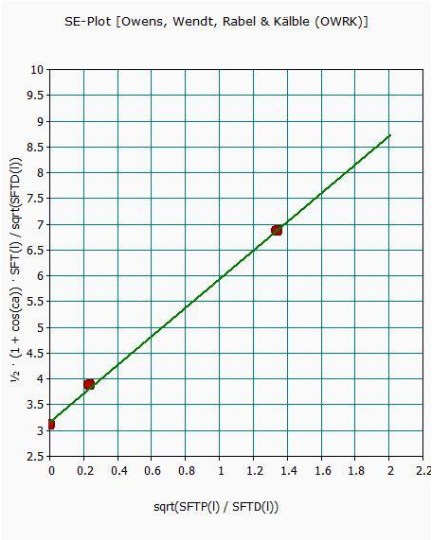

Figure C.15. Steel coated with 100-OX50(POCS)

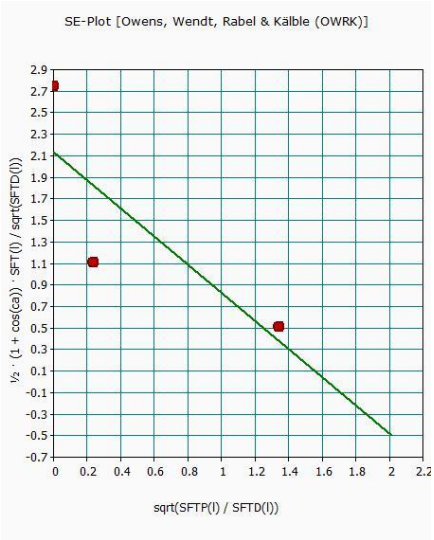

Figure C.16. Glass coated with 100-R972(POCS)

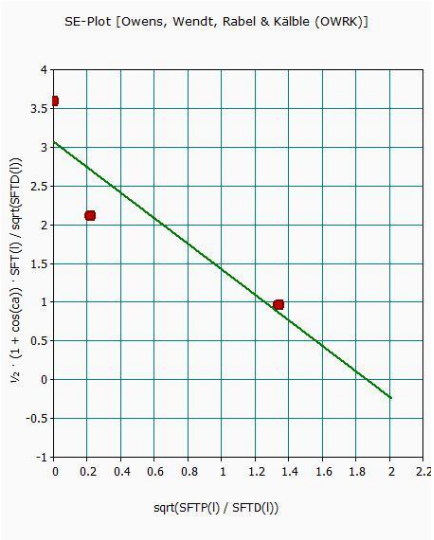

Figure C.17. Steel coated with 100-R972(POCS)

C.4 Silicon Oil DC 200

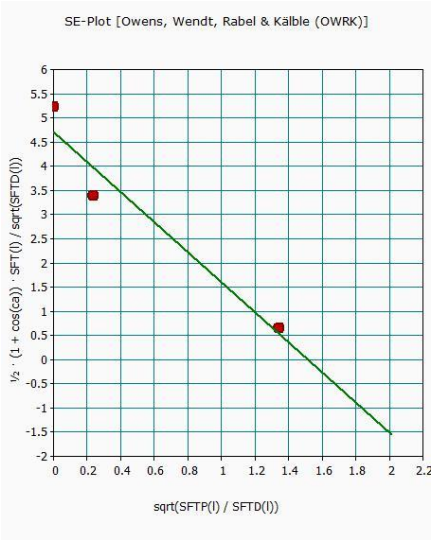

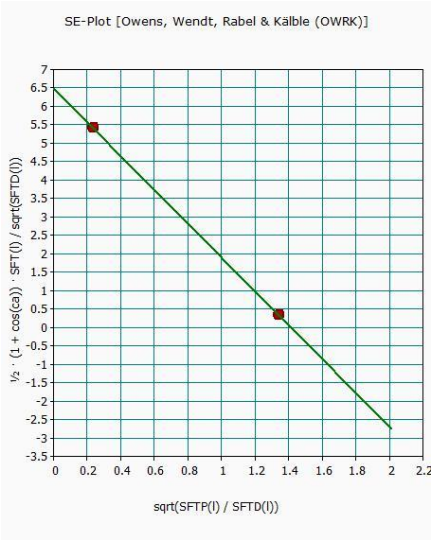

Figure C.18. Glass coated with Silicon oil DC 200 **Figure C.19.** Steel coated with Silicon oil DC 200

C.5 Sylgard 184

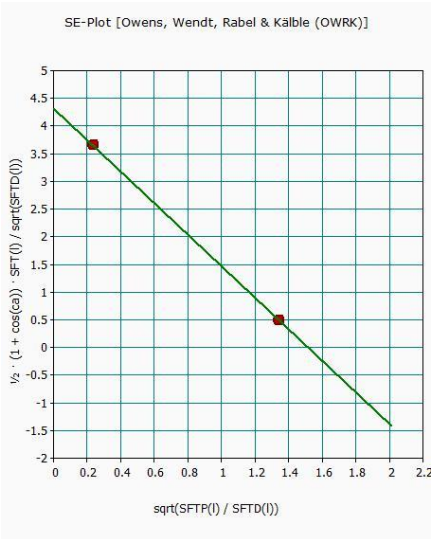

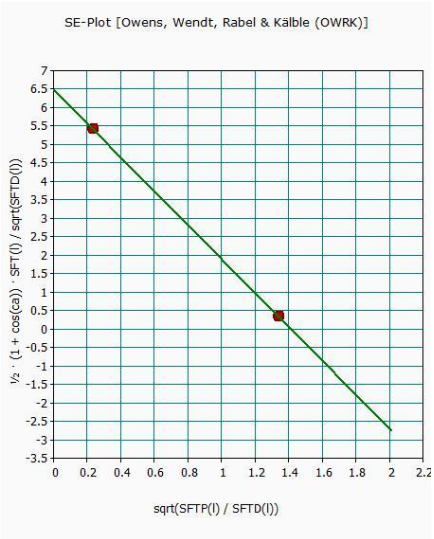

Figure C.20. Glass coated with Sylgard 184 **Figure C.21.** Steel coated with Sylgard 184

C.6 Etched and coated aluminum slide (10 minutes)

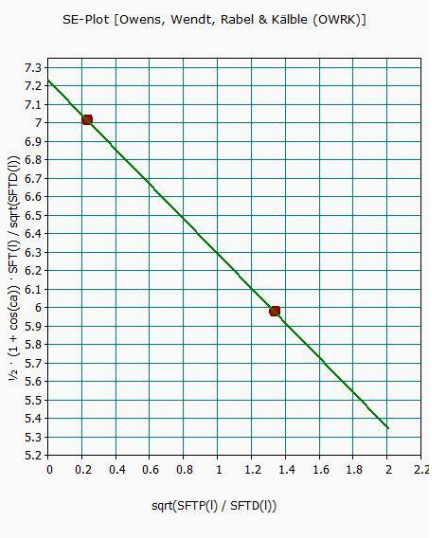

Figure C.22. Etched aluminum slide (10 minutes)

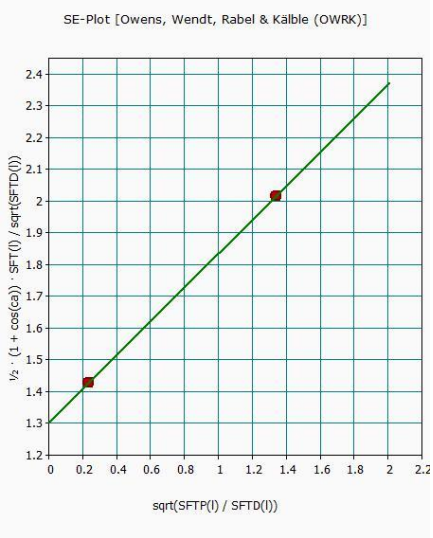

Figure C.23. Etched and coated aluminum slide (10 minutes)

C.7 Etched and coated aluminum slide (22 minutes)

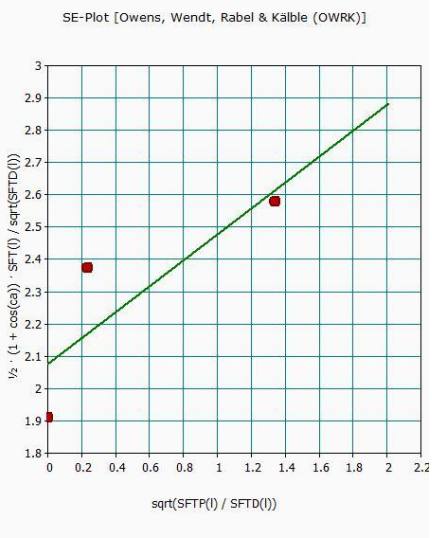

Figure C.24. First parallel aluminum slide etched and coated

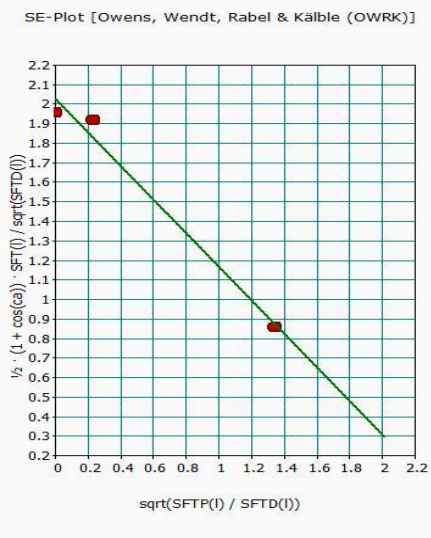

Figure C.25. Second parallel aluminum slide etched and coated

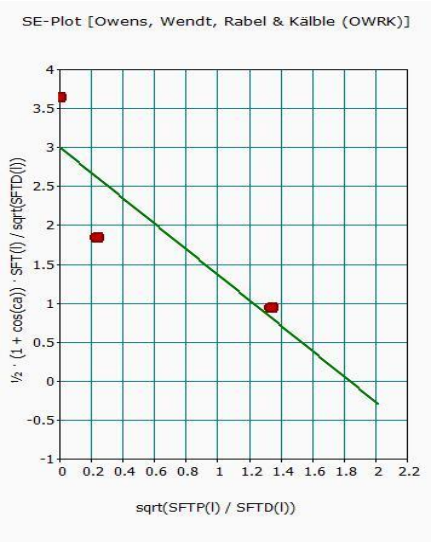

Figure C.26. Third parallel aluminum slide etched and coated.